A study of the polarization of Cherenkov Radiation in Extensive Air Showers of Energy around 1 TeV

Ignacio de la Calle Pérez

Trabajo de investigación dirigido por:

José Luis Contreras

y

Victoria Fonseca González

Dpto. Física Atómica, Molecular y Nuclear
Facultad de Ciencias Físicas
Universidad Complutense de Madrid

Contents

Introduction

Gamma ray is the generic term applied to the rather extensive band of photons seen at the shortest wavelengths of the electromagnetic spectrum. This term was first applied to the penetrating radiation from radiactive atoms. This radiation has energies in the range of 1 to 5 megaelectron volts. Although the electromagnetic spectrum extends far beyond this, the same term *gamma ray* is used to describe even photons a million million times more energetic.

The universe presents many constrains views when observed through different bands of the electromagnetic spectrum. Through the last decades astronomers had study the universe from radio to gamma waves. In the optical range the sky is essentiatilly populated by stable objects where stars and galaxies are the mayor components. At shorter wavelengths, X-ray and ultraviolet, a much more dynamic and unstable universe appears in which change is the rule rather than the exception. Finally, the gamma universe is violent, chaotic and explosive. Long before experiments could detect gamma-rays emitted by cosmic sources, scientist had known that the universe should be producing these photons. The study of the gamma spectrum show us a unique view of the hottest, most energetic regions of the cosmos. This view is also unique in that gamma-ray astronomy is an infant science and is currently in a period of discovery and vigor unparalleled in its history. In particular, the Energetic Gamma-Ray Experiment Telescope (EGRET) on the Compton Gamma Ray Observatory (CGRO) has moved the field from a few detections of a small number of sources to multi-faceted studies of several classes of Galactic and extra galactic objects.

Because gamma rays coming from space are mostly absorbed by the Earth's atmosphere they cannot be detected directly on ground, this being the reason for gamma-ray astronomy not to develop until it was possible to get our detectors above all or most of the atmosphere, using ballons or spacecraft. The latest and relatively new technique for the study of gamma ray sources is the ground-based imaging air Cherenkov technique.

The imaging air Cherenkov techique is based on the detection of secondary particles originated when a cosmic-ray arrives to the Earth's atmosphere. When a cosmic-ray plunges into the atmosphere it produces a cascade of secondary particles which develop to the ground where they can be detected. This cascade receives the name of Extensive Air Shower or EAS. Among the particles produced in an EAS there is a charged component which is known to be responsible for the emision of a bluish light known as Cherenkov radiation. This radiation reaches the ground where the Cherenkov telescopes can collect it. Thus while energetic cosmic-rays themselves cannot reach the ground, the secondary particles and the Cherenkov photons they spawn can. For the search of gamma-ray sources the gamma photons have to be selected over the whole range of cosmic-rays that reaches the Earth's atmosphere, the so called hadronic background. This method is called γ/hadron separation and the improvement of the method is one of the main tasks of the Cherenkov Technique.

The Cherenkov radiation is a big source of information for the study of EAS and from this study we can obtain information such as the energy of the primary particle and point of origin of the gamma-ray on the celestial sphere. One important feature of the Cherenkov radiation is its intrinsic polarization which has a characteristic pattern on ground from which important information can be achieved on topics such as γ/hadron separation above mentioned. Nevertheless this intrinsic polarization is one of the less studied features of Extensive Air Showers.

The goal of this work is the study of the intrinsic polarization of the Cherenkov radiation an its further aplication on the imaging air Cherenkov technique with two main implications: the improvement of the γ/hadron separation and the reduction of the telescope energy threshold.

By means of an Air Shower Monte Carlo simulation we have studied some of the characteristics of the net polarization of Cherenkov Light and results will be presented on this work. Taking into account geometrical considerations we found that there is a net polarization over one particular direction. This assumption will be the begining point of this work and will lead us to propose an experimental setup that could be used on Imaging Atmospheric Cherenkov Telescopes, to take advantage of the information contained in the Cherenkov Light polarization.

Chapter 1

Physical Basis

1.1 Cherenkov Radiation

Cherenkov radiation was first observed in the early 1900's by the experiments developed by Mary and Pierre Curie when studying radioactivity emission. The nature of such a radiation, afterwards called Cherenkov radiation was unknown. The first attempt to understand the phenomenon was made by Mallet in 1926. He found that the light emitted from a wide variety of transparent bodies placed close to a radioactive source always had the same bluish-white quality, and the spectrum was continuous, not possessing the line or band structure characteristic of fluorescence. Mallet found such an emission but he could not find the nature of it.

It was not until the experimental work carried out between years 1934-1937 by P. A. Cherenkov and the theoretical interpretation by I. E. Tamm and I. M. Frank (1937) that this radiation was described, although it was not until 1958 that the effect was well understood and recognize. In between lots of experiments were carried out. For example in 1947 the first experimental device was proposed by Getting for detecting single particles by the Cherenkov effect, and it is important to mention the first detection of Cherenkov radiation in a gas by Ascoli in 1953, or the observation of light pulses from the nigh sky by Galbraith and Jelley in 1953, experiments that started the search for Cherenkov radiation in the atmosphere.

It is not the aim of this work to give a complete mathematical description of the Cherenkov effect. Rather than that a more qualitative description will be given for a better understanding of future references.

The Cherenkov radiation is produced when a charged particle moves in a transparent medium, understanding by transparent medium the one in which the absorption coefficient is zero and thus the refraction index is real, at a speed higher that the speed of light in the medium.

Before starting the description of the Cherenkov effect it must be emphasized that the Cherenkov radiation is entirely unrelated to the bremsstrahlung, which is emitted by the moving electron itself when it collides with atoms in the medium. The Cherenkov effect involves radiation emitted by the medium under the action of the field of the particle moving in it. The distinction between the two types of radiation appears with particular clarity when the particle has a very large mass: bremsstrahlung disappears, but the Cherenkov radiation is unaffected.

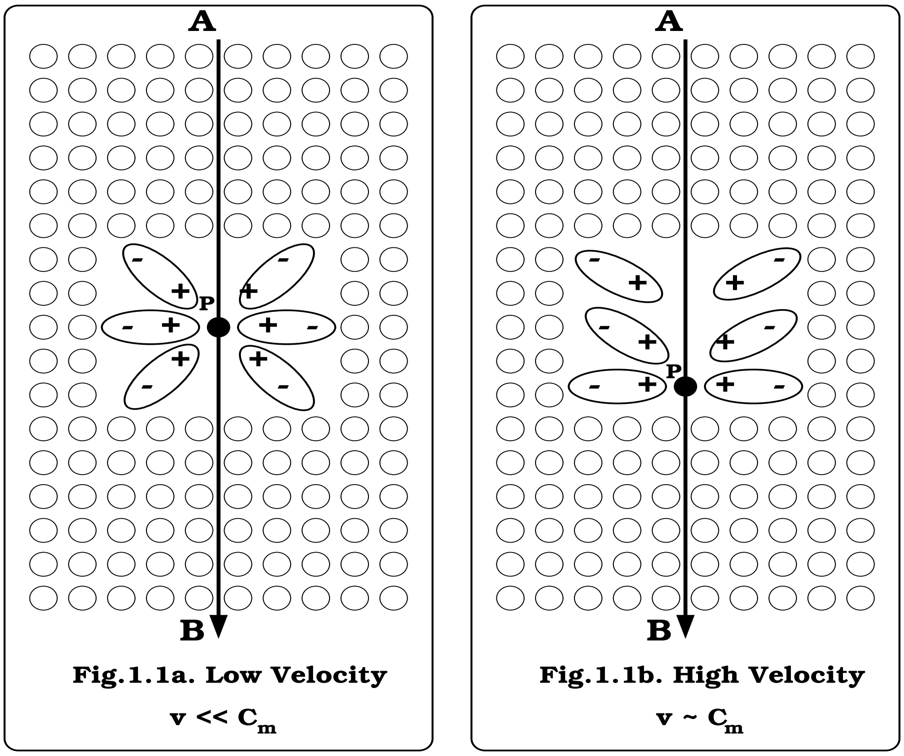

Figure 1.1: *The polarization set up in a dielectric when a charged particle passes through.*

Lets illustrate two cases, an electron moving slower than the speed of light and an electron moving at a speed faster than the speed of light through a piece of glass or other transparent medium. For the first case Fig.(1.1a) shows a section of the glass in the vicinity of the track AB of this electron, the circles represent the individual atoms composing the glass. At a certain time the particle is in point P, the electric field of the particle distorts the atoms so that the negative charges of the nuclei are displaced to one side while the positive charges are displaced towards the moving electron. The medium thus becomes polarized about the point P. When the electron moves to point P' the atoms in point P return to the normal position radiating electro-magnetic pulses. We can say that the electron polarizes the medium as it goes through it leaving regions of instant dipoles. Owing to the complete symmetry of the polarization field surrounding the electron, there will be no resultant field at large distances and thus no emission. If we take a look at Fig.(1.1a) we can see that there is symmetry both in azimuth and along the axis AB.

If, however, the electron is moving fast the situation is quite different as you can see in Fig.(1.1b). In the azimuthal plane, symmetry is preserved, but along the axis there is a resultant dipole field which will be apparent even at large distances from the track of the electron. Such a field will be momentarily set up by the electron at each element along the track, in turn each element will radiate a brief electro-magnetic pulse. The waves coming form each element of the track interfere constructively being the reason for the existence of a resultant field not equal to zero.

The reason why there is a dependence in the emission of Cherenkov radiation with the velocity of the particle is the following. The instant dipoles in the medium are set by the electro-magnetic field of the particle moving. When the particle moves slower than the speed of light the electro-magnetic waves travel ahead of the particle setting instant dipoles in the medium before the particle reaches those regions (see Fig.(1.1a)). That is the reason why no net polarization is set along the track of the particle. When the particle moves at a speed higher than the speed of light in the medium no instant dipoles are set ahead of the particle because the particle travels at a speed greater than the electro-magnetic waves emitted by the particle (see Fig.(1.1b)). This sets instant dipoles along the track of the particle being the reson for the existance of a net polarization along the track of the particle.

In Fig.(1.2) a geometrical interpretation of the emission of the Cherenkov radiation is shown.

From this figure it is understood that this radiation is only observed at a particular angle Θ called Cherenkov angle, with respect to the track of the particle. This angle represents the position in which waves from arbitrary point such as P1, P2 and P3 over the track AB are coherent and combine to form a plane wave front BC. This coherence takes place when the particle travels from A to B in the same time that the light travels from A to C. If the velocity of the particle is v or $\beta \cdot$ c where c is the velocity of light *in vacuo* and $\frac{c}{n}$ is the velocity of the

Cherenkov light in the medium, then we can write the Cherenkov angle in the following way only taking into account geometrical considerations;

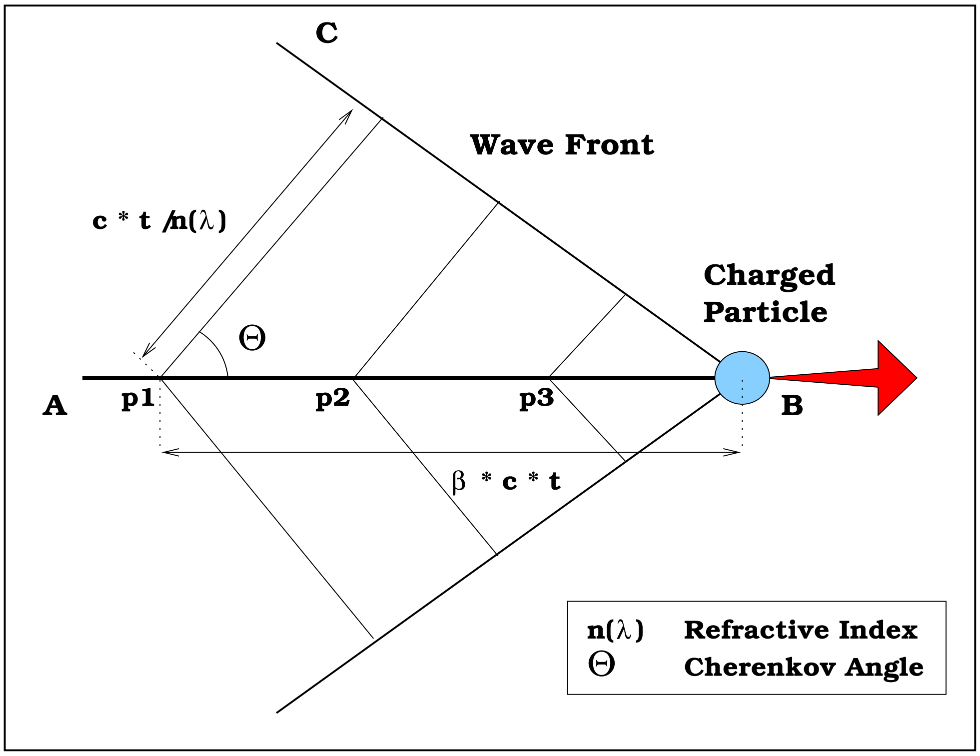

Figure 1.2: *Huygens construction to illustrate coherence.*

$$\cos\Theta = \frac{\frac{c}{n(\lambda)}\cdot\Delta T}{\beta\cdot c\cdot\Delta T} \tag{1.1}$$

$$\boxed{\cos\Theta = \frac{1}{\beta\cdot n(\lambda)}} \tag{1.2}$$

where n is the refractive index of the medium and ΔT is the time in which the particle moves from A to B.

From equation (1.2) we can take out some particular implications:

- (i) For a medium of a given refractive index n, there is a threshold velocity $\beta_{min} = \frac{1}{n}$, below which no radiation takes place. At this critical velocity the direction of radiation coincides with that of the particle. To see this we could write (1.2) in the following way:

$$\cos\Theta = \frac{1}{\beta \cdot n(\lambda)} = \frac{c_{medium}}{v_{part}} \tag{1.3}$$

so when v_{part} is lower than c_{medium} the equation does not have solution, and no radiation takes place.

We can see all this from a different point of view. The wave vector and frequency of an electro-magnetic wave propagating in a transparent medium are related by $k = \frac{nw}{c}$, where n is again the refractive index. The frequency of the field created by a particle moving uniformly in the x-direction in a medium is related to the x-component of the wave vector by $w = k_x \cdot v$. If this component is a freely propagated wave, these two relations must be consistent. Since k $>$ k_x it follows that we must have,

$$v > \frac{c}{n(\omega)} \tag{1.4}$$

Thus radiation of frequency ω occurs if the velocity of the particle exceeds the phase velocity of waves of that frequency in the medium concerned. On the other hand we have the relation between k and k_x:

$$k_x = k \cdot cos\Theta = \frac{nw}{c} \cdot cos\Theta \tag{1.5}$$

where, as we just show, cos $\Theta = \frac{c}{nv}$.

So when $\frac{c}{nv} \sim 1$ then $\Theta \sim 0$ and $k_x \sim$ k, that is, the direction of radiation coincides with that of the particle.

- (ii) For an ultra-relativistic particle, for which $\beta = 1$, there is a maximum angle of emission, given by,

$$\cos\Theta = \frac{1}{n} \tag{1.6}$$

- (iii) The radiation occurs in the visible and near visible regions of the spectrum, for which $n > 1$. A real medium is always dispersive, so actually radiation is restricted to those frequencies bands for which $n(\omega) > \frac{1}{\beta}$. In the x-ray region $n(\omega)$ is always < 1 and radiation is forbidden. So emission in the x-ray region is impossible for n is less than unity and equation (1.6) cannot be satisfied.

There are two further conditions to be fulfilled to achieve coherence, in addition to that stated in point (i). First, the length l of the track of the particle in the medium should be large compared with the wavelength λ of the radiation in question, otherwise diffraction effects will become dominant. Secondly, the velocity of the particle must be constant during its passage through the medium, or, to be more specific, the differences in the times for particle to traverse successive distances λ should be small compared with the period $\frac{\lambda}{c}$ of the emitted light. If we take into consideration the Maxwell theory of electro-magnetic waves a charged particle moving uniformly does not irradiate and this is the prove that the Cherenkov radiation is not related with Bremsstrahlung.

We would like to underline the following point as being important for further explanations, the Cherenkov radiation originated in each element of the track is propagated along a surface of a cone whose apex is at the element, whose axis coincides with the track, and whose semi-vertical angle is the angle Θ.

The main part of this work is based on the polarization of the Cherenkov radiation. We will discuss in a geometrical way how this polarization is set and in following chapters we will see how this set is the crucial point of this work.

Looking at Fig.(1.3) we can assume a charged particle moving along the z axis. Along its path, and as we just showed before, the Cherenkov photons are emitted with a certain angle called Cherenkov angle Θ. In this frame the polarization vector is everywhere perpedicular to the Cherenkov cone and it is contained in the plane defined by the direction of propagation of the charged particle and the direction of propagation of the photon. If we could take a look at the Cherenkov cone from its apex the distribution of the polarization vectors would be as the one you can see in Fig.(1.4).

This particular distribution will have big implications in the development of this work and it is the basis of it.

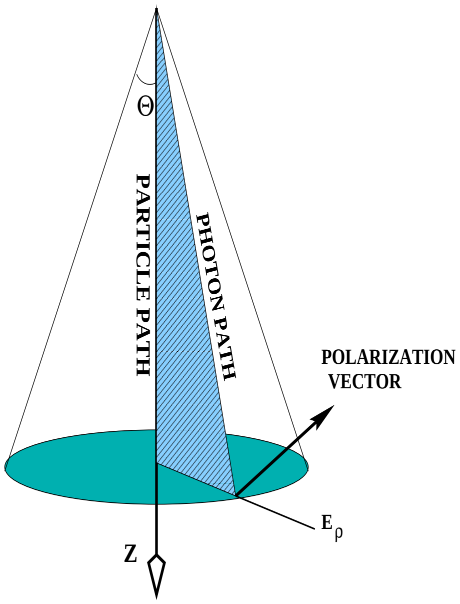

Figure 1.3: *The formation of the Cherenkov cone, and the polarization vectors.*

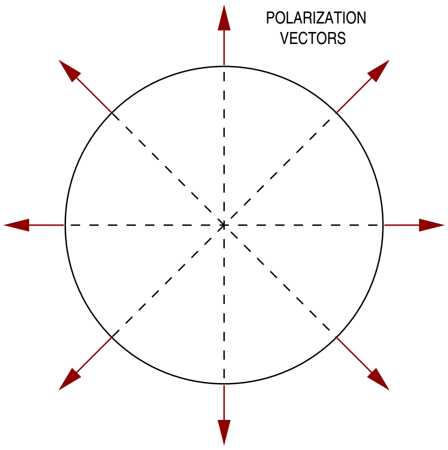

Figure 1.4: *Distribution of the polarization vectors.*

Before finishing this point we are going to comment briefly some important aspects of the Cherenkov radiation as it is the energy spectrum and the number of particles emitted as well as the duration of the light flashes.

The number of photons emitted by a charged particle of charge **ze** per unit path length and per unit energy interval, or equivalently to λ, of the photons is

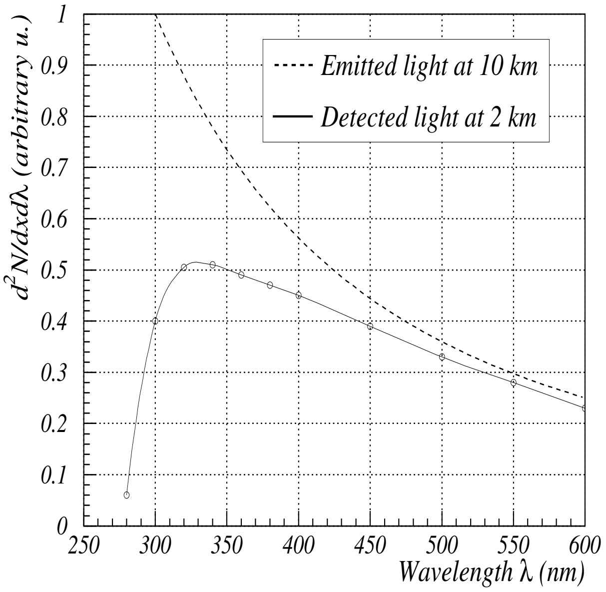

Figure 1.5: *Differential Cherenkov photon spectrum. Continuous line includes absorption by ozone and Rayleigh and Mie scattering. The spectrum has a peak at around 330 nm.*

equal to:

$$\boxed{\frac{dN^2}{dx d\lambda} = \frac{2\pi\alpha z^2}{\lambda^2} \cdot (1 - \frac{1}{\beta^2 \cdot n^2(\lambda)})} \tag{1.7}$$

For the particular case of an electron moving along a track of length l within a spectral region defined by wavelengths λ_1 and λ_2 we will have:

$$\boxed{N = 2\pi\alpha l \cdot (\frac{1}{\lambda_2} - \frac{1}{\lambda_1}) \cdot (1 - \frac{1}{\beta^2 \cdot n^2(\lambda)})} \tag{1.8}$$

where α is the structure constant $= \frac{e^2}{\hbar \cdot c} = \frac{1}{137}$ and n is the refraction index of the medium that is a function of the photon energy, or equivalently to λ.

The spectral distribution of the radiation may be expressed in several ways. Since the intensity of light of frequency ν, or $\frac{\omega}{2\pi}$, may be written as $\mathbf{W} = N \cdot h\ \nu$

where h is the Plank's constant, the spectral distribution may be written in any of the following four ways:

$$(\frac{d^2W}{dldw}) \propto w \tag{1.9}$$

energy per unit path and frequency interval

$$(\frac{d^2W}{dld\lambda}) \propto \frac{1}{\lambda^3} \tag{1.10}$$

energy per unit path and wavelength interval

$$(\frac{d^2N}{dldw}) \propto const \tag{1.11}$$

number of photons per unit path and frequency interval

$$(\frac{d^2N}{dld\lambda}) \propto \frac{1}{\lambda^2} \tag{1.12}$$

number of photons per unit path and wavelength interval

The energy carried off by Cherenkov radiation can be written in the following way,

$$-\frac{dE}{dx} = \frac{4\pi e^2}{c^2} \int w dw (1 - \frac{1}{\beta^2 \cdot n^2}) \tag{1.13}$$

where the integration is only over those frequencies for which $\beta \cdot n(w) > 1$.

About the duration of the light flashes we can say that in a non-dispersive medium, the wavefront is infinitely thin, so the duration of the light pulse at any given point within the Cherenkov cone is infinitely short. If however the medium is dispersive, the Cherenkov angle is different for different wavelengths and the wave trains will spread out. This turns in a duration Δt of the light pulse, Fig.(1.6). This duration observed along a line parallel to the axis of the particle, at a distance ρ from the axis, will be given by:

$$\Delta t = \frac{\rho}{\beta \cdot c} \cdot (tan(\theta_2) - tan(\theta_1)) \tag{1.14}$$

With this we finish the overview of the general basis of the Cherenkov radiation. Lets move all this into the frame of Extensive Air Showers.

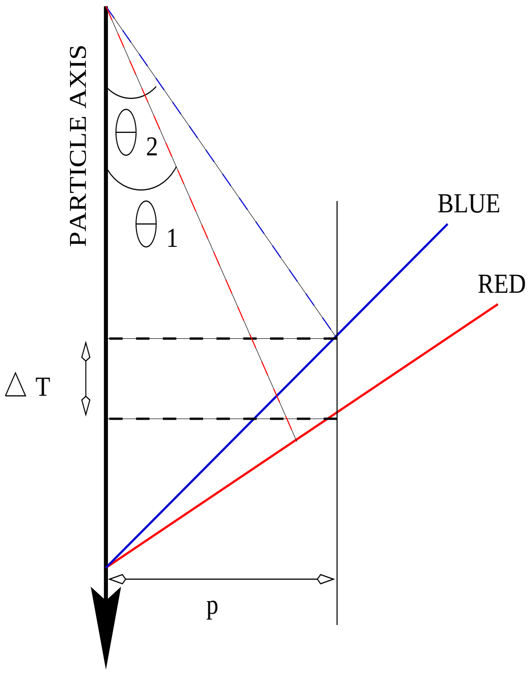

Figure 1.6: *The duration of light pulses in a dispersive medium.*

1.2 Extensive Air Showers

It was not until 1927 that all doubt was removed about the existence of what initialy was called cosmic-radiation and not until 1948 when the nature of such a radiation began to be understood. By *Cosmic Radiation* (CR) we understand all kinds of particles and high energetic radiation reaching the Earth from the outer space. Basically the cosmic radiation is integrated by atomic nuclei (96% H, 3% He, 1% C,N,O,Fe), γ-rays, electrons and positrons, neutrinos and other types of elemental particles. Nowadays only charged particles with sufficiently high energies are called cosmic-rays. In the following figure (Fig.1.7) the spectrum of comic-rays is plotted. The cosmic-ray spectrum extends in energy up to at least 10^{20} eV.

The cosmic radiation travels from the emission source until it reaches the Earth. On its way through the outer space some interactions with the intergalactic or interstellar medium can take place, as for example fragmentation of the nuclei, ionization, particle production and many more. This sub-products of the original cosmic particles are the ones that reaches the earth's atmosphere. When

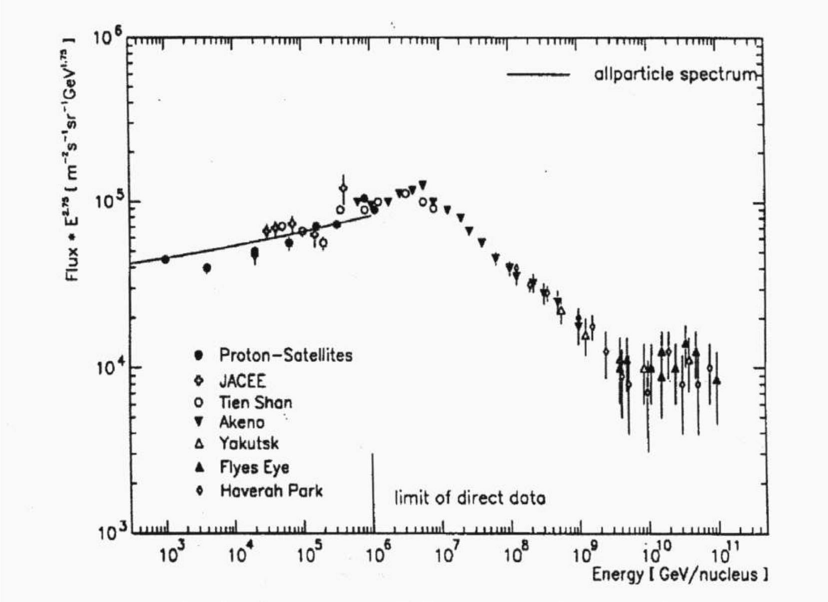

Figure 1.7: *The energy spectrum of cosmic radiation.*

the cosmic rays enter the earth's atmosphere they have extremely high energy and give rise to a number of complicated processes through the interaction with an atmospheric nuclei that gives rise to a certain number of *secondary particles* turning into what is called Estensive Air Shower or EAS. The secondary particles experiment more interactions through the atmosphere that are of two kinds depending on the nature of the particles; interaction *charged particle-matter* and interaction *radiation-matter*. For the first case two principle features characterize the passage of charged particles through matter: (1) a loss of energy by the particle and (2) a deflection of the particle from its incident direction. These effects are primarily the result of two processes:

- *inelastic collisions* with the atomic electrons of the material where energy is transferred from the particle to the atom causing an ionization or excitation of the latter.

- *elastic scattering* from nuclei, where the charged particle experiments successive elastic collision in the field of a nuclei. In general very little energy is transfered in these collisions.

These, however, are not the only reactions which can occur. Other processes include,

- emission of *Cherenkov radiation*.

- *nuclear reactions.*
- *bremsstrahlung.*

For the second case, interaction radiation-matter, three effects can take place:

- *photoelectric effect.* Dominant at energies E $\leq$ 100 KeV.
- *Compton scattering.* Dominant at energies around 1 TeV.
- *pair production.* Begins to be important at energies higher than 1 MeV and it is the dominant effect at energies higher than 25 MeV.

The final result of all this processes that take place in the atmosphere with the arrival of a cosmic-ray is a shower of particles that travels through the atmosphere until they reach the ground. It has to be mentioned that the shower does not keep growing until it reaches the ground. In every process the energy per particle is reduce so the shower gets to a critical point where dissipation processes become more important than creation processes and the shower begins to extinguish.

As already mentioned, amongst this high energy particles reaching the Earth there is small flux of gamma-rays, about 1 out 1000 air showers produced in the atmosphere are gamma initiated. There is some differences in the development of an air shower depending on the primary particle originating the shower. Lets take a look at both cases, a gamma-ray initiated shower and an hadronic initiated shower.

- *Gamma-ray Initiated Shower*: At the energies involved in the process that take place in the upper atmosphere when a γ-ray plunges into the atmosphere the pair production is the dominant effect. This is the situation in EAS. The process of pair production takes place in the field of an atmospheric nuclei or electron in order to conserve momentum. A high energy photon, of at least an energy of 1.022 MeV, in matter converts into an electron and positron pair. If the energy is sufficient, the resulting electron pair does not quickly lose its energy by ionizating interactions. Instead, an electron in the field of a nucleus can produce a secondary gamma ray. This process is called bremsstrahlung. This gamma ray, if its energy is still higher than 1.022 MeV, can then produce another electron pair that can undergo further bremsstrahlung interactions. The result is a cascade of photons, electrons and positrons, which continues traveling in the original direction of the primary gamma ray and sharing its total energy.

  We are going to take a closer look at the gamma-ray initiated shower. A simple model ([32, M.S. Longair 1992]) could be made to explain the processes that take place when a gamma-ray reaches the atmosphere.

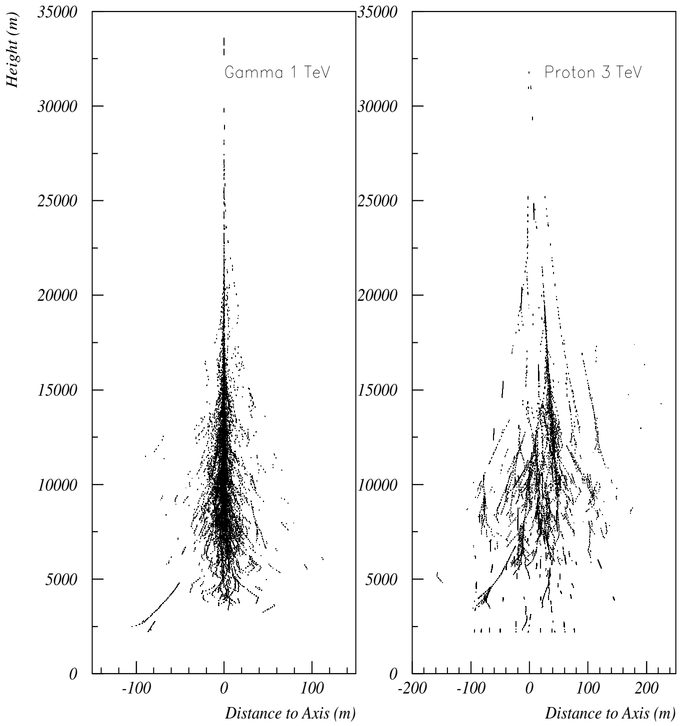

Figure 1.8: *Gamma initiated shower of energy 1 TeV and proton shower of energy 3 TeV.*

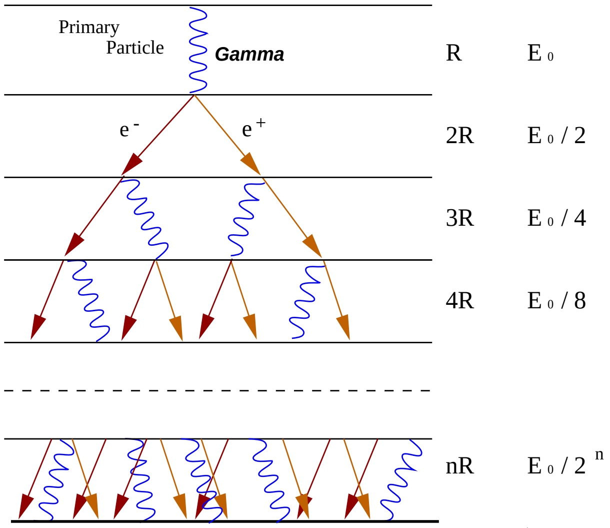

Figure 1.9: *Model of an electro-magnetic shower.*

Let us assume that an incident photon of energy E_0 traverses a distance R before creating an electron-positron pair. This distance can be expresed in terms of radiation length. One *radiation length* is the mean distance over which a high energy electron loses all but $1/e$ of its energy by Bremsstrahlung. At these high energies this is also the distance a beam of gamma photons must traverse so that all but $1/e$ of them have produced an $e^{\pm}$ pair. For the atmosphere this quantity equals $\xi_0 \simeq 36.7$ g$/cm^2$. So actually R $= \xi_0 \cdot \ln 2$, in terms of radiation lengths. The probability of a photon or electron to interact along a distance R is therefore, exp(-R$/\xi_0) = 1/2$. It is considered that in each interaction the energy is equally divided between $e^{\pm}$ and γ's. Then in the first interation each particle has half of the initial energy on the average. After traveling another distance R, each particle will bremsstrahlung and produce a photon of average energy $\frac{E_0}{4}$. At a distance nR into the shower, there will then be 2^n particles created, each with an average energy $\frac{E_0}{2^n}$. This multiplicative process continues until the average energy of the particle drops bellow some energy E_c, called the *critical energy*. This energy is defined as the energy below which the dominant energy loss is by ionization, via atomic collisions, rather than by bremsstrahlung emission, thus halting the cascade. This energy in the air is around 81 MeV per particle. At this point, no further multiplication occurs except for very low energy electron-ion pair production. For γ rays, the critical energy correspond to a point where Compton scattering begins to be more important than pair production.

Critical energy:

$$\text{photons} \longrightarrow \sigma_{com} \approx \sigma_{pair}$$

$$e^{\pm} \longrightarrow (\tfrac{dE}{dx})_{rad} \approx (\tfrac{dE}{dx})_{col}$$

The shower thus reaches its maximum development when the average energy of the cascade particles equals the critical energy. The total number of photons and electrons at the shower maximum is then given by the total energy E_0 divided by the critical energy E_c.

$$N_{max} = \frac{E_0}{E_c} \tag{1.15}$$

The maximum penetration depth of the cascade X_{max}, if we assume that the shower stops abruptly at the critical energy E_c, is,

$$E(X_{max}) = \frac{E_0}{2^n} = E_c \tag{1.16}$$

which solving for n, gives a value for X_{max}, as a function of primary energy and ξ_0,

$$X_{max} = \frac{Ln\frac{E_0}{E_c}}{Ln2} \cdot R = Ln\frac{E_0}{E_c} \cdot \xi_0 \tag{1.17}$$

A better approximation for the number of particles ($e^{\pm}$) produced in a shower as a function of the primary energy and atmospheric depth, is given by Greisen equation (1.18) ([33, K. Greisen 1956]). In figure Fig.(1.10) is represented the number of shower particles ($e^{\pm}$) in terms of the atmospheric depth (measured in radiation lengths) with the aid of:

$$N_e(t) = \frac{0.31}{\sqrt{[ln(E_0/E_c)]}} \cdot \exp\left[t \cdot (1 - 1.5 \cdot lns\right] \tag{1.18}$$

where $s = \frac{3 \cdot t}{t + 2ln(E_0/E_c)}$ is known as the age parameter that indicates the degree of development of the shower, and t is the atmospheric depth in terms of radiation length. A value of s = 0 indicates the first interaction point, s = 1 indicates the maximum development of the shower and s = 2 the point in which the shower begins to extinguish.

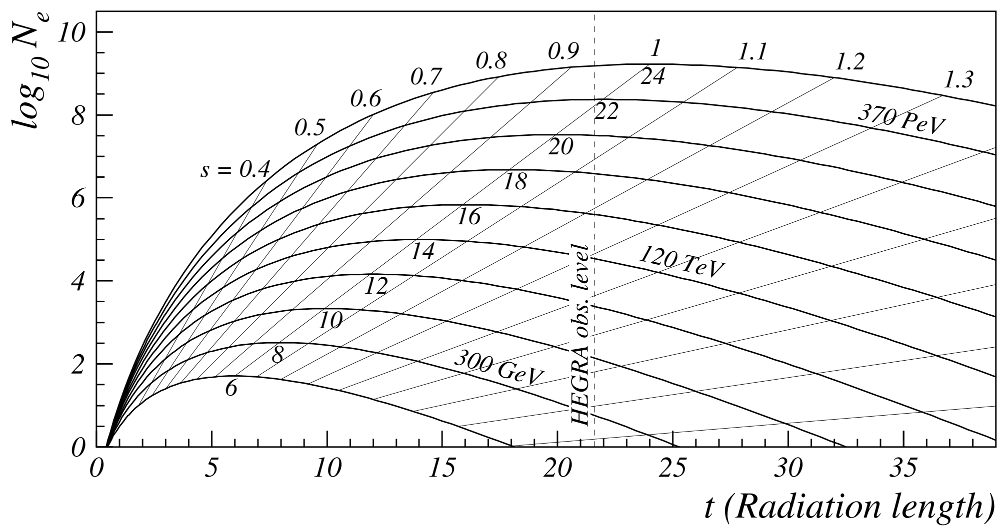

Figure 1.10: *Longitudinal development of an atmospheric shower in terms of atmospheric depth according to the Greisen approximation. Different curves represent different energies of primary photons E_0. The value $ln(E_0/E_c)$ are shown under the curves. At sea level the atmospheric depth is around 27 radiation lengths.*

This models, of course, only give a rough qualitative picture of the shower. In reality, the number of particles in an electro-magnetic shower rises exponentially to a broad maximum after which it declines gradually. In general, a precise calculation cannot be made analytically and recourse must be made to such techniques as Monte Carlo simulations.

- *Hadronic Initiated Shower*: These particles, most of which are protons, cause nuclear disintegration at the top of the atmosphere, with the emission of further particles which in turn themselves produce disintegrations. We could write this interaction in the following way:

$$\text{Cosmic Ray (CR)} + \text{Atmospheric Nuclei (AN)} \Rightarrow \text{CR'} + \text{AN'} + \text{n}\pi^{\pm} + \text{m}\pi^{0} + \text{other mesons.}$$

where CR' is a fragment of the original cosmic ray that can keep producing more interaction with atmospheric nuclei. If the original cosmic ray has enough energy some of its fragments could reach the ground. AN' are fragments of atmospheric nuclei in a high energy state. Among the products of the nuclear disintegrations are the π-mesons, which can decay in the following sub-products,

$$\pi^0 \rightarrow 2\,\gamma \qquad \tau = 1.8 * 10^{-16} s$$
$$\pi^{\pm} \rightarrow \mu^{\pm} + \nu_{\mu} \qquad \tau = 2.5 * 10^{-8} s$$
$$\mu^{\pm} \rightarrow e^{\pm} + \nu_e + \nu_{\mu} \qquad \tau = 2.2 * 10^{-6} s$$

The decay of the π^0 in two high energy γ-rays originates what it is called the electro-magnetic component of the shower because from here on only electrons and γ-rays will be produced having a component made up by electrons and gammas by the processes of bremsstrahlung and pair production. The process by which this sub-cascade develops is the same as the one describe for the pure electro-magnetic showers.

The whole process is summarize in the following figure:

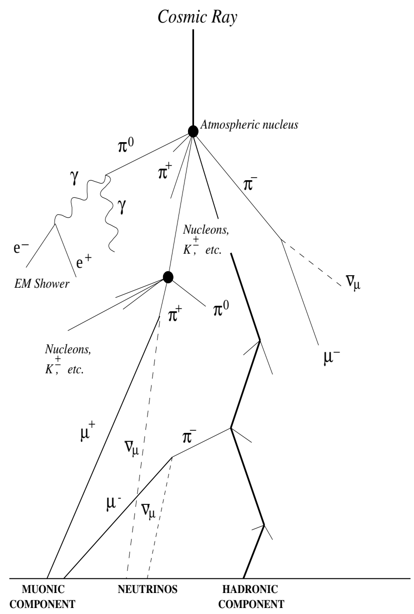

Model of an Extensive Air Shower initiated by a cosmic ray.

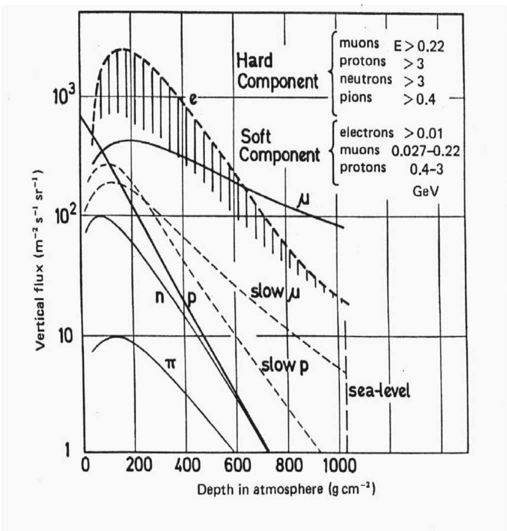

The vertical fluxes of different components of cosmic rays within the atmosphere.

Lets take a more qualitative look at the differences between an hadronic initiated shower and a gamma-ray initiated shower on the basis of the longitudinal and transversal development and the implications of this development on the pattern left on ground by the Cherenkov radiation. The knowledge of the longitudinal development of the shower it is important to understand the polarization vector distribution on ground and the existence of a net polarization.

1.3 Cherenkov Radiation in EAS

For primary energies less than 20 TeV the cascades dies out in the upper atmosphere but the Cherenkov radiation produced by the charged component of the shower, penetrates to ground level where it might be collected. Although subject to fluctuations in the point of origin of the cascade and its subsequent development, the Cherenkov light carries with it information pertaining to the exact point of origin of the primary γ-ray on the celestial sphere and also the energy of the primary particle.

In electro-magnetic showers electrons and positrons are the main charged component that radiates Cherenkov light. This is true if the energy of this particles exceeds a minimum threshold E_{min}, as can be pointed out from equation (1.21). This threshold is 21 MeV at see level and increases to 35 MeV at 7.5 kilometers above sea level. The reason for this change in the E_{min} is the variation of the Cherenkov threshold velocity with index of refraction of the atmosphere. We can make an estimation of E_{min} an its dependence with the index of refraction. We know that the velocity of the light in a certain medium is given by,

$$v = \frac{c}{n(H)} \tag{1.19}$$

where c is the speed of light *in vacuum* and n is the refraction index at a given atmospheric height H.

We can then write E_{min} in the following way, where E_{min} is the energy of a relativistic particle moving along a medium at a certain speed,

$$E_{min} = m_0 \cdot c^2 + E_c = \gamma_{min} \cdot m_e \qquad \gamma_{min} = \frac{1}{\sqrt{1 - \frac{1}{n^2}}} \tag{1.20}$$

so if we write n $= 1 + \delta$, with $\delta << 1$, then $\gamma_{min} \approx \frac{1}{\sqrt{2\delta}}$, so

$$\boxed{E_{min} \approx \frac{m_e}{\sqrt{2\delta}}} \tag{1.21}$$

We can approach the study the Cherenkov radiation in an EAS in terms of the longitudinal development of the EAS, or in terms of the lateral distribution of shower particles. The longitudinal spread of the shower is the distribution in points of emission of Cherenkov photons with height, Fig.(1.11). From this figure it is clearly seen that the showers reaches a maximum development after which it starts to blur.

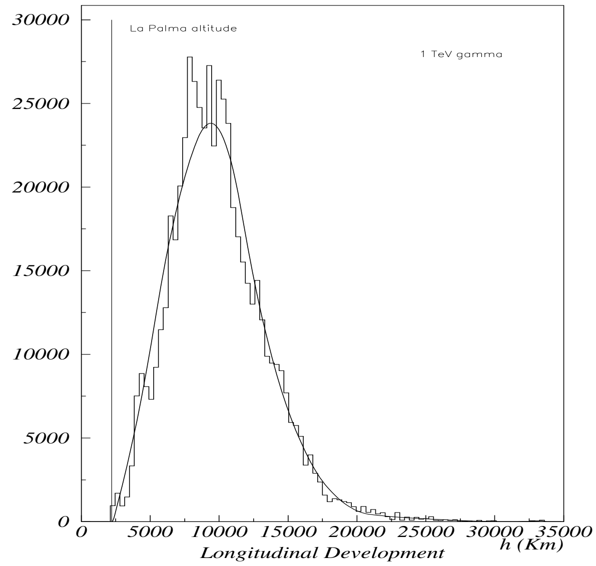

Figure 1.11: *Monte Carlo simulation of the longitudinal distribution of an electromagnetic shower of 1 TeV.*

The lateral distribution of an EAS in terms of Cherenkov radiation is the study of the emission points of Cherenkov radiation in planes perpendiculars to the shower axis. The lateral distribution is thus sensitive to the longitudinal shower development. On the basis of the lateral distribution we can say that steep lateral distributions are associated with showers which develop close to the observer, while showers developing high in the atmosphere have broader distribution exhibiting a characteristic pattern on ground called *Cherenkov ring* that will be discuss now.

The angle of maximum emission of Cherenkov light with respect to the particle direction varies with height because of the change in the refraction index with height, and is given by,

$$cos(\Theta_{max}) = \frac{1}{n} = \frac{1}{1+\delta} \simeq 1 - \delta \qquad (1.22)$$

We can then approximate Θ_{max} (rad) $= \sqrt{2\delta}$. With this value we can establish a relation to obtain the distance R_{core} between emitted Cherenkov photons and the particle trajectory at a certain observation height h_{obs}:

$$R_{core} \equiv (h - h_{obs}) \cdot tan(\Theta_{max}) \qquad (1.23)$$

In figure Fig.(1.12) the dependence of E_{min} and R_{core} with height above sea level is presented. The values for R_{core} were obtained for an ultrarrelativistic electron of vertical incidence and for two observation levels, the one corresponding to the HEGRA experiment, h_{obs}=2200. m, and for the sea level. We can see that R_{core} has a maximum between 10 and 20 km. This makes all the Cherenkov light emitted by the particle between this two heights to reach the observation level in a ring at a distance R_{core}, of around 120 m. (sea level).

For a single relativistic particle radiating high in the atmosphere, the Cherenkov angle is less than a degree, but opens to about 1 degree at 8 km altitude and, due to greater air density, opens to about 1.5 degrees at see level. Because all of the emitting particles are ultra relativistic the Cherenkov angle is saturated.

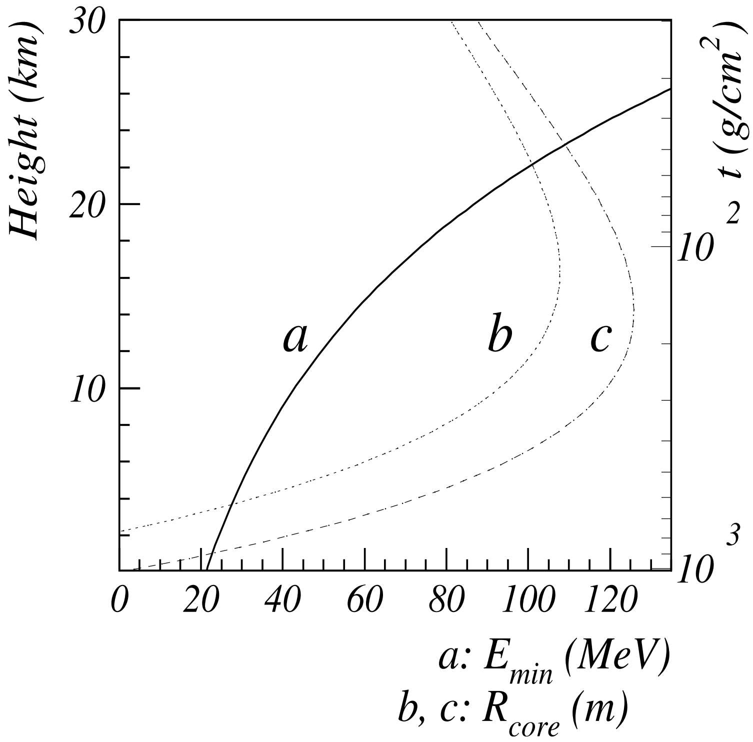

Figure 1.12: *Dependence of E_{min} and R_{core} with height above sea level for an ultra-rrelativistic electron of vertical incidence at two observation levels, sea level* (**c**) *and 2200. m above sea level* (**b**).

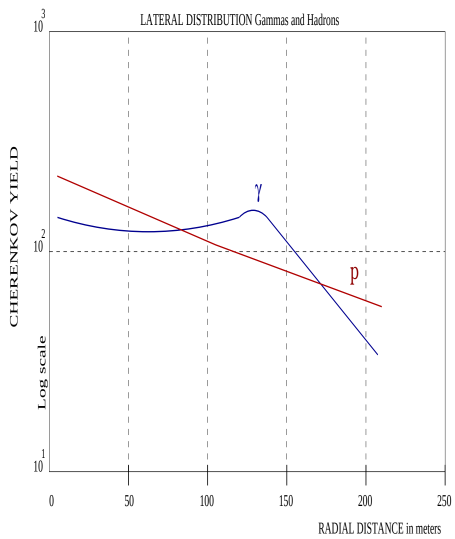

Lateral distribution of Cherenkov light yield on the ground for typical γ-ray and hadron showers. The γ-ray induced shower shows a relatively flat lateral distribution of light out to about 125m radial distance from the center.

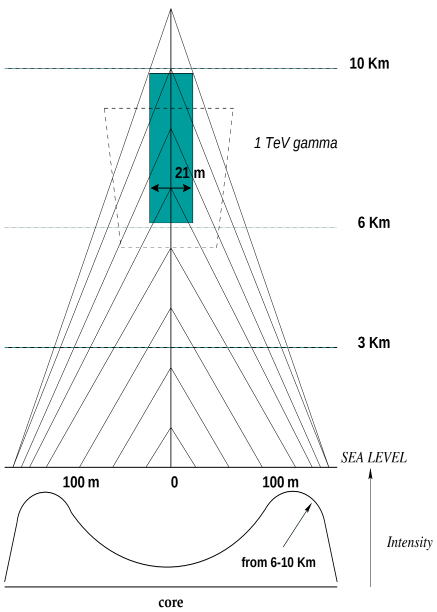

Geometric model of emission of Cherenkov radiation for γ-ray and hadron showers. The stippled region encloses the main emission region for production of Cherenkov light from γ-ray showers. The intensity profiles on the ground reflect the peaking in the Cherenkov lateral distribution for γ-ray showers at distances to about 126 m

The variation of the Cherenkov angle with height combined with the fact that the emitting particles move to the ground gives rise to a geometrical effect. If all the charged particles move along the shower axis, with no lateral displacement, the light would be emitted at the characteristic Cherenkov angle, which is around 1 degree. As the emitting particle speeds up to ground the Cherenkov angle opens focusing the Cherenkov radiation into a narrow annular strip. As an approximation, for a 1 TeV gamma shower light generated from heights between 6 to 10 kilometers above sea level would fall on ground within a ring of 110 to 145 meters in radius from the shower impact point on ground, if electrons did not multiple scatter. Electron multiple scattering broadens this Cherenkov ring but does not totally eliminate it. We can see the effect in the above figure, 50 % of the light is generated between 6 to 10 km and falls in what is called the hump of the Cherenkov pool. The other 50 % is split equally between both higher and lower altitudes. For a proton cascade of the same primary energy the same column is represented in dashed line. The Cherenkov ring is most prominent when the shower dies out far above the observation level, as in low energy gamma showers. The intensity near the shower axis rises when the tail of the shower penetrates close to the observation level, like at high energies, because light emitted closer to the ground has a shorter distance to travel, out weighting the somewhat larger Cherenkov angle, and so it strikes the ground closer to the axis.

As can be seen in the figure above of the lateral distribution, every radial distance on ground from the core, represents a different atmospheric height: the main bulk of particles particles, near shower maximum, produces the light seen at 100-130m from the shower axis; close to the shower axis (within 40m) one sees the light from local particles, the tail of the shower.

When the lateral distribution of light for different energies is compared, the hump (Cherenkov ring) has been shown to be due to high energy electrons above 1 GeV [25, Rao and Sinha 1998]. Electrons of lower energies are more scattered and the Cherenkov ring is washed out.

Another important fact of the Cherenkov radiation is the pulse shape. The Cherenkov pulse shape seen at a distance R from the core depends on the shower geometry and shower development, as well as on the variation of the refractive index with altitude. Simulation shows that at small core distances Cherenkov light produced low in the atmosphere reaches the ground first (see Fig.(1.13)). We can assume that light reaching ground at a given time t comes from a particular atmospheric height.

Lets now comment some differences between gamma initiated showers and hadron initiated shower. The interaction length for a primary proton in the atmosphere is about 80 gm cm^{-2} compared to about 38 gm cm^{-2} for γ rays, therefore proton showers will develop further into the atmosphere. By propa-

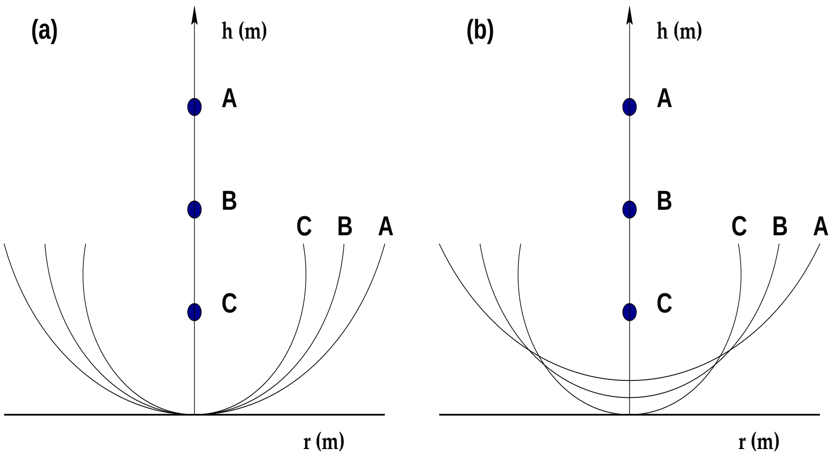

Figure 1.13: *Shapes of Cherenkov light fronts:(a) assuming no variation of atmospheric index of refraction; and (b) realistic case.*

gating much further into the atmosphere, the proton induced shower carries a Cherenkov component much closer to the ground level than γ induced showers, and this is reflected in a more intense pool of Cherenkov light close to the shower axis not presenting the ring shown in gamma initiated showers.

On the basis of the longitudinal development proton showers show much greater shower to shower fluctuations than gamma showers because a greater number of process can take place in the first ones, making the longitudinal development more chaotic and unpredictable. About the lateral distribution we could say that because of high transverse momentum flow to pions arising in the strong interactions, the hadronic shower will show a greater transverse development at all points of its longitudinal development than gamma showers as can be seen in (Fig.(1.8)). This will have further implication in the analysis of the images left on a detector by an extensive air showers as we will see further on.

One interesting feature of the Cherenkov pool left by gammas is the regularity of it in contrast to the hadron one that shows more irregularities. We can find the reason for this if we take a look at the longitudinal development of the hadronic initiated showers. As we saw earlier when a cosmic ray enters the atmosphere among other particles three types of pi-mesons can appeared. Only the neutral pion can decay to produce γ-ray pairs, thus sustaining electro-magnetic processes within the cascade. In first order we could say that 1/3 of the energy of the primary particle goes to the electro-magnetic component of the shower. So in principle for the same primary energy hadronic showers will show a Cherenkov pool on ground less intense. On the other hand, in hadronic showers there is other sources of Cherenkov emission other than electrons and positrons that contribute to the Cherenkov pool as can be the muons. This muons do penetrate to the ground over a wide area and an intense local peak of Cherenkov light is seen around each muon impact point. Comparing figures Fig.(1.14) and Fig.(1.15) it is clearly seen than the Cherenkov photon distribution on ground shows more irregularities for the proton initiated showers due to the different components of emission, being the pattern more chaotic. The rms in Cherenkov photon density (measured over a 10 m^2 area) is calculated to be 16 % for gamma showers, and 36 % for proton showers (at around 1 TeV), at 100 m from the axis. With greater particle transverse momentum spread and a more ragged penetration into the atmosphere, hadronic showers fail to exhibit any discernible focused ring.

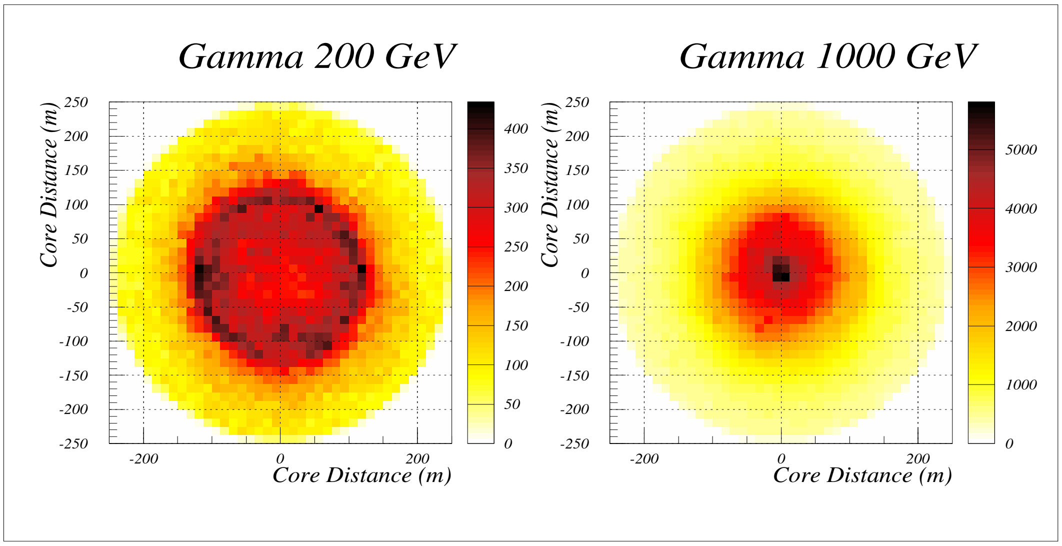

Figure 1.14: *Distribution of the impact point of the Cherenkov photons on ground for a γ-ray of energy 200 GeV at* 0^o *zenith angle.*

Just as a small overview, for the purpose of this work what matters is that gamma ray showers are more compact and this will be one of the basis of the shape and compactness of Cherenkov images recorded by suitable focusing instrument, and plays an important role for the separation process.

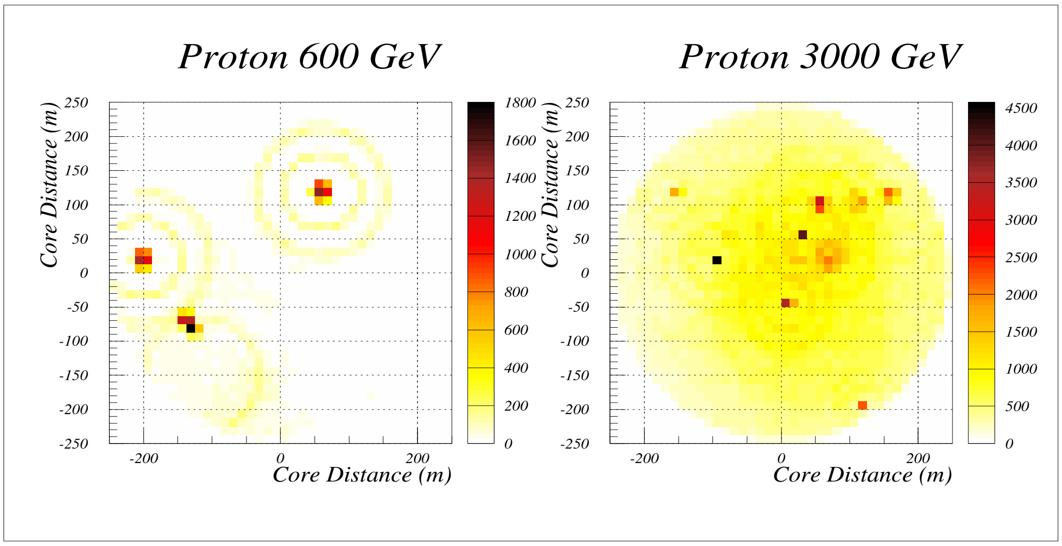

Figure 1.15: *Distribution of the impact point of the Cherenkov photons on ground for a proton shower of energy 500 GeV at* 0^o *zenith angle.*

Chapter 2

The Imaging Atmospheric Cherenkov Technique

2.1 Cherenkov Telescopes

The Cherenkov radiation generated in EAS is an important source of information that can be easily exploited with the appropriate experimental device. The first experiments developed for the detection of Cherenkov radiation were carried out in the early 50's by a group of the British Atomic Energy Research Establishment in Harwell. The idea was very simple, since each shower produces a vast spray of electrons over a very short time, then Cherenkov light might accompany each shower. This lead them to construct a very simple device, a garbage can with a 30 cm parabolic mirror inside and a photomultiplier tube placed on its focal plane. On the very first night this assembly provided rewards; large pulses were detected at a rate of about one every two minutes. Here was a promising ground-based technique for searching for point gamma-rays sources. Around thirty years ago, in 1968, the first Cherenkov telescope of around 10 meters of diameter was built, and since then, the Cherenkov technique has being improving steadily.

The Imaging Atmospheric Cherenkov Technique (IACT) as its name states, consist on the obtaining of an image of the atmospheric shower by collecting the Cherenkov photons spread on ground. We understand by image of a shower a geometrical projection of the shower into a detector. The basic idea of the technique is the collection of the Cherenkov photons and the subsequent analysis of the images with the final aim of detecting point gamma-ray sources. For such a purpose a Cherenkov telescope is used.

A Cherenkov telescope is a very simple instrument consisting of a parabolic reflector and a camera placed on the focal plane of the parabolic reflector. Usually the reflector surface is a tessellated mirror made out of smaller mirrors. The gross mirror profile follows a parabola for minimal time spread while individual mirrors elements are spherical with a radius that gives the best image quality. The mirror is supported by a frame structure placed either on an azimuthal mount or an equatorial mount. The mount has to be able to make a precise highly drive for tracking sources through their diurnal motion. It has to be kept in mind that a Cherenkov telescopes differs from an optical telescope in the large field of view required and in the extremely fast detector optics which rule out present CCD detectors and ungated image intensifiers. Usually the reflector of an imaging telescope must provide an optical resolution of better than 0.1^o - 0.2^o, that is the characteristic difference in size between the images of gammas and hadrons, within a field of view of 2^o - 3^o in diameter.

The camera is the most important element of the telescope and is decisive for the improvement of a good γ sensitivity. Usually, the camera is made out of photomultipliers tubes and is accompanied by fast signal processing electronics. Through the years cameras have develop from a single photomultiplier, usually called pixels, to a few hundreds. The number of pixels in a camera and in particular the angular size of each pixel is very important because it determines the minimum angular resolution that the telescope can achieve. In the table bellow some characteristic parameters of some Cherenkov telescopes existing at the moment are summarized.

Telescope	**Whipple**	**CAT**	**HEGRA**	**CANGAROO**
Mirror diameter (m)	10	5	5	3.8
Mirror area (m^2)	74	18	8.4	11.3
Number of pixels	151	546+54	271	256
Pixel deg	0.25	0.12	0.25	0.18

In the following pictures a Cherenkov telescope is shown together with a camera.

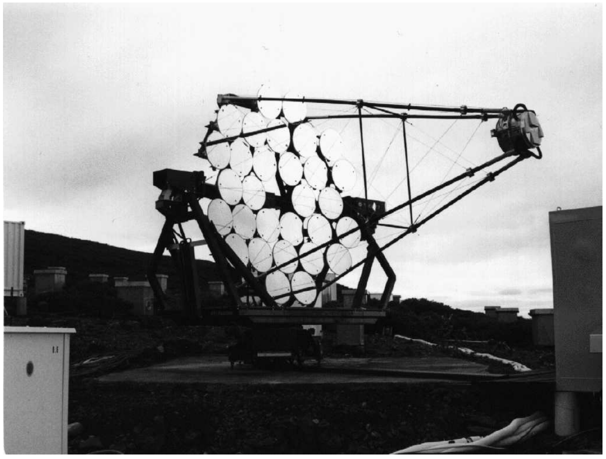

Cherenkov Telescope.

Camera of a CT.

The Cherenkov pool of a typical EAS of around 1 TeV of energy covers an extensive area up to the hump and around the core approximately equal to 100.000 m^2. A detector, such as a Cherenkov telescope, has to be placed on the Cherenkov pool in order to collect as much of this light as possible.

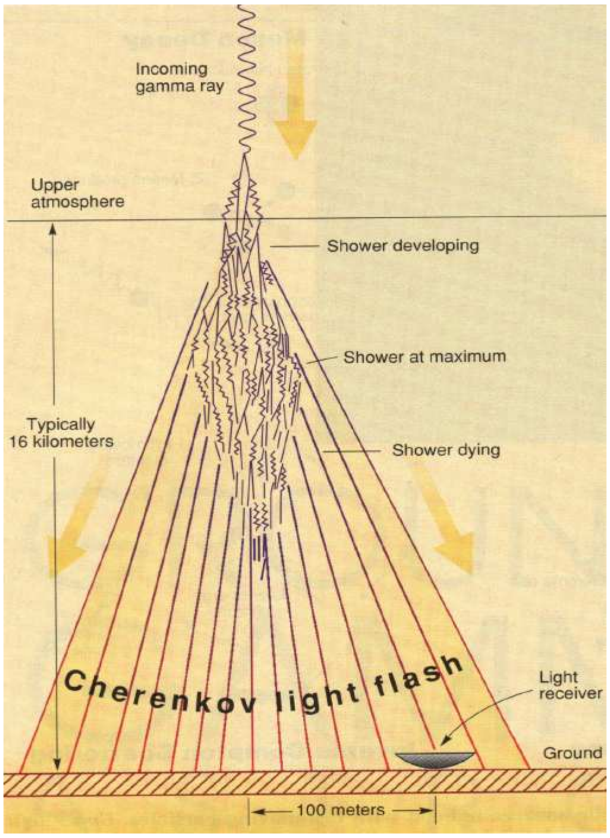

Figure 2.1: *Diagram of an Extensive Air Shower.*

After collecting Cherenkov light, a Cherenkov Telescope (CT) uses a coordinate-sensitive light detector in its focal plane to provide images of showers in Cherenkov light. We will see later on how this images are formed on the camera and how the differences in the shape and orientation of this spots will provide a method for determining the nature of the image, whether was originated by a gamma or hadron event, thus providing a method for discriminating hadron events. But first lets take a quick look at the factors that determine the amount of light that we can obtain from a shower. One obvious factor that limits the amount of Cherenkov light produced in an EAS is the energy of the primary particle. The very low energy primaries produce less Cherenkov light than more energetic primary particle. This is mainly due to the smaller number of secondaries produced in the former case, but also, as we have seen in Chapter 1, the dependence of the Cherenkov threshold with the variable refractive index of the atmosphere plays an important role. At higher altitudes this threshold is higher and less particles are above the emission energy threshold so the amount of light emitted is low. Starting from the amount of light produced depending on the energy of the primary particle we have other factors that limit the amount of light collected from an EAS, listed below.

- We have the atmospheric absorption that is not going to be discussed in detail and further references can be found in [8, P. Sokolsky 1988], just as an estimation we can say that around 85 % of the light emitted in an EAS is absorbed ([19, A. Konopelko 1998]).

- The next factor that determines the total amount of light collected is the mirror reflectivity. The reflectivity depends on the material the mirrors are made and on the wavelength of the radiation. For aluminum mirrors and from 300nm on, this reflectivity is around 90 %.

- Then we go on to the camera. Here several factors afects the photon collection, but the fundamental one is the *Quantum Efficiency*, QE, of the photomultipliers. This is the efficiency in which photons are converted into electrons in order to be sampled by the electronics. Normallly for good photomultipliers this QE is around 20%, depending on the wavelength.

So if we take into account all the efficiencies involved in the process of the Cherenkov light propagation which starts with emission of Cherenkov photons and ends with the digitization of the PMT signal, the total amount of light converted into signal is around **10%** of the total light emited in an EAS.

There is another important, and not so evident, effect that limits the amount of light collected by a telescope and that is, the field of view of the detector. Ususally an angular aperture stop is used to limit the field of view on the detector. For example lets suposse an angular aperture of 0.5^o. From geometry, if a shower falls 100m away from the telescope, only the part above an altitude of $100\text{m}/\sin(0.5^o) \sim 12$ Km, is seen. In the previous chapter we have see that this is above the emitting region (6-10 Km). Thus the limitation of the field of view will make the amount of light collected fall off more rapidily with core distance than previously and reduces the effect of the Cherenkov ring. Because imaging cameras possess a wide field of view ($\sim 3.5^o$ full field), showers whose core falls out to about 200 m away from the detectors's optic axis can be recorded.

Once we know the amount of light that we can collect from an EAS the next question that comes into mind is if there is a relation between this amount of light collected and the minimum energy of a shower that we can detect. In order to measure a shower of a given energy E_0 one has to measure enough signal from it. There is a certain amount of facts that limit the energy E_0 that a detector can reach. This energy is called *energy threshold* of a telescope bellow which the detector is unable to detect any shower. Lets take a look at the factors that define this energy threshold.

The main one is evident and arises from the fact that our detector has a limited size. A tipical Cherenkov telescope has a collection area of around 10 m^2, that means that only 0.001 % of the Cherenkov light reaching ground is collected (for a Cherenkov pool $\sim$ 100.000 m^2). We can take a look at the following formula that gives us an idea of the area needed to provide the necessary minimum signal for detecting a shower of energy E_0.

$$N(ph/m^2) \cdot A_{mirror} \cdot M_{ph.e./ph.} \geq minimum \quad signal \tag{2.1}$$

Where N(ph/m^2) is the average number of photons provided by a gamma shower of energy E_0 up to the impact parameter $\sim$ 125 m; A_{mirror} is the mirror area; $M_{ph.e./ph.}$ is the Cherenkov photon conversion factor that takes into account all the factors listed before and *minimum signal* is the minimum number of photoelectrons needed to reconstruct a reliable image. Both $M_{ph.e./ph.}$ and *minimum signal* are provided by the experience. For example for the HEGRA telescopes $M_{ph.e./ph.} \sim 12\%$ and *minimum signal* is between 60 - 100 ph.e. in order to have a good image to parameterize it reliably for a given pixel size of 0.25^o.

When dealing with this technique one has two fight against two difficulties. The first one is the light of the night sky (LONS) and the other one is the shower background produced by the cosmic ray from which gamma showers have to be picked out. The LONS is the integrated light arriving at the detector over the typical time measurement gate of the arrival of an EAS. The LONS has a very important role in IACT. For example in full moon nights measurements become unable. We will talk some more of this LONS in further Chapters. For now lets just say that the amplitude fluctuations of detected LONS determine the threshold of a detector. In terms of this fluctuations we can define in a more precise way the energy threshold, defining it as the shower energy which provides a minimum given signal/noise ratio during the given measuring time thus the energy threshold scales with the mirror surface area A_{mirror} as:

$$E_{thr} \sim \frac{1}{\sqrt{A_{mirror}}} \tag{2.2}$$

This is due to the fact that the signal is almost linearly to the mirror area, while the noise fluctuations are proportional only to the square root of it.

Once we have reconstructed and selected our gamma candidates images the final steep in the IAC technique is the analysis of them. This will be treated in detail in the next point of this chapter.

As an overview lets say that the Imaging Atmospheric Cherenkov Technique is used to differentiate between gamma and hadron initiated showers on the basis of shape and orientation of the images recorded using a very fast, multipixel photomultiplier detector on the focal plane of a Cherenkov Telescope.

2.2 Gamma/hadron separation technique

More than 99% of the air showers in the atmosphere are caused by the isotropic flux of hadronic cosmic rays, so the study of gamma-ray requires an efficient technique for recognizing and rejecting the hadronic showers, and accepting only pure electron-photon showers. All of this techniques receive the name of *γ-hadron separation*. Lots of strategies exist to achieve a good γ-hadron separation but all of them are based on geometrical consideration arising from the different ways the two kind of showers develop on their way down to the ground through the atmosphere. Before entering into the discussion on how images of the different showers can be exploited to achieve a γ-hadron separation method lets take a look at how are this images formed in the detector.

The gamma photons emitted by a gamma-ray source arrive to the earth atmosphere keeping the original direction of emission thus when pointing to an hypothetical gamma source with a Cherenkov telescope the shower axis of this gamma events are aligned with the optical axis of the telescope. In contrast, the hadronic component of the cosmic rays does not keep track of the original direction of emission due to the deflection it suffers by the magnetic fields it finds on the way through. So when they arrive to Earth they do it from all directions of the sky conforming an isotropic background of hadronic events. This will determine a difference in the orientation of the images left by a gamma shower and an hadronic shower on the detector as we will see right now.

Lets start with showers whose core land on the detector with axes parallel to the optic axis. This showers produce circularly symmetric images. As the point of impact of the shower on the ground is displaced away from the detector, images become progressively more elongated and comet shaped. The position of the maximum light intensity no longer corresponds to the core location. The true direction of the shower moves away from the point of maximum light intensity toward the head of the image, always lying on the major axis of the elliptical image. Figure (2.2) gives an intuitive view of how the elliptical image is formed when the trajectory of the incident γ-ray is parallel to the optic axis but with impact parameter some distance away from the detector. In section 2.3 we will see how the elliptical image can be characterize on the basis of shape and orientation parameters.

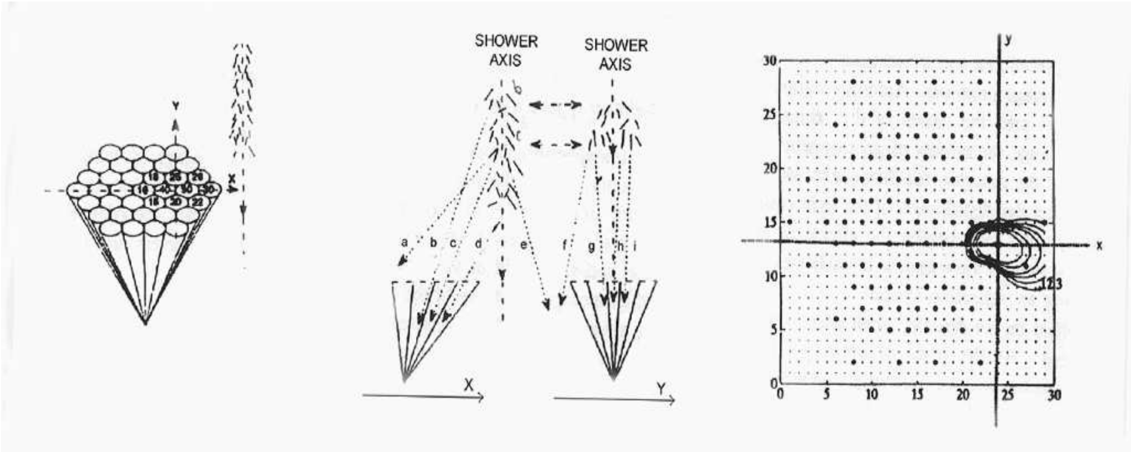

Figure 2.2: *Model of how Cherenkov photons from the development of a shower in the atmosphere might be mapped to a focal plane detector. Rays such as (a-e) map the longitudinal shower development which correspond to the length of the resulting image in the focal plane detector (length parameter). Conversely rays such as (f-i) map the transverse shower development which corresponds to width of the corresponding image in the focal plane (width parameter).*

On the figure it is considered that the Cherenkov angle is equal to zero, that is, the actual direction of the rays are determined mainly by the Coulomb scattering angles. The figure on the left represents a pixelated camera with an xy coordinate system over it. Pixels with signal are marked. The figure in the middle shows how photons from different heights reach the camera, both, along the x-axis and along the y-axis. Pixels such as those which intercept photon b are more likely to detect light generated high up in the cascade, while pixels on the edge of the detector have higher probability of detecting light from closer to ground level. Thus, the scale of the image along the major axis corresponds some how to the longitudinal development of the shower. In contrast the pixels aligned along the y-axis, intercept light from photons such as those labeled g, h and i. These pixels are inclined at approximately the same angle to the vertical and therefore look at roughly the same altitude, i.e. the part of the shower that is between rays b and c of figure 2.2. The figure on the right shows the coordinate plane xy with intensity outlines.

Just taking into account geometrical considerations lets find the basical ideas that leads to look for a γ-hadron separation method on the basis of the shape and orientation of shower images. Both, **shape** and **orientation** of Cherenkov images are exploited to suppress cosmic-ray background. Related to the shape, calculation showed that gamma-ray initiated showers start higher up in the atmosphere and spread out less than cosmic-ray initiated showers, as already mentioned in the first chapter of this work. Thus γ events are characterized by narrow and compact images in contrast with cosmic-ray generated hadronic showers with wider and more diffuse images. Respect to the orientation lets take a closer look at it.

If the axes of the shower are aligned parallel with the optic axis of the detector, as will always be true for γ-rays emanating from a point source located at the center of the telescope field of view, then the major axes of the images will be orientated so as to point radially at, or close to, the center of the detector. This is true even if the core distance from the telescope is greater then 100 m. While such images will be quite elliptical in shape, nevertheless they will exhibit strong orientation of the major axis, towards the center of the field of view of the camera. In contrast, hadronic showers can arrive isotropically distributed within the field of view and with random shower axis orientation relative to the optic axis of the reflector. The major axes of hadronic images left in the detector will therefore show no preferential radial pointing characteristic but rather will be distributed isotropically. Furthermore, since the hadronic showers images are, on average, considerably broader and longer than their γ-ray counterparts, then the γ-hadron separation becomes feasible on the basis of both shower shape and shower orientation. Preferential selection of γ-rays might be possible on the basis of such differences.

Other minor factors, other than the nature of the primary particle, which determine the appearance of the images are:

- the cascade fluctuations.
- the effects of geomagnetic deflection.
- the angle between shower axis and optic axis of the detector.
- the distance to the point of impact of the shower core from the detector.
- the angular distribution of the light emitted by the shower itself.
- the Cherenkov angle and its variation with height.
- the effects of multiple Coulomb scattering.
- the finite size of the detector field of view.

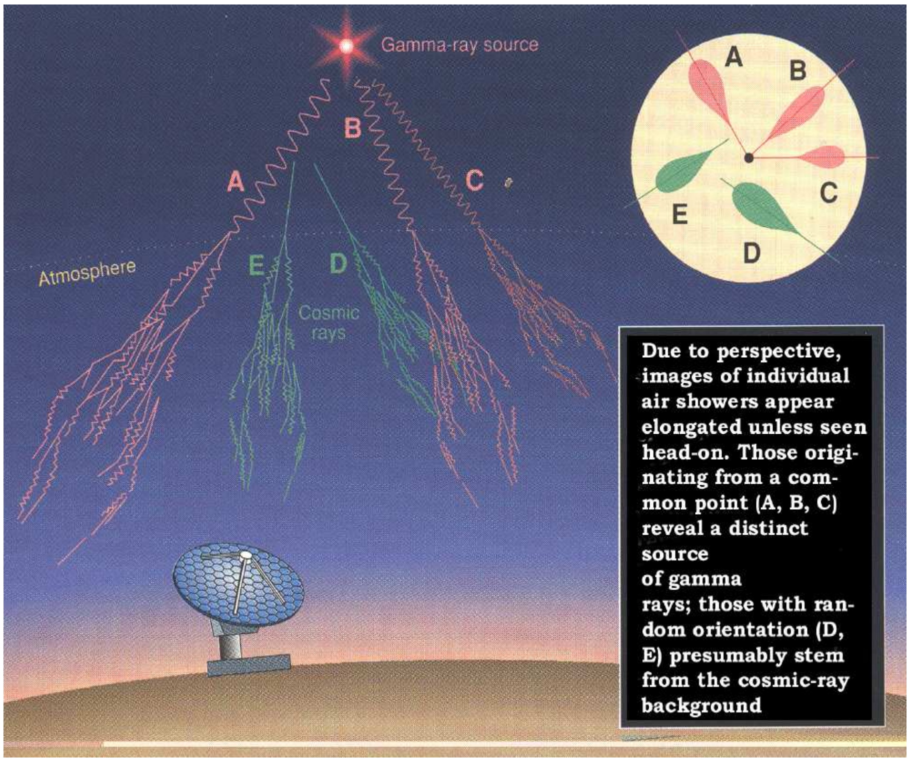

Figure 2.3: *Diagram of the formation of images depending on the nature of the primary particle initiating the shower.*

The different studies and parameterization of images recorded using IACT detectors is the reason for the existence of a big number of γ-hadron discrimination strategies, but before commenting some of this strategies based on the image parameters we are going to define them.

2.3 Image Parameters

The process of γ-hadron separation begins with some form of parameterization of shower images based on either a second moments approach ([23, A. M. Hillas 1985]) or else on some form of semi-analytical fitting of shower images. Given the essentially elliptical nature of the shower images it was natural that the parameterization of images was originally performed in terms of a moment analysis of the recorded pixel signal amplitudes. Moments are based on the ADC counts in each pixel, together with the particular pixel coordinate, thus image parameters are reconstructed from the pixel information. With finer pixels the shower images will contain more information which could be used for further improvements in

γ-hadron separation.

The ellipse parameters can be classified as *shape parameters* which characterize the size of the image and *orientation parameters*. In figure (2.4) an ellipse is drawn to represent a shower image. From this single figure we could take out the shape parameters:

- Size:The total integrated light content of the shower. Sometimes another parameter similar to size is used, and that is **Conc**, that represents the degree of light concentration as determined from the ratio of the two largest pixel signals to the sum of all signals.
- Length: The rms spread of light along the major axis of the image. Carries information of the longitudinal development of the shower.
- Width: The rms spread of light along the minor axis of the image. Carries with it information of the lateral development of the shower.

If we place an image like this onto a camera some more quantities are needed to describe an image. These quantities are the orientation parameters:

- Distance: The distance from the centroid of the image to the center of the field of view of the camera. Gives information of the impact parameter of the shower with respect to the CT. From another point of view if we take a line to join the shower maximum and the telescope is the angle between that line and the shower axis.
- Miss: The perpendicular distance between the major axis of the image and the center of the field of view of the camera. Its a measure of the shower orientation.
- Azwidth: The rms spread light perpendicular to the line connecting the centroid of the image to the center of the field of view. In other word is the projection of width along a line which is perpendicular to a line joining the center of the camera and the center of the image and which contains the centroid. This is a measure of both the shape and orientation of the image.
- Alpha: Is the angle between the major axis of the image and the radius drawn from the center of the camera to the center of the image. It is some how related to the angle between the shower axis and the axis of the telescope.

Other parameters have been proposed from time to time for the analysis of the images but the ones listed above have prove to be more efficient.

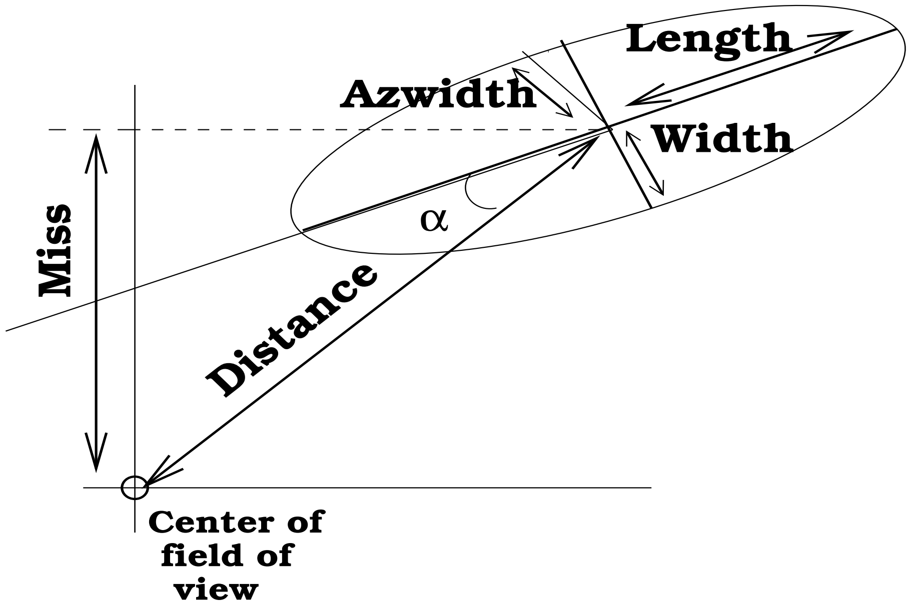

Figure 2.4: *Image parameters.*

2.3.1 Image moment estimation

We are going to take a look at the mathematical procedure to obtain the parameters above mentioned. On the basis of moment we can estimate the value of the image parameters and define the order moments in the following way. The *zero-order* moment is the sum of all the ADC signals in all the pixels which are non-zero after the cleaning of the image. The *first-order* moments describe the position of the image in the focal plane of the camera and the *second-order* moments describe the extent of the image. In general only first and second order moments are used on the parameterization of the images.

To obtain the parameters we need to calculate the first and second order moments. The moments are defined as:

$$\langle x\rangle = \frac{\sum n_i * x_i}{\sum n_i} \qquad \langle y\rangle = \frac{\sum n_i * y_i}{\sum n_i} \tag{2.3}$$

$$\langle x^2\rangle = \frac{\sum n_i * x_i^2}{\sum n_i} \qquad \langle y^2\rangle = \frac{\sum n_i * y_i^2}{\sum n_i} \tag{2.4}$$

$$\langle xy\rangle = \frac{\sum n_i * x_i * y_i}{\sum n_i} \tag{2.5}$$

$$\langle x^2 y\rangle = \frac{\sum n_i * x_i^2 * y_i}{\sum n_i} \qquad \langle xy^2\rangle = \frac{\sum n_i * x_i * y_i^2}{\sum n_i} \tag{2.6}$$

$$\tag{2.7}$$

Spreads of the images in different directions are then defined in terms of the moments as follows:

$$\sigma_{x^2} = \langle x^2\rangle - \langle x\rangle^2 \tag{2.8}$$

$$\sigma_{y^2} = \langle y^2\rangle - \langle y\rangle^2 \tag{2.9}$$

$$\sigma_{xy} = \langle xy\rangle - \langle x\rangle\langle y\rangle \tag{2.10}$$

The various image parameters can be calculated form the previously defined moments and the image spreads as follows:

$$length = \sqrt{\frac{\sigma_{x^2} + \sigma_{y^2} + s}{2}} \tag{2.11}$$

$$width = \sqrt{\frac{\sigma_{x^2} + \sigma_{y^2} - s}{2}} \tag{2.12}$$

$$distance = \sqrt{\langle x\rangle^2 \langle y\rangle^2} \tag{2.13}$$

$$alpha = \arcsin \frac{miss}{distance} \tag{2.14}$$

$$miss = \sqrt{\frac{1}{3} * (u\langle x\rangle^2 + v\langle y\rangle^2) - (\frac{2\sigma_{xy}\langle x\rangle\langle y\rangle}{s})} \tag{2.15}$$

$$azwidth = \sqrt{\frac{\langle x\rangle^2\langle y^2\rangle - 2\langle x\rangle\langle y\rangle\langle xy\rangle + \langle x^2\rangle\langle y\rangle}{distance^2}} \tag{2.16}$$

where:

$$s = \sqrt{d^2 + 4(\sigma_{xy})^2} \tag{2.17}$$

$$d = \sigma_{y^2} - \sigma_{x^2} \tag{2.18}$$

$$u = 1 + \frac{d}{s} \qquad v = 2 - u \tag{2.19}$$

For the real estimation of the ellipse parameters what we have are not discrete points representing each one of them a single photon, but much larger extension, the pixels. In one pixel we could have more than one photon, so the pixel weight would be this number of photons. Then, what we actually have is a pixelated image with different pixel weight depending on the photons each pixel has. Thus in order to achieve a good estimation of the parameters it is necessary that the size of the pixels are at least half the value we want to measure. For example, to measure the width parameter, that is of the order of 0.2^o, the appropriate pixel size should be 0.1^o. As we can see the pixel size is very important because not choosing an appropriate size could represent a cut off in our images that could affect further calculations.

Once we have the image parameterized we could use them to elaborate a γ-hadron separation method as we are going to see in the following point.

2.4 Image parameters in the context of the γ-hadron separation method

Successful strategies aimed at γ-hadron separation have been developed on sets of parameterized Monte Carlo simulations to optimize strategies aspiring to the efficient rejection of hadronic background. Simulations tend to make the most reliable model and how the resulting parameterized simulated images might appear, following detection by particular model reflectors. Strong discrimination of background seem possible on the basis of the parameters length, width, alpha, azwidth and miss although the most useful of the latter pair of parameters attributes may already be contained within the width and alpha parameters.

In the following figure we can see a set of parameters for a typical hadron and gamma initiated shower.

Lets briefly comment what this plots represent for the γ-hadron separation technique and the different appearance of this plots for gammas and for hadron events:

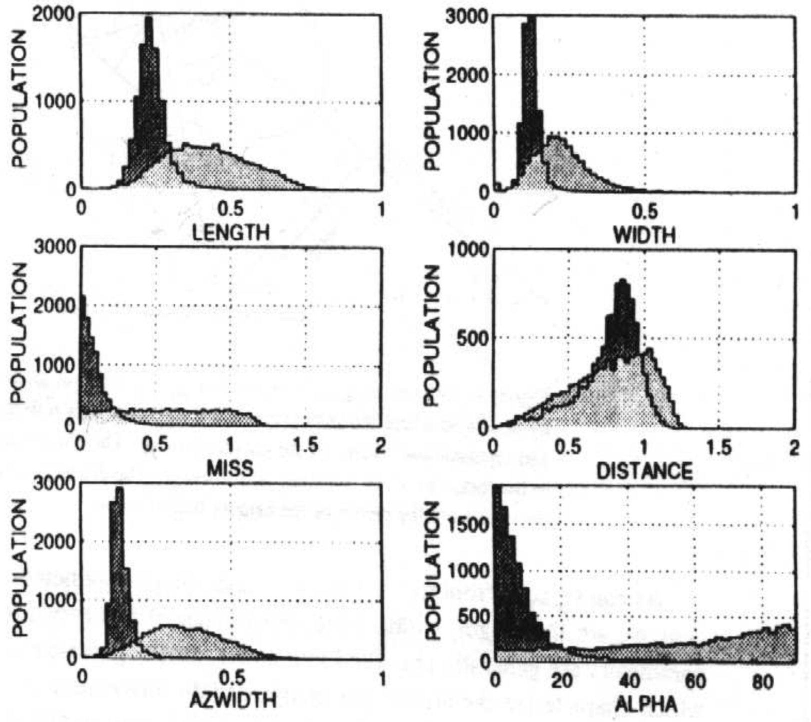

Figure 2.5: *Image parameters for gamma events and hadron events.*

- **Length**: While in electro-magnetics showers the maximum shower development is well localized for the hadrons showers it is not true due to greater fluctuation existing in this showers. This turns into a higher length distribution for the last ones, as we can see in the plot.

- **Width**: As already mention electro-magnetic showers are more compact than the hadronic ones. This turns also in more compact images. As happens with the length parameter the distribution in width for hadron showers is much wider and can be use to distinguish between both types of showers.

- **Distance**: The distance parameter distributions indicate how the collection efficiency of an IACT system is. Images that comes from showers with big impact parameter are cut out in the camera because they lay too close of the edge. On the other hand showers with impact parameter too close to the detector produces circularly images, thus making the estimation of the orientation parameters of the image rather uncertain. So upper and lower cuts have to be use to discriminate this images with the implication of rejecting showers too close to the detector or showers far from the detector thus limiting the effective area of the telescope. We can clearly see how the gamma distribution has a peak value around one. Just by taking into account geometrical consideration we can see that showers falling with impact parameter of 120m (the hump) the maximum of the shower is produce at an angle of 1^o as subtended from the optical axis of the telescope to the maximum of the shower. Hadron showers do not present this characteristic because as we already saw they do not present the hump on their lateral distributions and thus the distribution does not peak at any distance.

- **Miss**: Because hadronic showers are distributed randomly in orientation over the camera the miss parameter is about flat for hadron events. For gamma events the distribution is much narrow because the orientation tends to be towards the center of the field of view (center of the camera).

- **Azwidth**: Because images for gamma events are orientated towards the center of the field of view the azwidth parameter is much about the same than the width parameter. For hadron events the distribution is a little bit wider as compared to the width parameter. The reason is that azwidth is the projection of width along a line which is perpendicular to a line joining the center of the camera and the center of the image containing the centroid an thus takes longer values.

- **Alpha**: This is the most important and significant parameter and is the pillar of a good γ-hadron separation technique. We already explained why the alpha parameter for gamma events should be expected to be distributed around zero degrees, while for hadron showers should present a flat distribution on the basis of their random orientation. The main reason to explain the broadened alpha distribution for gammas is the the pixel size that limits the resolution in which image parameters are estimated as explained before. For a good estimation of alpha it is important to limit the distance parameter in order to not have cut images or too circularly images.

- **Size**: Electro-magnetic showers are much compact and uniform than hadronic ones. Hadronic showers show more diffuse images. For the same energy electro-magnetic showers show more concentration than hadronic showers because in the last ones more energy dissipation processes take place, so there is not as many particles as in electro-magnetic showers to give rise to the Cherenkov radiation.

Historically, γ events were selected by applying a fixed set of cuts to the image parameters. This set of parameters condition applied to achieve a good γ-hadron separation strategy are simply called *image cuts*. In principle, each experimental detection system requires its own specific set of selection cuts. On the basis of the plots shown above it is clearly seen how this cuts can be defined to reject background with maximum efficiency, while at the same time retaining as much as genuine signal as possible. Normally cuts are defined as to maximize the relation accepted gamma - rejected background.

Recently, refined cut procedures were developed by various groups. The combination of several cuts in each parameter are called *Supercuts* strategy and was developed by the Whipple collaboration [26, P. T. Reynolds *et al* 1993]. The γ-hadron rejection achieved by Supercuts discriminates very efficiently against background on the basis of exploitation of angular resolution, image intensity (size) and intrinsic parameter differences based upon both image shape and orientation characteristics. For example, the set of Supercuts used by the HEGRA experiment are the following:

$$\begin{gathered}\mathrm{CONC} > 0.5\\ 0.6 < \mathrm{DIST} < 1.2\\ 0.18 < \mathrm{LENGTH} < 0.375\\ 0.06 < \mathrm{WIDTH} < 0.2\end{gathered}$$

There is further strategies like the *Extended Supercuts* strategy originally described in [27, Lewis *et al* 1993] and summarized in detail in [28, Mohanty *et al* 1997]. This method of γ-hadron combines the traditional supercuts but allowing for scaling of the specific parameter cuts with total light intensity (size) as sampled by the camera. The motivation of defining the Extended Supercuts is the access of γ-ray events which might otherwise have been rejected with the Supercuts on the basis of being either too long or too wide, thus producing a significantly larger sample of sources events for evaluation of the power-law exponent of the energy spectra associated with primary γ-rays from sources. The range of applicable Extended Supercuts is optimized using Monte Carlo simulations.

Just to mention them we have other strategies like the *Hypersphere* or *cluster* originally applied by [30, Hillas and West 1991], based on a multidimensional metric with a combination of more than three parameters; *Dynamical Supercuts* with the general ideas of taking image parameters which are most correlated with the primary energy, impact parameter and the zenith angle of the showers and optimize the cuts on the remaining parameters as functions of them.

Some other methods have been proposed not depending on the second moments approach to image parameterization but use χ^2 minimization and maximum likelihood techniques, in conjunction with Monte Carlo simulations, in order to optimize species separation ([29, S. Le Bohec and B. Degrange 1995]).

As a general consideration for all the strategies, the effectiveness of a γ-hadron separation method is characterize by what is called *Quality Factor*, Q. A higher

Q states for a better method than a low Q. This quality factor is defined as:

$$Q = \frac{\epsilon_\gamma}{\sqrt{\epsilon_h}} \tag{2.20}$$

where ϵ_γ is the efficiency in accepting γ events, that is:

$$\epsilon_\gamma = \frac{\gamma\ events\ accepted}{Total\ \gamma\ events} \tag{2.21}$$

and ϵ_h is the suppression factor of the hadronic background, that is:

$$\epsilon_h = \frac{hadron\ events\ accepted}{Total\ hadron\ events} \tag{2.22}$$

Since the IACT technique is dominated by background fluctuations, Q is the factor by which the strategy enhances the statical significance of the signal, that is, it is a measure of the signal to noise ratio. It should also be mention the difficulty in the comparison of the Q factors estimated by different experiments, due to uncertainties associated with cross calibrations and instrumental systematics.

To date, no strategy has surpassed the accomplishments of Supercuts in terms of Q factor.

Chapter 3

On the Use of Polarization in IACTs

3.1 Basic Physical Ideas

As already stated one important source of information in the study of EAS comes from the Cherenkov radiation emitted by the charged cascade particles on their way to the ground. One feature of this radiation it is its intrinsic polarization which, as we will see, has a characteristic pattern on ground that could be exploited for the IACT. In this chapter we are going to see first how this particular distribution is set on ground and how it is expected to be on the basis of geometrical considerations. Secondly we will study the differences in such a distribution for gamma initiated showers and hadron initiated showers. Once we know the features of the polarization vectors distribution on ground we will discuss how can we take advantage of it using a Cherenkov Telescope and afterwards how the polarization vector distribution on ground is carried onto the camera. Finally we will make a study of the shower images on the basis of the polarization vector distribution for gamma and hadron initiated shower with the implication of this distribution for the IAC technique, concretely for the image parameters.

So lets start with some basic physical ideas. We saw that an EAS is initiated by a cosmic-ray particle when it plunges into the atmosphere. The processes that take place when this happens have already been explained in detail. Now the only thing that we want to point out for our study is the approach to the problem of the propagation of the relativistic charged particles through the atmosphere in a geometrical way. In section 1.1 we saw that the Cherenkov radiation emitted by a charged particle is distributed along a cone whose apex moves with the particle. The angle at which Cherenkov radiation is emitted in air is of the order of one degree. The Cherenkov radiation shows an intrinsic polarization such that the electric vector is contained in the plane defined by the electron and photon paths (figure (1.3)) and is everywhere perpendicular to the Cherenkov cone. This means that the polarization vectors point to the axis of the cone.

Moving to ground, we can approach the problem of polarization vector distribution from two different points of view.

- **Ideal case**. Two approximations are made in the ideal case. The first approximation is to consider all the particles to be moving along the shower axis, thus we consider that the shower does not spread due to dispersive effects; all the particles move parallel and along the shower axis. The second approximation is to consider the shower axis to be perpendicular to the plane defined by the detector, that is, the shower axis is parallel to the optical axis of the detector. In this ideal case each particle will emit a Cherenkov cone and, as a result of it, will leave a ring on ground. Taking into account all the emitting particles we will have on ground concentric rings of Cherenkov radiation centered on the core. The polarization vectors will be on ground over those rings perpendicular to them and, on the basis of the ideal case, pointing to the center of the ring, that would be, pointing to the core. We will say for this particular situation that we are in the *total polarization* approximation. This approximation is represented in figure(3.1).

- **Real case**. The situation described above does not fit to the real situation in EAS. If we want to describe the problem in a more realistic way we have to take into account some particular effects. This are, in order from less to more important:

  - *Pair production and Bremsstrahlung.* This two effects have already been described. Both will make the particles to get away from the ideal case.
  - *Coulomb scattering.* The charged particle suffers elastic collisions in the field of an atmospheric nuclei.
  - *High transverse momentum in hadronic interactions.* This is the dominant effect in hadronic initiated showers.

  All this effects gives rise to small deviations from the ideal case, that turns into deviations in the direction of propagation of the particles on their way

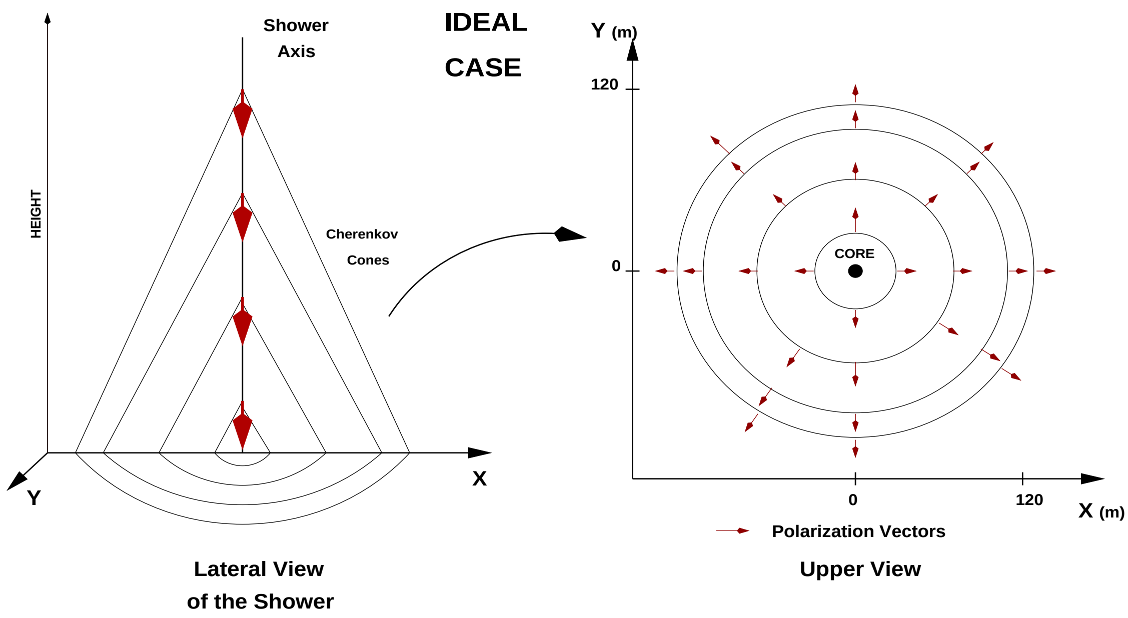

Figure 3.1: *Ideal case.*

through the ground with respect to the shower axis. In this case we wont have concentric rings on ground, this time for most of the particles we will have ellipses, and rings for those particles propagating parallel to the shower axis. The polarization vector distribution over the ellipses is such that the polarization vectors are over it orientated towards the crosspoint of the mayor and minor axes. This approximation is represented in figure(3.2).

We can translate all this into an EAS to clearly define in which situations we can say that we are close to the ideal case and in which situations we are far form the ideal case, so lets look at the following considerations. Suppose an EAS at zero degrees zenith angle. When we move away from the shower impact point we see the shower with less transverse angular spread. As we move away from the core the shower begins to seem more narrow. So from this particular point of view as we move away from the core we get closer to the ideal case. All the particles seem to be moving along the shower axis. As the polarization vectors refers we get closer to the total polarization approximation, vectors pointing to the core location. If we get closer to the shower axis the shower seems to have more transverse angular spread, and we move away from the ideal case. The situation then is quiet different at closer distances from the shower core. What we have here are ellipses and the polarization vector distribution is more chaotic moving away from the total polarization approximation. On the other hand we

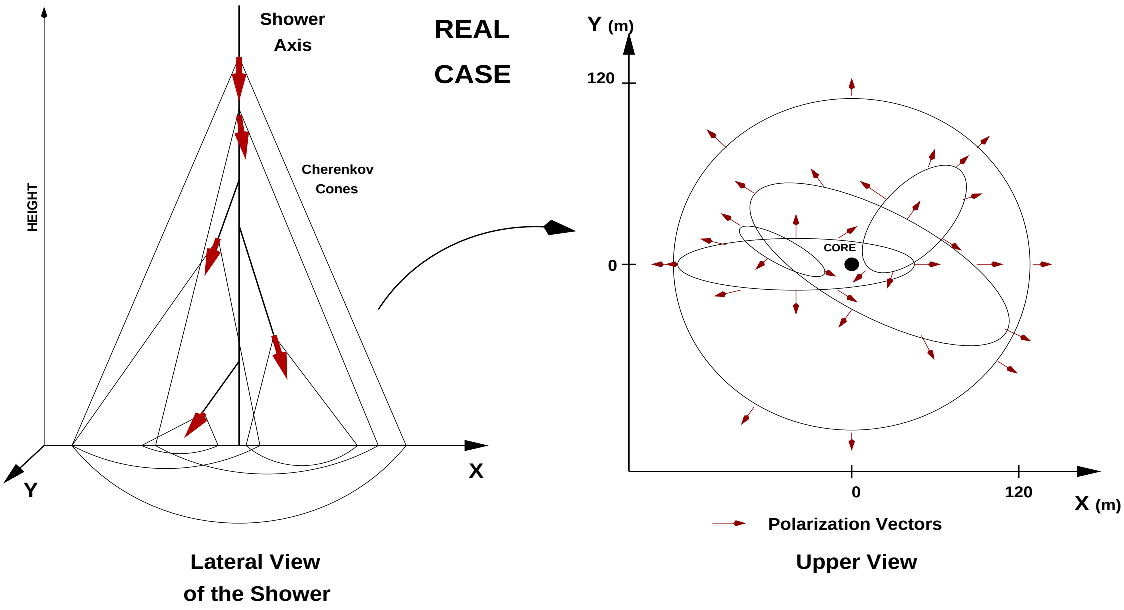

Figure 3.2: *Real case.*

can approach the problem from a different point of view. Light reaching ground at large distances from the shower core come from higher layers of the shower, so emitting particles had suffer less the dispersive effects and move along the shower axis, being again close to the ideal case. Particles reaching ground at closer distances from the core come from lower layers of the shower, so emitting particles had suffer more the dispersive effects moving away from the ideal case.

Summarizing, deviations from the ideal case will be more important at closer distances from the shower core having a more chaotic polarization vector distribution on ground. At large core distances we are closer to the ideal case and polarization vector distribution tends to the total polarization situation.

On the basis of the above considerations we can find a privilege direction over which a net polarization exists. First lets define the radial direction as the one joining the shower core with the impact point of the photons on ground and the transverse direction as the one perpendicular to it. If we plot the following relation:

$$\frac{transverse\ component\ of\ polarization\ vector}{radial\ component\ of\ polarization\ vector} \tag{3.1}$$

as a function of the core distance, we would expect the following result: at closer distances, because of more chaotic polarization vector distribution (real case), no component should dominate over the other, and as we move away towards larger core distances, the radial component should start to dominate over the transverse component (ideal case). If we plot the relation for a gamma event and for background events this is what we obtain:

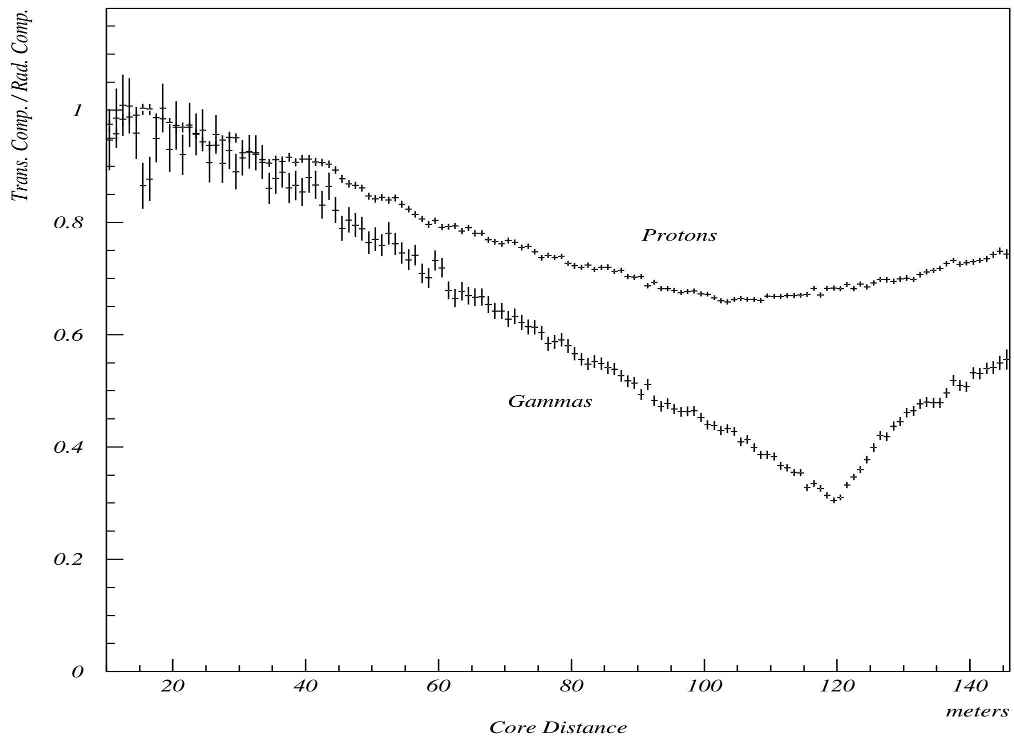

Figure 3.3: *Relation between the transverse and radial component of the polarization vector for different core distance, both for gamma events of 1 TeV with zenithal angle of 0 degrees and proton events of 3 TeV with a zenithal angle range between 0 and 3 degrees.*

This particular feature was first pointed out by Hillas, [6, A. M. Hillas 1996].

By taking a look at figure(3.3) a difference between the gamma and the hadron-background events is clearly seen. This difference is expected and can be explained taking into account the differences in the longitudinal development between hadron and gamma induced air showers. Due to the high transverse momentum existing in hadronic air showers, the EAS spreads more and we get away from the ideal case and, as we explained, this turns in differences in the polarization vector distribution on ground. In general, for an hadron event, the distribution is more chaotic everywhere and no component clearly dominate over the other. For the gamma event the situation is quite different. The EAS are more compact and the distribution on ground seems to have preference for the radial direction. For the gamma events we can clearly see a peak at a distance of about 120 meters from the center of the light pool. At this distance we are close to the ideal case thus polarization vectors point towards the core and the radial component dominates over the transverse component. The reason why the hadron events show a slightly peak around the hump is because hadrons with zero degrees of zenith angle have been simulated too. In contrast close to the core, for both kinds of events, because we get away from the ideal case, the polarization vector distribution seems more chaotic so no component dominates over the other.

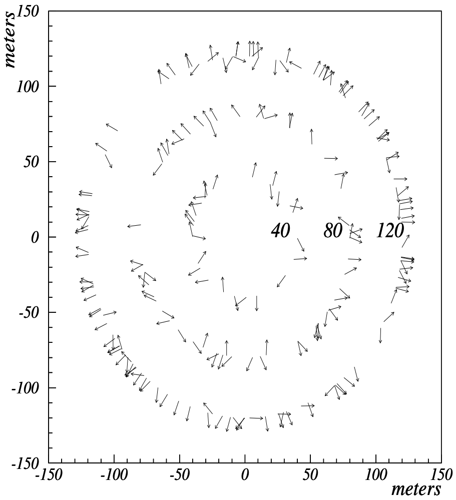

Monte Carlo simulation of the geometrical distribution of polarization vectors on ground for different core distances for a gamma event of 1 TeV at 0 degrees zenith angle.

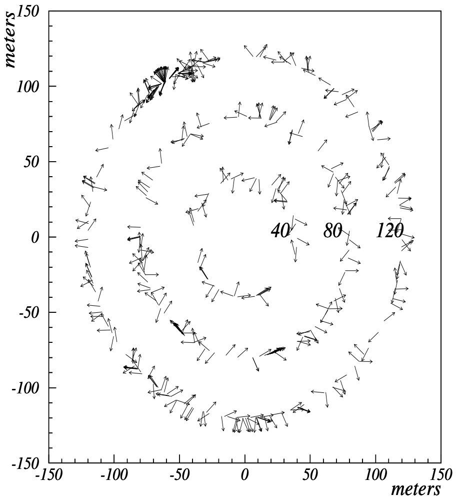

Monte Carlo simulation of the geometrical distribution of polarization vectors on ground for different core distances for an hadron event of 3 TeV at 0 degrees zenith angle.

Again, to summarize, what we see is that as we move away from the core the radial component of the polarization vector dominates over the transverse one. This feature has more relevance for the gamma events than for the hadron events and it is the main reason that leads to look for a method to reject background events on the basis of polarization vector distribution.

This particular ground distribution turns into a characteristic distribution of the shower image mapped on the focal plane of the detector but it is very important that the information contained on ground is carried onto the camera without changes, because if the information is lost then the method would be worthless. So lets see how is this information, contained on ground, carried onto the camera and why Cherenkov telescopes can take advantage of this information.

First lets see why with a Cherenkov telescope we can take advantage of the polarization vector distribution on ground. For such a purpose, first, suppose an array of detectors distributed on ground over a wide are of lets say 100.000 m^2. In order to measure the polarization vector distribution we need to place in each detector a polarizer orientated towards the core location, to measure the radial component, and another polarizer perpendicular to the first one to measure the transverse component. The problem is that the radial direction has to be known in advance, that is the core location, so actually no advantage can be take out with this particular setup from the polarization distribution on ground.

Nevertheless the situation is quite different for a Cherenkov telescope. With the appropriate setup of polarizers on the telescope camera we do not need to know the core location, and thus the radial direction, in advance. This particular setup will be discussed later on this work, lets just say for now that linear polarizers have to be placed on the camera with the transmission axis aligned with the radial direction of the camera.

Once that we know that the core location is not needed in advance and the problem is solved the other problem that we have to deal with, is the reflexion in the mirrors of the Cherenkov radiation and the possible rotation of the polarization vectors in this reflexion. To obtain information out of the polarization distribution on ground it is important the conservation of this distribution after the mirror reflection. If polarization vectors are rotated in the reflexion then the information contained in the polarization vector distribution on ground wont be carried onto the camera. So lets take a closer look at this problem.

Detailed description on how does light reflects on a metal medium such as the mirror of a telescope is not going to be given. Instead, we are going to give some definitions and on the basis of them we will see the approximations that can be done. For the study of light reaching a reflective surface a particular coordinate system is chosen in order to describe what happens to the polarization vector of such a radiation. Only the plane of the reflective surface and what it is called plane of incidence are needed. The plane of incidence is the one defined by the normal to the surface of incidence an the wave vector of the radiation reaching the surface. We can define too, the angle of incident as the one between the normal to the surface and the wave vector. On the basis of the incident plane we have a component of the polarization vector contained on this plane and the other component perpendicular to it. Both components have different phase and it is the difference in phase of both components what characterizes the polarization state of the wave. For example a difference in phase of 0 or π gives rise to linear polarization. When a reflexion takes place a change in the difference of phase is produced depending on the incident angle, so in principle a change in the state of polarization of the radiation takes place in a reflexion.

Lets particularice this for our case. We have Cherenkov polarized radiation coming from an EAS reaching the telescope and focusing onto a camera after the corresponding reflexion on the telescope mirrors. Two approximations are going to be made.

- If we consider light to be produced high up in the atmosphere, the relation between ground effective distance and vertical distance is rather small so in first order of approximation we can consider angles of incident close to zero. In this case the plane of incidence is not defined so in this approximation of normal incident the state of polarization is preserved after the reflexion and carried on to the camera.

- For a more realistic description of the polarization conservation after a reflexion in an optical system such as a Cherenkov telescope, we are going to consider the arguments given in reference [21, J. Sanchez Almeida and V. Martinez Pillet 1992]. Details of the basic principles and analytical description can be found in the reference. It is not the aim of this work to enter in the discussion of such a matter, rather than that we would only point out the following result. Taking into account that the mirror of the telescope has revolutionary symmetry, we can take a look at two cases: a point source on the axis and a point source off-axis. For a point source on-axis the conservation of the polarization vector orientation after the reflexion is better than 10^{-4}, and for a point source off-axis (few arc minutes) the deviation turns out to be negligible.

So as far as we can get the state and orientation of the polarization of Cherenkov radiation is conserved after the reflexion and no information of the polarization vector distribution on ground is lost due to the mirror reflexion. This is a very important result that indicates us that we can take advantage of the ground distribution of the polarization vectors for further applications. The results will be given in the corresponding chapter of this work.

Now that we have the polarization vectors on the focal plane of the detector we can move on to the description of how this vectors are set in the camera and how are they distributed along the shower images.

To explain how is the polarization vector distribution along a shower image lets make a simple model of an EAS and its image. This model is represented in Figure(3.4).

First we are going to see how the polarization vectors are set in each one of the regions represented over the image and then we will see how this distribution

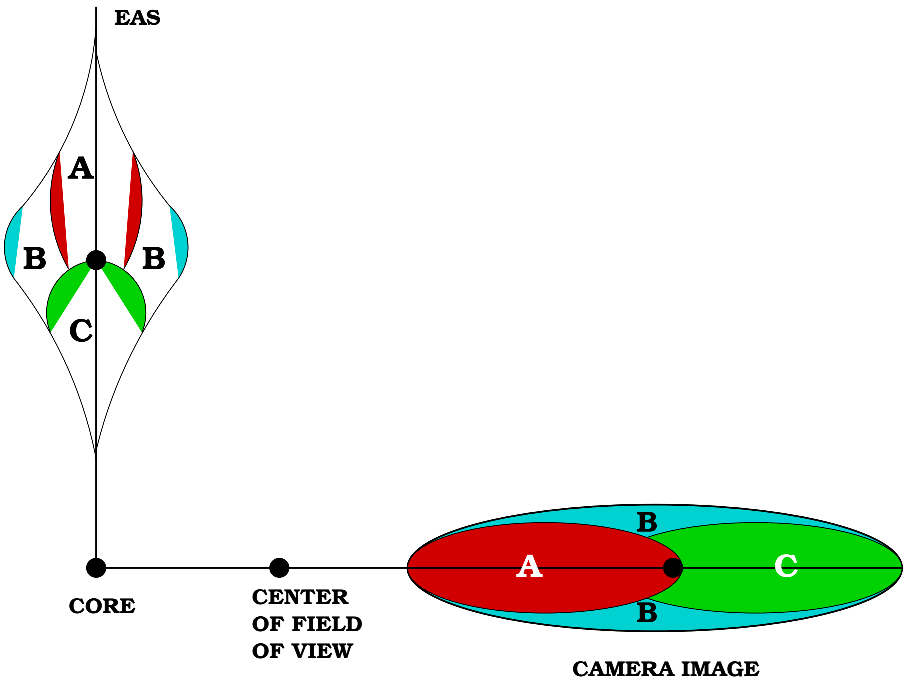

Figure 3.4: *Model of an EAS together with the shower image. In the model the shower is divided into four different regions attending the different source of the light. Over the image the corresponding regions of the shower are represented too.*

changes with the impact parameter of the shower with respect to the telescope. Finally we will make a comparison for both gammas and hadron images.

For this simple model we are going to consider that the telescope is pointing at a source so the corresponding shower image on the focal plane will have an elliptical shape with the mayor axis orientated towards the center of the camera. We are going to consider that the impact parameter of the shower with respect to the telescope is somewhere between 50m and 100m. We already know that the mayor axis give us information about the longitudinal development while the minor axis give us information about the transverse development. By taking a look at figure (3.4) we are going to identify each one of parts A, B and C of the shower with a region A, B and C over the image. We identify too, the shower axis with the major axis of the ellipse. Another important fact to keep in mind is that light generated high up in the cascade lays close to the center of the camera while light coming from lower parts of the cascade lays on the outer part of the image. With the consideration made, the polarization vector distribution over the image is as follows:

- **Major axis.** Moving along the major axis towards the edge of the camera we find light coming from different heights of the shower, but all the light coming from what we will call *shower slice* as seen from the telescope. This slice contains the shower axis and the telescope axis. Then, over the major axis we only see Cherenkov photons emitted along this slice. As the polarization vectors refers, it depends on the following: if the electrons that emit the light move along the slice too, the polarization vector would be contained in the slice and it would reach the camera over the major axis pointing towards the center of the camera. But if the emitting electron does not move along the slice but happens to cross it at the emission time and emits the photon along the slice, then the photon would reach the major axis but the polarization vector wont be orientated towards the center of the camera. The first situation dominates at higher parts of the shower when the shower is not dominated by dispersive effects, and the second situation dominates at lower parts of the shower. So along the major axis of the shower the polarization vectors are better orientated towards the center of the camera at closer distances from it and as we move along the major axis away from the center of the camera the polarization vectors tend to slightly orientate away from the major axis. This situation can change with the distance parameter as we will see later on.

- **Region A.** In this region we can consider light to be coming from higher parts of the shower and close to the shower axis. In this region, and on the basis of this, we are close to the ideal case and polarization vectors are more likely to be orientated away from the center of the camera.

- **Region B.** We consider those regions to be coming from the outer parts of the shower, so this light is far from the ideal case and polarization vector distribution seems more chaotic. As we move away from the major axis along the minor axis the vectors start to orientate towards the mayor axis.

- **Region C.** We consider this region made out of light coming from lower parts of the shower, far from the ideal case, so in this region C of the image, the polarization distribution is more aleatory.

How does this distribution changes with the impact parameter ?. We can give the same arguments as for the distribution on ground since after the reflexion the polarization vector distribution is conserved. For short distance parameter we only see the lower parts of the shower so we are far from the ideal case and the polarization vector distribution is more chaotic everywhere over it. In terms of the regions shown in Fig.(3.4), we could say that as we move towards shorter core distances region C starts to grow towards the center of the image covering it when the distance parameter is equal to zero. In this case region C will be a circle centered in the camera. As we move towards larger core distances we get closer to the ideal case. Region A is the one growing this time as we move away. As region A grows, region B gets more narrow. The image gets sharp and for high distance parameters region C tends to disappear too, under region A. About the distribution over the major axis we can say that as we move away from the core, the photons that reach the camera are more likely to be emitted by electrons moving along the slice, so the dominant distribution over the axis is, polarization vectors pointing towards the center of the camera.

Now we can take a look at the differences between gamma and hadron images on the basis of polarization vector distribution. Hadron images are more disperse and chaotic. On the basis of our model for hadron events the connection between regions on the shower and regions over the image is not so well establish. The elliptical shape is not so clear. We could say that region B dominates more over the others in hadron images than in gamma images, and region C would be more dispersive and wider. In general we can say that the polarization vector distribution over an hadron image is more or less chaotic everywhere with a small tendency to the radial direction in parts of the image close to the center of the camera and over the major axis of the image.

In the following figures some images are represented at different core distances for a gamma event of 1 TeV at zero degrees zenith angle, and some hadron events at 3 TeV at zero degrees zenith angle. The simulation procedure will be explained in the following chapter along with all the approximations and parameters used for the simulation. The image are not pixelizated, each photon impact point is drawn together with the polarization vector. The field of view of the camera is the typical field of view of a Cherenkov telescope, $4,75^o$.

To finish this chapter we are going to take a look at some implications of this particular polarization vector distribution over the images without entering into the discussion of results, that will be given in the last chapter. We will just mention what do we expect from the combination of such a distribution with the experimental setup proposed: radial polarizers on the camera.

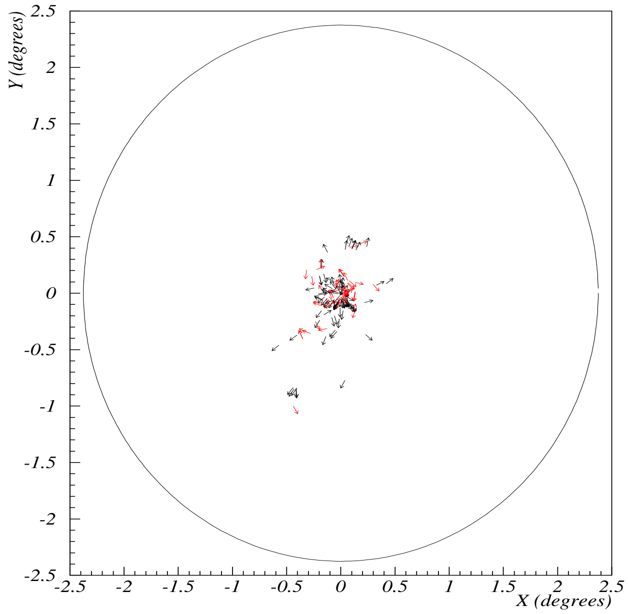

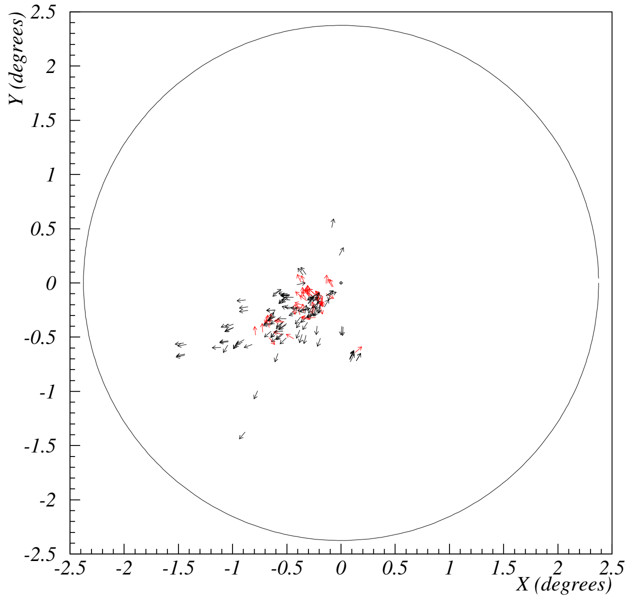

Figure 3.5: *Images of a 1 TeV gamma event at core distances of 0m and 40m respectively.*

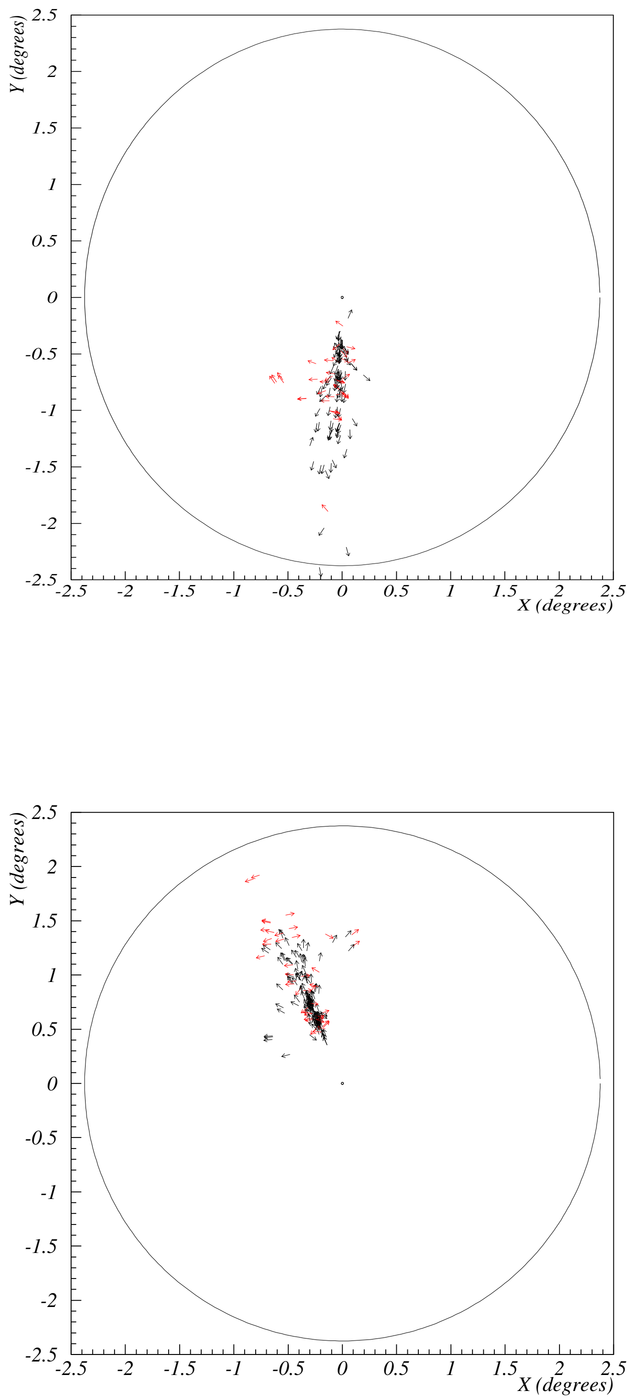

Figure 3.6: *Images of a 1 TeV gamma event at core distances of 80m and 120m respectively.*

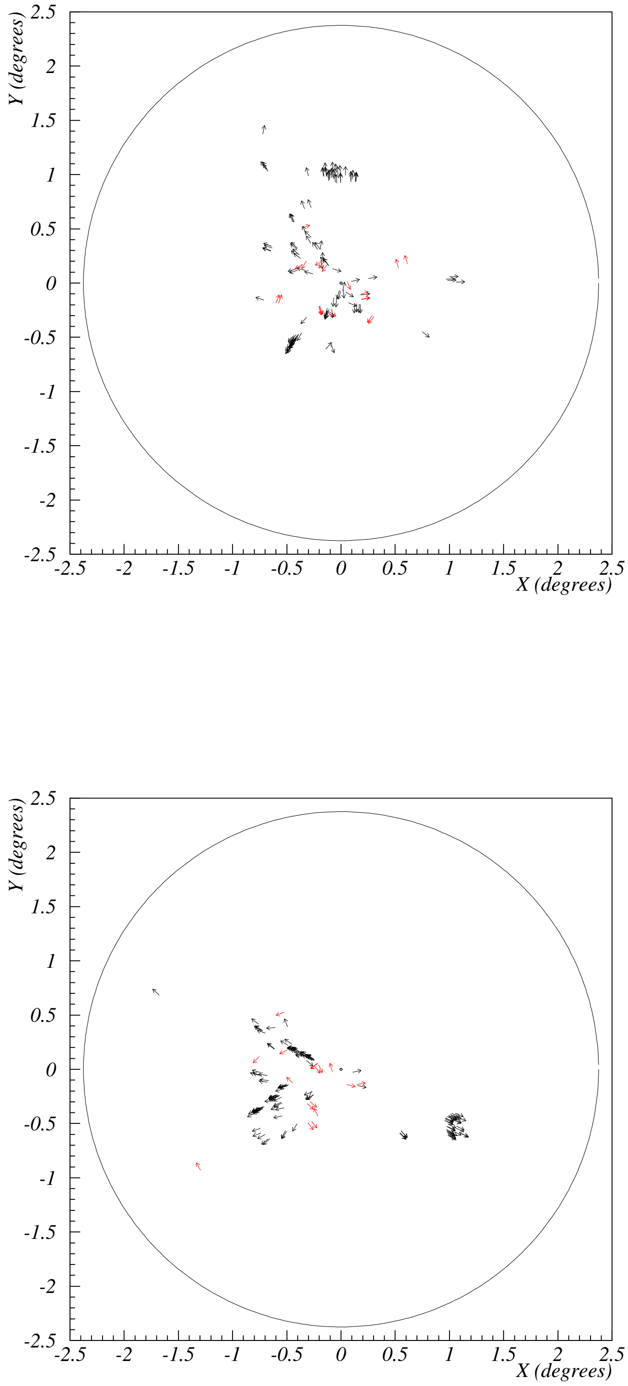

Figure 3.7: *Images of a 3 TeV hadron event at* 0° *zenith angle at core distances of 0m and 40m respectively.*

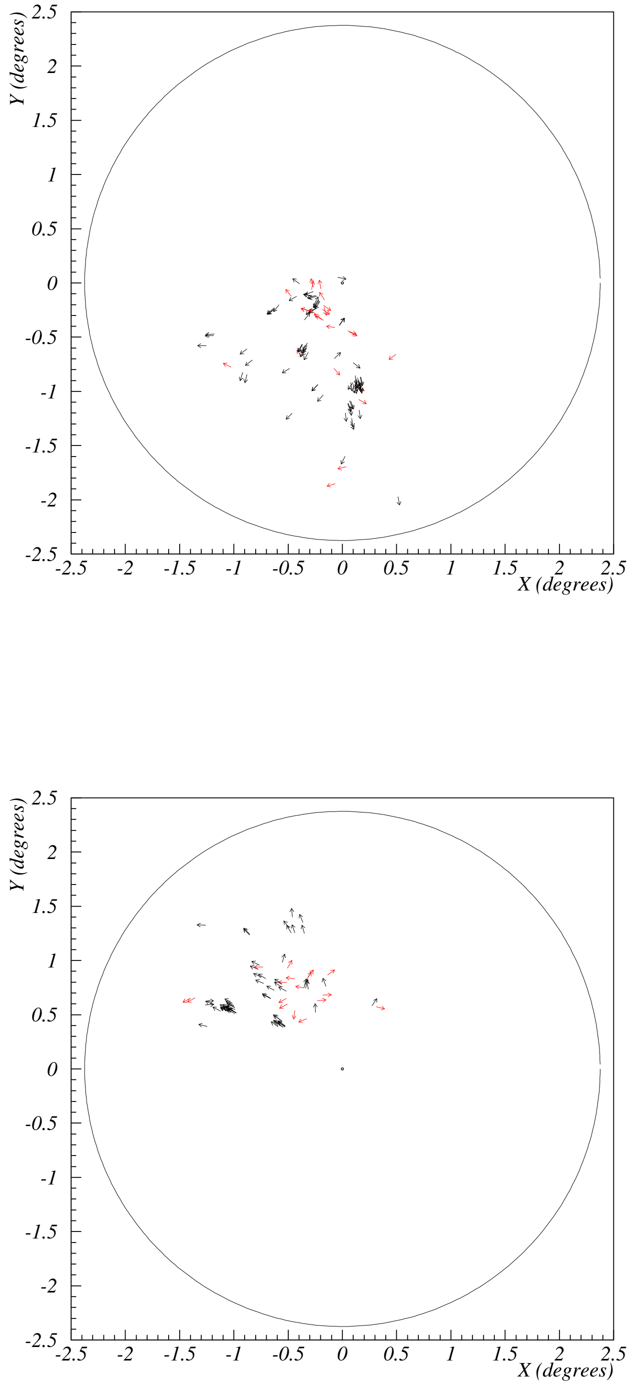

Figure 3.8: *Images of a 3 TeV hadron event at* 0^o *zenith angle at core distances of 80m and 120m respectively.*

3.2 Implications

We are going to summarize the points of our study in terms of what we expect. The detailed study and results of it, would be presented in the corresponding chapter. The points are:

- **NSB.** This is the first conclusion that can by point out *a priori* without further studies. The light of the night sky is a not polarizated light, what is called natural light. If a linear polarizer is placed on the way of such a radiation 50% of the light is cut out. The intensity is reduced by a factor of 2. We have pointed out that the LONS is the limiting factor for determining the energy threshold of a telescope. Because the $E_{threshold}$ scales with ϕ_{LONS} as the square root of it, then the $E_{threshold}$ of a telescope is reduce by a factor $\sqrt{2}$:

$$E_{new.thre} = \frac{E_{thre}}{\sqrt{2}} \tag{3.2}$$

  Of course the energy threshold depends on some other factors. For example we are cutting out light coming from the EAS too. This has to be study in detail in terms of detection rates. This rates would be obtained and presented in the results chapter for this new situation to see if the energy threshold actually changes or rather stays unaffected.

- **Length and Width parameters.** This is a quiet interesting study that could have implications for the γ-hadron separation strategies. Just to remember what we have just seen, lets make this small overview. In terms of regions A, B, C and major axis of the image, we have that the polarization vector distribution is more chaotic for regions C and B, and for region A the radial component dominates over the transverse component. Over the major axis the radial component dominates in regions close to the center of the camera and polarization vectors move away from the major axis as we move towards the edge of the camera. On the basis of this and using regions A, B and C, if we place radial polarizers on the camera we expect the following results: light intensity would be cut out more efficiently from regions B and C, so we expect images to be more compact and shorter. Light from the edges of the images (B and C) would be cut out. The image becomes more defined, what lead us to the following point. Just as an example we can take a look at the following camera image (figure(3.9)). The simulation procedure will be explained later on. Now we only want to point out the following: the image becomes more compact when the polarization assumption is made.

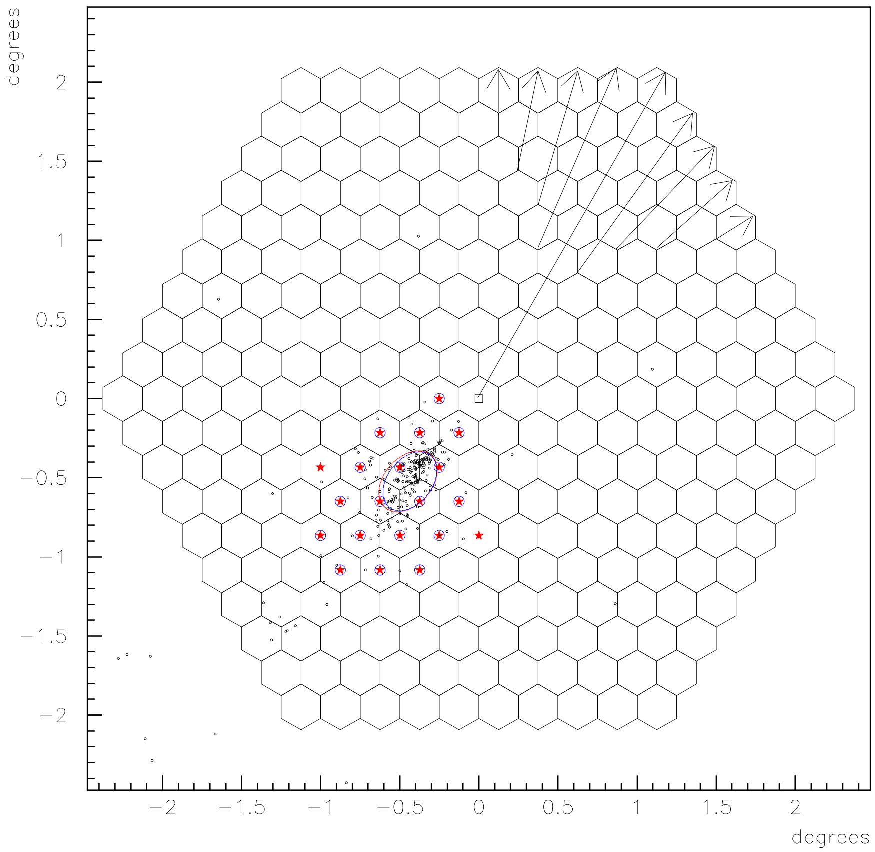

Figure 3.9: *Camera image. The dots are the photon impact points on the focal plane. The stars stand for the pixelized image after tail-cuts without polarization assumption. The circles stand for the pixelize image after tail-cuts taking into account the polarization effect. On the right upper corner there is a detail of how the polarizers should be display on the camera*

- **Alpha parameter.** If the image is better determined then the alpha parameter should be better established. The alpha parameter plays a decisive roll in any γ-hadron separation strategy, so any method to give a good estimation of it is always welcome. For our purpose the alpha parameter has to be compared with and without using radial polarizers to see if any change is noticed, and then the new alpha estimated parameter for gamma events has to be compared with the new alpha parameter for background events to see if any advantage can be taken out of it.

- **Quality factor.** Actually, to see if a γ-hadron separation strategy achieves good results, the quality factor is needed. This quality factor depends very strongly on the experiment parameters so quality factors are not easy to compare between different experiments. For example, in our study, as we pointed out in the previous points, the image parameters might change due to the application of our simulation method. That means that for determining the quality factor with good accuracy for our method we would need to define a new set of Supercuts. This is not going to be done in this work and is left for further studies. Instead the quality factor would be obtained using the same set of Supercuts with and without the polarization assumption.

- **Energy threshold.** For determining the energy threshold of a telescope the effective area is needed as a function of the energy. What is expected a priori is the following. Because of more chaotic polarization vector distribution on hadron images light intensity would be cut out more efficiently in hadron images than in gamma images. So the effective area for hadron events would be reduce, thus incrementing the energy threshold for them. But also light for gamma events is going to be cut out, but with less efficiency than for hadron images. So in principle the effective area is going to be reduce for gamma events too, but less than for hadron events. This fact together with the suppresion of 50% of night sky noise will lead us to study the modification of the enregy threshold of the telescope.

- **Time distribution.** Another interesting feature that we found out and that will be explained further on, is the time distribution of arrival of the light to the detector as a function of the polarization orientation. Results would be presented.

With this we finish this chapter and move on to the next one. Before result are presented, the operational setup together with the simulation procedure is going to be presented. The Monte Carlo data base will be given too.

Chapter 4

Operational Setup

4.1 Introduction

As we showed in the previous chapter the IACT is a common well established technique for the study of EAS which implies the use of a Cherenkov telescope. So it is not enough, when studying CR though EAS, a good understanding of the physical processes that takes place in an EAS, but also a good understanding of the detector with its limited acceptance and efficiency is needed.

We are going to divide this chapter in two main sections: the **EAS simulation** and the **detector simulation**. For each one of this sections we will make a brief discussion of the programs used and then we will present and discuss our approximations on the frame of this programs, explaining the physical basis for such approximations. Finally we will show the data base of our simulation used for this study.

4.2 Extensive Air Showers simulation

4.2.1 CORSIKA physics

The standard simulation program used for the simulation of EAS is the CORSIKA program. CORSIKA (COsmic Ray SImulations for KAskade) is a detailed Monte Carlo program to study the evolution of EAS in the atmosphere initiated by photons, protons, nuclei, or any other particle.

The CORSIKA code was originally developed to perform simulations for the KASKADE experiment at Karlsruhe and has been refined over the past years. The development of CORSIKA is guided by the idea to predict not only correct average values of observable with this EAS simulated code, but also to reproduce the correct fluctuations around the average value. In two words, the program simulates the transport of particles through the atmosphere as well as their interactions with air targets. All particles are tracked along their trajectories.

It is not the aim of this work to give a complete and detailed description of the physics used in CORSIKA ([14, D. Heck et al 1998]) but to mention the main physical considerations and how CORSIKA deals with them. We will remark the Cherenkov photon production because it is important for this work.

Analyzing experimental data of an EAS requires a detailed theoretical modeling, for comparison, of the cascade processes. This can only be achieved by detailed Monte Carlo calculations taking into account all knowledge of high energy strong and electromagnetic interactions. We have seen in Chapter 1 the main processes that take place in an EAS, so it is easy to see the difficulty in modeling such interactions for all the secondary particles generated in an EAS. Other than this technical problem we have the physical problem that is also rather complicated for two main reasons: there is a big amount of parameters to be taken into account and most crucial is that the knowledge of high energy interactions is still incomplete in important features. The following could be a small list of the main facts that have to be taken into account when simulating an EAS:

- Electromagnetic interactions.
- Hadronic interactions.
- Decay of instable particles, ionization energy loss and deflection by multiple scattering.

- Environmental parameters; mainly the atmosphere.

CORSIKA implements several routines to take into account each one of the above listed facts. Without entering in detail in everyone of the routines we would like to briefly comment some general aspects of them in order to know what are we working with.

1. *Decay of unstable particles, ionization energy loss and deflection by multiple scattering:* For propagating particles between two interactions points their space and time coordinates as well as their energy have to be updated. For electrons and photons this is done in EGS4. Charged particles lose energy by ionization whereas neutral particles proceed without energy loss. The coulomb scattering is also taken into account. Most of the particles produced in high energy interactions are unstable and may decay into other stable or unstable particles. Neutral pions and η mesons as well as all resonance states have such a short life time that interactions is negligible before the decay. Muons are prevented from penetrating the complete atmosphere by decay only. Neutrons are treated as stable particles due to their long life time. For all the other unstable particles there is a competition between interaction and decay processes and the decision is taken when calculating the actual mean free path.

    - **Decay of unstable particles**: The distance a particle travels before it undergoes its next interaction or decay is determined by the cross section for a hadronic reaction together with the atmospheric density distribution along the flight path, and the probability to decay. A decay length and an interaction length are determined independently at random and the shorter one is taken as the actual path length. By this procedure it is also decided whether a particle decay or interacts.

    - **Ionization energy loss**: The energy loss by ionization of a charged particle which traverse matter of thickness λ is described by the Bethe-Bloch stopping power formula. The ionization energy loss is computed along the particle trajectory.

    - **Coulomb multiple scattering**: Charged particles are scattered in the electric Coulomb field of a nuclei in the air. As these nuclei are generally more massive than the scattered particles, the direction of flight might be altered, but not the energy. In CORSIKA the process of Coulomb multiple scattering is considered only for muons and only once for each tracking step in the middle of the tracking distance.

2. *Hadronic interaction models:* For the hadronic interaction models a division is made depending on the energy:

- **High energy interactions:** For the hadronic interactions of nuclei and hadrons with the air nuclei at energies above $\sim$ **80 GeV** the following models are used. This models work for energies above 80 GeV because below this energies the generation of strange baryons takes place, and a model for low energy interactions is needed:

  VENUS(K.Werner, Phys. Rep. 232 (1993) 87): Is a program developed to simulate ultra relativistic heavy ion collisions. Especially it handles nucleus-nucleus with an up to date theoretical approach based on the well founded manner of the Gribov-Regge formalism. The maximum energy reachable by this model is $2{\cdot}10^7$ GeV.

  QGSJET(N.N.Kalmykov et al., Physics of atomic nuclei 58 (1995) 1728): This program was developed to describe high energy hadronic interactions using the quasi-eikonal Pomeron parameterization for the elastic hadron-nucleon scattering amplitude. The hadronization process is treated in the quark gluon string model. The energies reachable by this model are $> 10^{11}$ GeV.

  DMPJET(J.Ranf, Phys. Rev. D 51 (1995) 64): This program was developed to describe high energy hadronic interactions of hadron-nucleus and nucleus-nucleus collision using the two-component Dual Parton Model with soft chains and multiple minijets at each elementary interaction. The energies reachable by this model are $> 10^{11}$ GeV.

  SIBYLL(R.S. Fletcher et al., Phys. Rev. D 50 (1994) 5710 ; J.Engel et al., Phys. Rev. D 46 (1992) 5013.): This program was developed to simulate hadronic interactions based on the QCD minijet model. The energies reachable by this model are $> 10^{11}$ GeV.

  HDPM(J.N Capdevielle et al., J. Phys. G: Nucl. Part. Phys. 15 (1989) 909): Is a set of routines to simulate high energy hadronic interactions. These routines are fast and adjusted to experimental data where available. Proton-proton interactions simulated with HDPM and other models agree fairly well with each other. The energies reachable by this model are around 10^8 GeV.

- **Low energy interactions:** For the hadronic interactions of nuclei and hadrons with the air nuclei at energies below $\sim$ **80 GeV** the following model is used:

  GHEISHA(H.Fesefeldt Aachen PITHA 85/02 (1985)): is used to calculate the elastic and inelastic cross sections of hadrons below 80 GeV in air and their interaction and particle production.

3. *Electromagnetic interactions model*(W.R.Nelson et al. SLAC 265 (1985)): For these interactions the EGS4 model is used. The photoproduction of muon pairs and hadrons is incorporated into EGS4. This allows the calculation of the muon content of photon induced showers. An alternative way of treating the electromagnetic component is to use the improved form of the analytical NKG formula for each electron or photon produced in the hadronic cascade. It allows to study the longitudinal development of the electromagnetic cascade and the electron density at particular coordinates at the observation level.

4. *Atmosphere and Earth's magnetic field:* The atmosphere adopted in CORSIKA consist of N_2, O_2 and Ar with the volume fractions of 78.1%, 21.0% and 0.9%. The density variation of the atmosphere with altitude is modeled by 5 layers and a flat atmosphere is considered, understanding by flat atmosphere a series of parallel layers not taking into account the earth's shape. This is an important fact that has to be taken into account if one wants to generate showers at high zenith angle where this approximation is no longer valid.

   About the magnetic field lets only say that in CORSIKA is characterized by its strength B_E, its declination angle δ, and its inclination angle θ. For an specific location this values has to be given.

To finish this small overview of the CORSIKA code we just remark that the major systematic uncertainties in EAS analysis arise from the lack of knowledge of the total cross-section and the details of particle production for nuclear and hadronic reactions at high energies with small momentum transfer. The energetic particles arising from this high energy interactions are of highest importance in the development of EAS, as they are the most energetic secondary particles, which bring the largest energy fraction of each collision deep into the atmosphere. The experimental findings at protons colliders have to be extrapolated, using theoretical models, over many orders of magnitude to CR energies, small emission angles and nuclear projectiles and targets.

4.2.2 Cherenkov Radiation in CORSIKA.

There are some more options in the CORSIKA code that are not going to be discussed in this work. Nevertheless, there is one with important relevance for our work, the Cherenkov photon production in EAS. The Cherenkov light production by electrons, positrons, muons, and charged hadrons is considered in the routines CERENE and CERENH respectively. The Cherenkov photons are considered within a wavelength band and the atmospheric absorption of the Cherenkov photons is not taken into account. Because these are the routines that are going to be used for our purpose we will take a closer look at how CORSIKA treats in those routines the generation of such a radiation.

Based on a program extension made by HEGRA collaborators [?, S. Martinez 1995] the Cherenkov radiation simulation option is implemented in the CORSIKA code. We have seen in Chapter 1 how and under what conditions this radiation is produced. In the program the condition:

$$\frac{nv}{c} = n \cdot \beta > 1 \tag{4.1}$$

is examined for every transportation step of a charged particle. The refractive index n is approximated by the local density $\rho(h)$ (in g/cm^3):

$$n = 1 + 0.000283 \cdot (\frac{\rho(h)}{\rho(0)}) \tag{4.2}$$

neglecting the wavelength dependence of n.

The number N_c of photons which are emitted per path length s at an angle θ_c is calculated as:

$$\frac{dN_c}{ds} = 2\pi\alpha \int \frac{sin^2\theta_c}{\lambda^2} d\lambda \tag{4.3}$$

where the integral extends over the wavelength band, within which the Cherenkov detector is sensitive; α is the fine structure constant, and the angle θ_c relative to the charged particle direction is given by:

$$\theta_c = acos \frac{1}{\beta \cdot n} \tag{4.4}$$

To adapt the Cherenkov simulation easily to various detector types, a wavelength band may be specified by data input in the INPUTS parameter file.

The emission of Cherenkov photons is treated in the following way: each charged particle path element is subdivided into smaller fractions such that, within each fractional element, the number of emitted photons is less than a predefined bunch size. This photon bunch is treated as a whole rather than each single Cherenkov photon, thus reducing the computational effort and time considerably. For each photon bunch the azimuthal emission angle is taken at random, and its arrival coordinates at the detector plane are calculated. The size of the bunch can be predefined but we will treat it when dealing with the INPUT file, where this parameter is set along with others. As already said, atmospheric absorption of the Cherenkov photons is not taken into account. But by writing the original height of each photon bunch onto the Cherenkov output, the absorption may be introduced later when analyzing the output data.

4.2.3 CORSIKA parameters and applied modifications.

After this short overview of the routines of CORSIKA with a brief description of the physical assumptions made in each one of them, we are going to comment the modifications we have made on the code for our purpose and the physical approximations made.

HEHi Model	LEHi Model	Electrom. Model	Cherenkov ver.
VENUS (*)	GHEISHA	EGS4	CERENE CERENH

Table 4.1: Models used in the CORSIKA code.

HEHi: High Energy Hadronic interaction
LEHi: Low Energy Hadronic interaction
(*): The VENUS model is also used for the inelastic hadron-nucleus interaction cross section at high energy above 80 GeV which are calculated by the subroutine VENSIG.

The version of CORSIKA used for our simulations is the 5.61 version from April 21, 1998. There is a Web site where the newest version of the program can be found: *http://ik1au1.fzk.de/~heck/corsika* and downloaded (*ftp-ik33.fzk.de*).

Once the code is downloaded in order to extract the executable file you have to chose among some options to adequate the code to your own necessities. Mainly this extraction consists in the selection of the Hadronic interaction model that is going to be used and if you want to implement the Cherenkov version or not. Our code implements the routines shown in table 4.1.

We are going to divide this subsection in three parts: INPUT file modifications, program code modifications, and finally we will see how is the output file that we obtain from CORSIKA.

INPUT file

Once we have selected the routines that our CORSIKA version is going to use, in order to run CORSIKA several input files are needed. For example input files exist with cross sections tables, data lists with atmosphere densities, etc.

VARIABLE	DEFAULT VALUE	OUR VALUE	COMMENT
OBSLEV	11000.	2.2E5	observation level (in cm)
CERARY	10 8 1200. 1500. 80. 50.	1 1 1. 1. 5.E4 5.E4	Cherenkov array
CERSIZ	0.	1.	bunch size
CSCAT	5 1000. 1000.	1 0. 0.	scatter Cherenkov events
MAGNET	20.4 43.23	29.5 23.0	magnetic field
ECUTS	.3 .3 .015 .015	4. 4. 0.02 0.02	energy cuts for particles
STEPFC	10.	1.	mult.scattering step fact.

Table 4.2: Input parameter modification.

We are not going to specify now how did we set the parameters, such as the zenith angle or the primary energy spectrum to generate our data base, we will do that later on. Now we only want to comment the parameters that are going to be general, the same, for all the shower events that we generated. The parameters with the values used are the ones listed in table (4.2).

- **OBSLEV**: The experiment is located at an altitude of 2200. meters above see level so we set the variable to that value.

- **CERARY**: For high primary energies it is impossible to write all the bunches of photons of one shower to the output file. Therefore, only those bunches are recorded if they hit an array set at the observation level. Our definition of the array completely covers an area of 500. x 500. m^2 because we are interested in recording Cherenkov photons up to a distance of 250. m from the location of the core. Later on this fact will be explained.

- **CERSIZ**: The bunch size might be selected by this command. The way CORSIKA works with the Cherenkov photon production is the following: A segment AB is taken and the total number of photons in that segment is obtained. This number is recorded by the variable PHOTCT. Once we have this number, the segment AB is divided into smaller segments in the following way:

$$NSTEPC = \frac{PHOTCT}{CERSIZ} + 1 \tag{4.5}$$

where CERSIZ is the variable set in the INPUT file. Once we have all the smaller segments the number of photons is again obtained for each one of them, and this time that number is recorded by the variable PHOTCM. So setting CERSIZ to the value of 1, as we did, means that we have as many smaller segments per AB segment as photons and hence that we have one photon per smaller segment with different properties with respect to the photons of other smaller segments inside the segment AB, obtaining this way a bigger sample of photons. This gives us, what is called *bunch size*, equals to one. We have to be careful when selecting CERSIZ equals to one because we might have some problems. We will comment this when talking about the modifications we made in the CORSIKA code because one of them is related with this problem.

- **CSCAT**: This factor allows the use of a shower multiple times and to fix the shower core impact point. We only used each shower event once and fixed the core in the 0. 0. position.

- **MAGNET**: The value chosen in our case are the components of the magnetic field of Central Europe.

- **ECUTS**: This four values are the cut-off (in GeV) of the particle kinetic energy. Our values are 4. 4. 0.02 0.02 in GeV, for hadrons(energy per nucleon), muons, electrons and photons respectively. For electrons we set the threshold at $\sim$ 21 MeV that it is the energy threshold for producing Cherenkov photons at sea level, and since we are interested in Cherenkov radiation only electrons with energies higher than that threshold interest us. The same is applied for positrons. For hadrons an muons the same argument is valid, but since the mass of the muon is around $\sim$200 times higher than that of the electron we multiplied 21 MeV by $\sim$200 to get $\sim$4 GeV for muons. For the hadrons, the lightest ones are the charged pions which have a mass around 200 times higher than the electrons, so we set the cut at $\sim$4 GeV, the same as for the muons.

- **STEPFC**: Is the factor by which the multiple scattering length for electrons and positrons in EGS4 simulations is elongated. We set STEPFC to the value of 1. A reduction of this factor may be necessary to reproduce experimental data since we are closer to the more realistic case.

CORSIKA code

Once we have set the values for this parameters, the next step is to take a look at the CORSIKA code and make the modifications necessary according to our needs. Mainly the modifications are made in the CERENE and CERENH subroutines.

- **CERENE subroutine:** The modifications in this subroutine are the same as for the CERENH subroutine. Basically the modifications are two:

  1. We only take 10% of the photons produced. This takes into account some effects as are the atmospheric absorption, reflectivity of the telescope mirror and some others that would be commented later on when talking about the detector simulation. We introduced some lines in the program in order to do this.
  2. When talking about the parameter CERSIZ that we set to 1, we said that there could be some problems related with it. The problem is the following: could be the case that PHOTCT equals 1. The way CORSIKA is written, NSTEPC equals 2. That means that one photon has to be divided into to steps. That is $\frac{1}{2}$ in each one of the steps. Since CORSIKA takes PHOTCM as an integer, we would have 0 photons in each one of the steps. What we did was the following: If in any step we have less than one photon we take a random number between 0 and 1 and if this number is less than the photon number then we take PHOTCM equals 1 and if it is greater we take PHOTCM equals 0. We actually applied this to all the values of PHOTCM. In other words what we are doing is round up correctly PHOTCM. For example if we have a value of 1.8 for PHOTCM we take out the integer part and keep the 0.8 and do the same as explained before. Take a random number between 0 and 1 and take for PHOTCM the value of 1 or 2 depending if the random number is higher or lower than 0.8 respectively.

Output file

There are several streams of the output of CORSIKA. One is control information about the simulation run itself which is directed to the logical unit MONIOU. The second output stream contains the information about all the particles that reach the observation level. It is directed to unit PATAPE. In order to extract from the code the information we need for our calculations we have to make some modifications in the code and make up our own output file. With our modifications the output file can be written in binary or ntuple format. Only the binary format would be use by the next program and the ntuple format is only used as a control to check the output data. Both files have exactly the same variables stored. The variable are listed in table (4.3).

NAME	TYPE	UNITS	COMMENT
PHOTCM	I	——	Num. of photons per bunch
XCER	R	meters	X-coor. of photons on ground (*)
YCER	R	meters	Y-coor. of photons on ground (*)
XEL	R	meters	X-coor. of emitting electron (**)
YEL	R	meters	Y-coor. of emitting electron (**)
HPROD	R	meters	Z-coor. of emitting electron (**)
TCER	R	ns	time of arrival of photons since emission
UEL	R	——	direction cos of the electron when emitting
VEL	R	——	direction cos of the electron when emitting

Table 4.3: Output Ntuple variables taken out from CORSIKA.

I $\equiv$ Integer
R $\equiv$ Real
(*) This are the coordinates of the photon impact point on ground in a reference coordinate system with its origin on the core.
(**) This are the coordinates of the electron by the time of emission of the Cherenkov photons in a reference coordinate system with its origin on the core.

In figure (4.1) the coordinate system with the variables is represented.

With this we finish the overview to the modifications we have made in the CORSIKA code.

4.3 Detector simulation

The simulation of the detector is one of the critical points of every work that studies EAS through the simulation procedure. The results of the work depend very strongly on the parameters that define the simulated telescope and camera so this parameters have to be chosen very carefully. In our simulation we tried to be as close as possible to the real situation so many parameters are needed

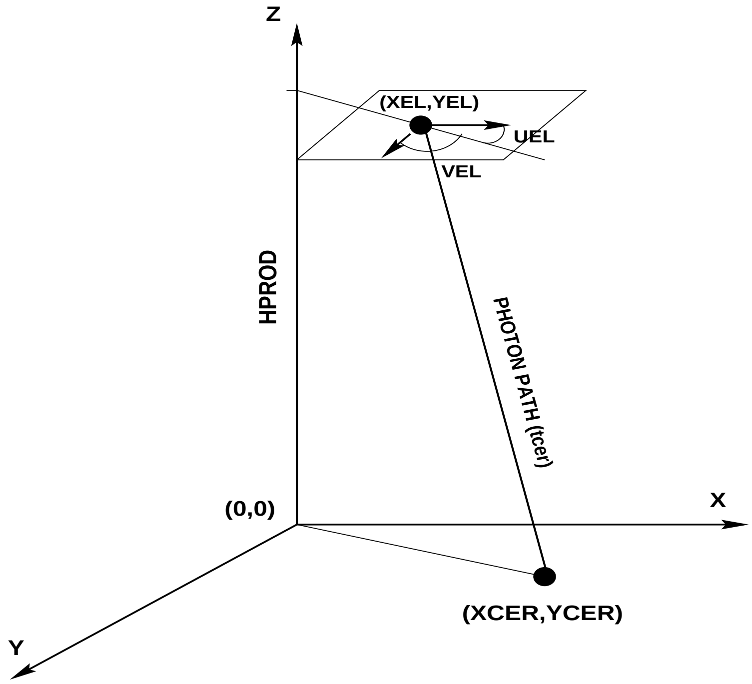

Figure 4.1: *Coordinate System.*

in order to achieve such an order of realism. Simulation parameters go from the mirror's reflectivity to the QE of the PM going through the area of the telescope, ADC gate, etc.. In order to simplify things and be able to make studies at two different levels, two main programs have been developed in order to fulfill our purposes. Both of them are going to be described in detail in this section. The first one takes the output of CORSIKA and simulates our detector translating the photons from the ground to the pixelated camera. All the parameters of the telescope and camera would be described in the correspondent section. With this program a first study can be done and images can be seen although its parameters cannot be obtained with it. The output of this first program is taken by a second program that will obtain the Hillas image parameters using the second moment fits already described in this work. This second program also simulates the LONS (Light Of the Night Sky), in order to achieve a more realistic situation. Since one of the applications of the polarizers is the reduction of half of the intensity of the LONS, a detailed study will be carried out. All parameters and approximations for this second program would be describe in the correspondent section.

4.3.1 Ray Tracing

First lets see what are we looking for with this first program and what do we need in order to achieve it. It has already been mentioned that the main goal of this work it is the study of the polarization vector distribution on the camera with the final aim, among other things, of using such a distribution to achieve a better γ-hadron separation strategy. So it is evident that in a first step we need to obtain the polarization vector for all the Cherenkov photons emitted in the EAS. Thus the first step it is the calculation of such a vector and then simulate the reflexion in the detector's mirror and calculate the camera pixel that the photon reaches. Once we have the polarization vectors onto the camera we will simulate the intensity cutoff that suffers each one of the photons reaching the camera by the polarizers. So the final aim of this first program is to obtain a camera intensity distribution with and without the polarizers simulation in order to compare both situations afterwards.

Attending to the above stated, we are going to divide this section in three different parts: 1) calculation of the polarization vectors for the Cherenkov photons, 2) simulation of the reflexion in the detector's mirror and finally 3) the simulation of the camera.

- **Calculation of the polarization vector:** We have already explained in Chapter 1 how is the distribution of the polarization vector over the Cherenkov cone: always perpendicular to the Cherenkov cone and in the plane defined by the electron path and photon path (see Figure 1.3). To begin with, we have to obtain the photon and electron direction and for that, all we need are the coordinates of the electron by the time of emission (xel,yel,hprod), the direction cosines of the electron by the time of emission (uel,vel,zel), and the photon impact point on ground (xcer,ycer,0). This coordinates are provided in the output file, that we create, taken out from CORSIKA. With these coordinates we can obtain all the directions needed and thus define the plane over which the polarization vector is set. We define four vectors (figure 4.2):

  1. Vector defining the photon path: γ (normalized).
  2. Vector defining the electron path: $\mathbf{e}$ (normalized).
  3. Characteristic vector of the plane defined by the electron and photon path: $\gamma\mathbf{e}$ (normalized).
  4. The polarization vector: **polar** (normalized).

  It follows that:

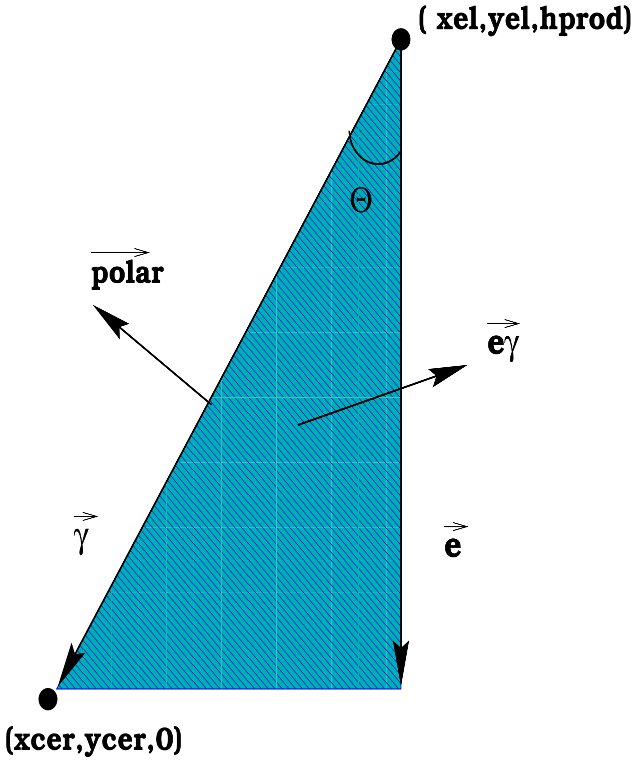

Figure 4.2: *Vector definition.*

$$\mathbf{polar} = \gamma \times \gamma\mathbf{e}$$

This vector is normalized afterwards.

We consider that the photon, from the time of emission until it reaches ground, suffers no deviations, thus the polarization vectors stays unchanged on its way through the atmosphere. Another thing that we would like to mention here is that as it was said before, only 10% of the photons produced in the EAS are taken in order to take into account some physical effects as are the atmospheric absorption, mirror reflectivity, funnel transmission and quantum efficiency of the photomultipliers.

Once we have the components of the polarization vector we can go on to the next step and simulate the reflexion of the light on the detector's mirrors.

- **Simulation of the reflexion in the detector's mirror:** We chose the parameters for our telescope according to the characteristics of the telescopes of the HEGRA experiment (table (4.4)).

TYPE	DIAMETER	FOCAL LENGTH
Parabollic	5 m	4.9 m

Table 4.4: Telescope parameters used in our simulation.

Before entering in detail on how the reflexion is simulated lets take a look at the way in which we simulate the telescopes. For every shower event we cover with telescopes an area around the core up to 250 meters. That is, a circle of 250 meters of radii is full covered with telescopes each one of 5 meters in diameter. This yields an approximate number of 9000 telescopes. An important fact is that all the images of an EAS as seen by the 9000 telescopes are highly correlated. This way, the results should be correct with respect to sampling fluctuations, but not to fluctuations of physical origin.

The reason we go up to 250m is that beyond that distance the efficiency to detect Cherenkov light of an EAS drops significantly.

To simulate the reflexion of the light on the telescope's mirror we follow the next steps:

1. In a first step the number of the telescope at which the photon arrives is obtained for each photon which reaches the ground.
2. Once we know the telescope in which the photon impacts, we have to find the exact point of the telescope surface that has reached. So we need the intersection point, (x_1,x_2,x_3), of the photon direction with the telescope. For the telescope we simulate a parabollic surface following the equation:

$$Z = \frac{1}{4f}x^2 - \frac{xtel}{2f}x + \frac{xtel^2}{4f} + \frac{1}{4f}y^2 - \frac{ytel}{2f}y + \frac{ytel^2}{4f} \qquad (4.6)$$

   where (xtel,ytel) are the telescope coordinates taking as the origin of the coordinate system the core, and f is the focal length.

3. Next we calculate the normal direction to the parabollic surface on that intersection point. This is calculated as the ∇Z(x,y,z) evaluated in the intersection point (x_1,x_2,x_3) and Z is the parabola equation.
4. Once we have this normal direction we can easily obtain the reflected direction just by projecting and adding vector components.

To finish with this part of the simulation just remark that we had justified with several arguments in Chapter 3 that the polarization vectors suffers no change in the state of polarization after the reflexion, so they are translated from the ground to the camera without change.

- **Simulation of the camera:** The parameters that define the camera used for the simulation are the following (table (4.5)):

NUMBER OF PIXELS	DEGREES per PIXEL
271	0.25

Table 4.5: Camera parameters used in our simulation.

This parameters are the same that define the HEGRA system of telescopes. The simulation of the camera includes a couple of things. We have to obtain the pixelated image and we have to evaluate the intensity cutoff by the polarizers that each photon suffers. The first step is quite simple. With the reflected direction of the photon we just have to find the intersection point of this reflected direction with the focal plane defined in our case at z = 4.90 (focal length in m). This intersection point is the impact point of the photon in the camera after the reflexion and with the coordinates of this point we obtain the number of the pixel at which this photon arrives.

For the intensity cutoff the simulation is as follows. The polarizers are set over each one of the camera pixels following the radial direction, that is, with the transmission axis oriented towards the center of the camera. A detailed picture is shown in figure (4.3). So for our simulation we know in every point over the camera how the polarizers are oriented. We just have to take the components of the polarization vector and make it go through a polarizer with the transmission axis set over a plane that we define as X_cY_c (a plane set on the camera parallel to the plane XY on ground as defined in figure (4.1) with the X_c and Y_c axis oriented along the same direction as the axis X and Y on ground). We have the components of the polarization vector from the first step of the simulation. To obtain the components x_p and y_p of the polarizer, defined in the X_cY_c plane, we just have to take the impact point of the photon on the camera and joint that point with the center of the camera. The situation is represented in figure (figure(4.4)).

The matrix of a polarizer, following the Jones matrix notation, with the transmission axis oriented respect to the X-axis with an angle that we will call *clam* (figure 4.4), is the following:

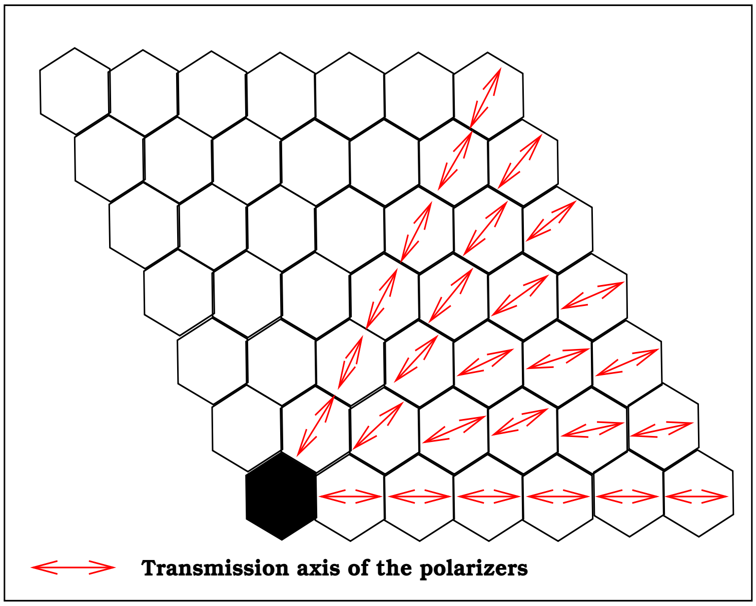

Figure 4.3: *Detail of the polarizers setup on the camera.*

$$A = \begin{pmatrix} cos^2(clam) & sin(clam) * cos(clam) \\ sin(clam) * cos(clam) & sin^2(clam) \end{pmatrix}$$

If we apply the Jones matrix algebra to study the pass through of a linear polarization state through a linear polarizer to obtain the intensity after going through it, to a given polarization vector, **polar** = (polarx, polary), we have for the intensity the following value:

$$\begin{pmatrix} cos^2(clam) & sin(clam) * cos(clam) \\ sin(clam) * cos(clam) & sin^2(clam) \end{pmatrix} * \begin{pmatrix} polarx \\ polary \end{pmatrix} =$$

$$\begin{pmatrix} polarx * cos^2(clam) + polary * sin(clam) * cos(clam) \\ polarx * sin(clam) * cos(clam) + polary * sin^2(clam) \end{pmatrix} = \begin{pmatrix} a \\ b \end{pmatrix}$$

The intensity is obtained as:

$$in = a^2 + b^2 + polarz^2 \tag{4.7}$$

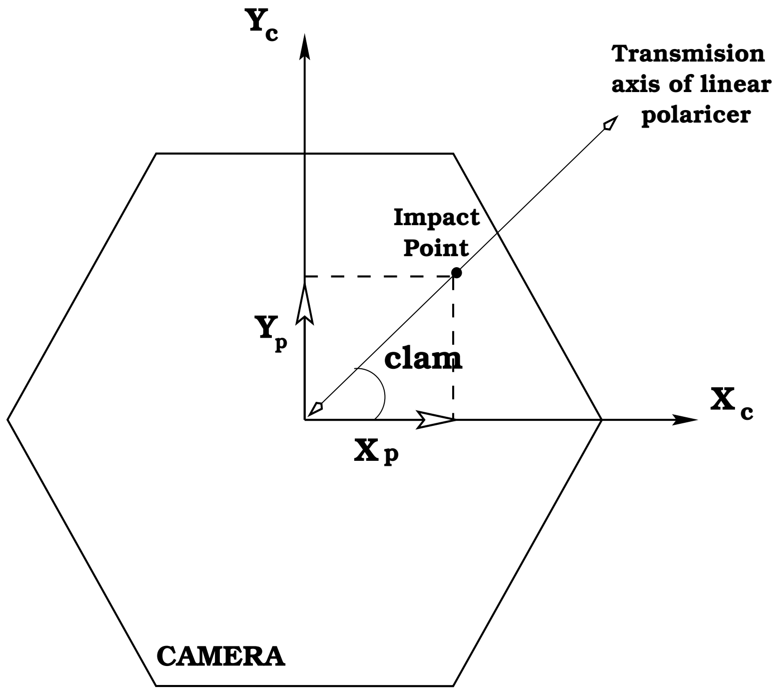

Figure 4.4: *Coordinate system on the camera. The orientation of the transmision axis of the polarizer is obtained from the impact point of the photon on the camera, just by joining this point with the center of the camera.*

where polarz is the z-component of the polarization vector that suffers no change when going through the linear polarizer placed on the XY plane. We calculate this value for every single photon. This value is between 1 and 0, and we consider it as the probability that the photon has of going through the linear polarizer. So we take a random number between 0 and 1 and if this number is greater that the value of *in* then *in* is set to 0 and if it is lower we set the value of *in* to 1.

The output of this first program are camera pixelated images for every single telescope that we have, not including yet the simulation of the LONS.

4.3.2 Light of the Night Sky

One of the main problems that the Cherenkov technique has to deal with is the light of the night sky (LONS). The LONS is the main limiting factor that determines the energy threshold of a telescope. LONS have several components and depends on an specific place and a given detector, as well as the zenith angle and for example man-made light. The LONS influences the detector in several ways such as the angular acceptance, the light collection area, the time response and the spectral sensitivity, therefore it is natural to measure the intensity of LONS in the spectral range where PMs are efficient. In order to understand how the LONS influences our measurements lets take a brief look at how the signal left on the camera by Cherenkov photons coming from an EAS is digitalized.

Lets start with a brief description of how does a photomultiplier work. A photomultiplier (PM) is a device that converts light into a measurable electric current. A PM consists of a cathode made of photosensitive material followed by an electron collection system, a set of what are called dynodes, and finally an anode from which the final signal can be taken. The conversion factor between arriving photons at the cathode and electrons produced at the cathode is called quantum efficiency (QE) of the PM. Another definition that we will introduce here is the term photo-electron (ph.e.). These are the electrons produced in the cathode with the arrival of one photon, and not the electrons collected at the anode.

Once you have the current at the anode you have to be able to measure it. In order to do that an analog to digital converter (ADC) is used. This device digitizes an analog signal into a discrete range of digital values. This instrument is the link between analog and digital electronics. ADC's can be of two types: peak sensitive and charge sensitive. In the former, the maximum of a voltage signal is digitized, while in the latter it is the total integrated current. The time of integration or the time period over which the ADC seeks a maximum is usually determined by the width of a gate signal, or ADC gate. Mainly this is all you need to measure the signal of a PM.

The electronics needed and the logic used in the IACT is quite complex and is not going to be described in detail in this work. Rather than that, we are only going to comment some general aspect that might be useful. Other than the PMs and the ADCs converters, another device that is needed is a discriminator. A discriminator is a device which responds only to input signals with a pulse height greater than a certain threshold value. If the criterion is satisfied, the discriminator responds by issuing a standard logic signal, if not, no response is made. Once we have introduced this definitions lets see what happens when a shower arrives to the detector.

Suppose a camera made out of 271 photomultipliers. Each one of the photomultipliers is connected to the following electronics. The PM is connected to an amplifier. After the amplifier the signal is divided in two. One output is connected via delay cable to the ADC while the other output feeds a leading-edge of a discriminator which is set to a certain value in mV, called threshold, and an output pulse duration of a few ns. For the HEGRA CT1 telescope the values are: amplifier X10, delay cable 85ns, threshold -30 mV and coincidence window around 10ns. When a signal arrives to one of the photomultipliers a certain current is originated at the anode. After going through the amplifier the signal is divided in two, one going to the delay cable and the other to the discriminator. In the discriminator the signal only goes through if it is up the threshold. If it passes the discriminator the signal is sent to the input of a coincidence unit which provides an output signal if N out of M inputs are coincident in time. In this case the trigger signal opens the gates for the ADCs, latches the rubidium clock bit pattern and generates a computer interrupt to start the readout cycle. The information of all the ADCs is read. The logic unit provides a 25 ns gate for the ADCs. Lets point out something here. If the logic unit provides a 25 ns gate for the ADCs, that means that every time the ADC gate opens, along with the signal coming from the EAS, the detector is integrating all the background light arriving to the PM within that time.

The important fact of all this is that to initiate the digitalization of the signal from the camera, and of the read out of data, a trigger signal is required. Something has to tell the electronics when to read the data. This is important because due to the LONS the detector is receiving photons continuously so if no trigger condition is set then, every time a photon reaches the photomultiplier the system would be triggered. This trigger caused by spurious signals is called accidental trigger. This situation has to be avoid, so in order to suppress the accidental triggers produced by background signal, a trigger condition has to be set. This condition is set at the discriminator in mV, that is equivalent to setting a condition in the number of photoelectrons produced at the cathode of the photomultiplier. From now on we will talk in terms of ph.e. and not in mV.

There are several trigger levels and every level gives a different trigger rate. A first level is to ask for a pixel threshold q_0 (q_0 is the value in ph.e. set in mV at the discriminator) in order to suppress the accidental trigger rate. An important fact is that the pixel trigger threshold, q_0, limits the minimum energy of the shower that we are able to detect and thus the energy threshold of the telescope, so q_0 is a very critical value that has to be chosen with care. Currently the trigger threshold of an atmospheric Cherenkov telescope is set to the fluctuations in the average charge due to the LONS integrated within a short time window τ. A second trigger level would be to ask for two pixels to fire in coincidence within a time window. And finally we could impose that not only they have to be fired in coincidence but they have to be next neighbors.

Next we are going to make a small study on how the trigger rate of a telescope changes with the different trigger levels and most important for our study, we are going to take a look at how the trigger rate depends on the intensity of the LONS and how this dependence is related to the pixel trigger threshold in order to see if this pixel trigger condition,q_0, can be lowered with the final aim of detecting showers of lower energy and thus lowering the energy threshold of a telescope.

Because for our work we are simulating as a detector one of the telescopes of the HEGRA experiment we are going to use the following value for the intensity of the LONS as measured at La Palma ([15, R. Mirzoyan and E. Lorentz]):

$$Flux^{LONS} = (1.7 \pm 0.4) \cdot 10^{12} ph/m^2 \cdot sr \cdot s \tag{4.8}$$

over the spectral range between 300-600nm

With this value for the flux of the LONS and the characteristic parameters of our detector we can obtain the single-pixel rate due to the night sky background light. The characteristic values of our detector are the following (table(4.6)):

Variable	Value
Mirror area	8.5 m^2
Number of pixels	271
Field of view	4.75^0
degrees/pixel	0.25^0
Solid angle/pixel	$1.5 \cdot 10^{-5}$ sr
Quantum Efficiency	0.10

Table 4.6: Parameters used to evaluate the pixel rate due to the LONS.

As can be seen in the table we are not considering in our study any absorbtion due to the polarizers.

The single pixel rate, R_{pixel}, due to the LONS is,

$$R_{pixel} = \mathbf{21.6\ MHz/pix}$$

This is the rate at which single photoelectrons are produced in a certain pixel. As can be easily seen this is a very high value for the rate and is the fact that leads to impose trigger conditions. With this value we can obtain the mean number of ph.e./pixel due to the LONS for different integration time windows (table(4.7)) :

In order to set a reasonable trigger rate, it is necessary to move to a higher trigger level and evaluate single pixel rates with different trigger thresholds as

Time Window	ph.e./pix
30 ns	0.6
15 ns	0.3
10 ns	0.2
5 ns	0.1

Table 4.7: Number of ph.e. for different integration times windows.

well as coincidences rate. In order to find single-PMT trigger rates and coincident rates, lets assume that the individual pixels of a camera fire at identical rates R_{pixel}, and that all discriminator output pulses have the same length T. If the coincidence unit reacts instantaneously, the rate R_n of random n-pixel coincidences is approximately (for R_{pixel}T << 1) ([17, G.Hermann, C. Kohler, T. Kutter and W. Hofmann 1995]):

$$R_n = n \cdot C_n \cdot R_{pixel} \cdot (R_{pixel} T)^{(n-1)} \tag{4.9}$$

where R_{pixel} is the single pixel rate. If no pixel threshold (q_0) condition is set, then the value of R_{pixel} would be the 21 MHz obtained above. The coefficient C_n gives the number of different n-pixel combinations; for a two-fold coincidence of M pixels,

$$C_n = \frac{M \cdot (M-1)}{2} \tag{4.10}$$

Typical coincidence windows T range from 10 to 20 ns; acceptable IACT trigger rates R_n are usually in the range of a few Hz, and as we will see in a moment this is only possible if single pixel rates (R_{pixel}) are of the order of some Hz ($\sim$ 100 Hz). The rate at which single photoelectrons are generated by LONS (21.6 MHz) is some orders of magnitude above those 100 Hz. Obviously, pixel trigger thresholds have to be chosen high enough in order to reduce that rate of 21 MHz such that only rare fluctuations trigger a pixel.

For our case, if we set the condition that two pixel have to be fired in coincidence without setting yet any pixel trigger threshold condition, we can evaluate the trigger rate with equation 4.9. We are looking for a two pixel coincidence out of 271 coincidence in a time window of 10 ns. In the next table are resume the values of the variables needed to apply that equation:

The coincidence rate, R_n, we obtain is the following,

n	M	Cn	R_{pixel}	T
2	271	36585	21.6 MHz	10 ns

Table 4.8: Coincidence rate parameters. *Cn* does not take into account the NN pixel condition.

$$R_n = \mathbf{3.3} \cdot 10^5 \mathbf{MHz}$$

We got a higher value than we had before. This is reasonable because we have 271 pixels firing each one at a rate of 21 MHz thus the number of coincidences in a time window of 10 ns measured over one second is very high. The number of pairs that we can make taking pairs of two pixels is very high. We can reduce this rate just by going into the next trigger condition. We can ask for two pixels to be next neighbors. In equation (4.9) we only have to evaluate the number of next neighbors pixels that we can make out of 271 pixels. This number can be easily obtained being 756, a factor 48 smaller than the value obtained before of 36585 for pixel pairs without the next neighbor condition. So the rate should be reduced by this factor:

$$R_n = \mathbf{6.9} \cdot 10^3 \mathbf{MHz}$$

The rate is still high and pixel threshold conditions have to be set. In equation (4.9) the new R_{pixel} has to be evaluated according to a certain pixel threshold q_0 . For such a purpose we assume the following: the single-photoelectron pulse response of the PM is approximated as a rectangle of length τ, the characteristic shaping time. A discriminator with its threshold set at q_0 photoelectrons will then trigger if within a time τ at least q_0 photoelectrons are generated. Assuming that the individual night sky photons, and hence the photoelectrons are uncorrelated, the rate $R_{pixel}(q_0)$ can be estimated as:

$$R_{pixel}(q_0) = R_{pe} \cdot \frac{(R_{pe} \cdot \tau)^{(q_0-1)}}{(q_0-1)!} \cdot e^{-R_{pe} \cdot \tau} \tag{4.11}$$

Where R_{pe} is the generation rate of photoelectrons due to the LONS (21.6 MHz). If $q_0 = 1$ then $R_{pixel} = R_{pe}$. This equation has the following interpretation: every time a photon arrives to the PM a time window τ is opened. In this case we have to ask ourselves for the probability of having (q_0 -1) photoelectrons every time a photoelectron is produced in order to have the minimum q_0. So in this case R_{pixel} would be the probability of having (q_0 -1) ph.e. multiply by the rate

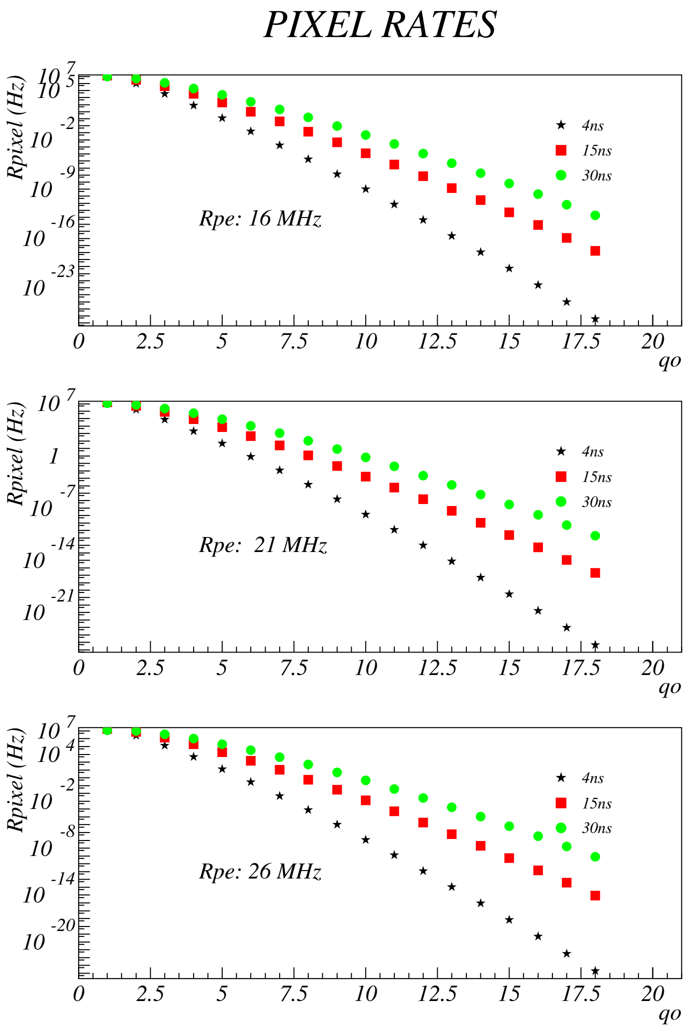

Figure 4.5: *Single-pixel trigger rates. In every plot R_{pixel} is represented against q_0, in ph.e., for a fixed value of the single-pixel rate (R_{pe}) due to the LONS. Each one of the curves is for a different response time τ.*

R_{pe} of the LONS. With this equation we obtained the plots represented in figures (4.5) and (4.6) where pixel rates are evaluated.

In those plots the pixel rate R_{pixel} has been represented against q_0 for different combinations of $R_{pe} \cdot \tau$. The values in table (4.9) have been used to do the plots.

As an example we could give the following. From the plots we can see that for τ = 4ns, R_{pe} = 21 MHz and q_0 = 5 we have a value for $R_{pixel} \sim 100$ Hz which

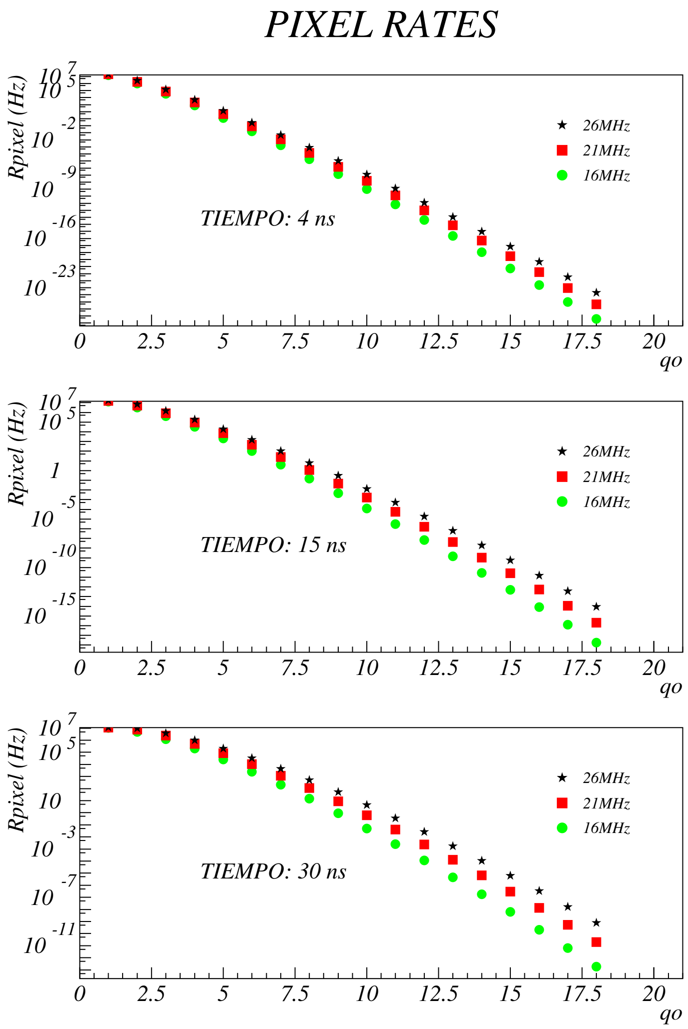

Figure 4.6: *Single-pixel trigger rates. In every plot R_{pixel} is represented against q_0, in ph.e., for a fixed value of the response time τ. Each one of the curves is for a different value of R_{pe}.*

$Flux^{LONS}$ (ph/$m^2 \cdot str\cdot$ s)	R_{pe} (MHz)	τ (ns)
$1.3 \cdot 10^{12}$	16.5	4, 15, 30
$1.7 \cdot 10^{12}$	21.6	4, 15, 30
$2.1 \cdot 10^{12}$	26.7	4, 15, 30

Table 4.9: Flux value, pixel rate and integration time windows.

using equation (4.9), for T = 10ns, n=2 and C_n = 756 (2NN), yields a value of $\sim$ 0.15 Hz for the pixel rate R_n. With this example we can see that with the appropriate value of q_0 we can reduce the accidental trigger rate to the value of a few Hz.

In order to reduce random IACT triggers, two factors appear to be relevant: a short coincidence resolution time window T (which in case of the usual two-fold coincidence it is not too crucial because the rate R_n depends in this case linearly on T), and a fast response time τ of the PM, ideally close to the spread of a few ns of the genuine Cherenkov photons. One more thing has to be pointed out. In equation (4.9) effects such as the afterpulsing have not been taken into account. The afterpulsing has not been taken into account for the development of this work although it is an important effect that has to be kept in mind because for moderates values of $< q >$ ($< q > \leq 20$ ph.e) it is not the fluctuations of the LONS which sets the threshold but the afterpulsing ([16, R.Mirzoyan, E. Lorenz, D. Petry, C. Prosch 1997]).

Once we have introduced the definition of single pixel rates and coincidence rates lets find out the effect of the polarizers on the rates and more particularly how the polarizers might affect the pixel trigger threshold condition with its implications.

The arrangement of linear polarizers on the camera has a direct effect on the intensity of the LONS: the intensity is reduced by a factor of 2. This is a simple effect of natural light, understood as natural unpolarized light, going through a linear polarizer. What we are looking for is how single pixel rates are modified by the reduction of the intensity of the LONS and most important what happens with the pixel trigger threshold condition q_0. In order to make this study we are going to make the following considerations. We are going to consider the next neighbor trigger condition with a single pixel threshold set at a certain value q_0. Because the polarizers reduce the intensity of the LONS by a factor of 2 the single pixel rate R_{pixel} would be lowered and thus the coincidence rate R_n. We are not going to deal with the appropriate value of this coincidence rate, instead we are going to assume that a few Hz is good enough according to the experimental values, so we are going to proceed in the following way. We are going to maintain the coincidence rate R_n, at the same value of a few Hz what implies, as can be seen from equation (4.9), maintaining the same single pixel rate. In order to maintain the same pixel rate R_{pixel} when reducing the intensity of the LONS by half its value, form equation (4.11) we can see that the pixel threshold, q_0, has to be reduced. So we are going to make the following comparison:

$$\frac{R_{n(notpol)}}{R_{n(pol)}} = 1 = \frac{R_{pixel(notpol)}}{R_{pixel(pol)}} \tag{4.12}$$

Understanding by $R_{n(notpol)}$ the coincidence rate without polarizers and $R_{n(pol)}$ the coincidence rate using polarizers (this notation of *notpol* $\equiv$ *without using polarizers* and *pol* $\equiv$ *using polarizers* is going to be used for other variables in the rest of the work having the same meaning as for the rates). So using equation (4.11) we have:

$$\frac{R_{pixel(notpol)}}{R_{pixel(pol)}} = 1 = \frac{q_{0pol} - 1}{q_{0notpol} - 1} \cdot e^{\frac{-R_{pe} \cdot \tau}{2}} \cdot \frac{((R_{pe}) \cdot \tau)^{(q_{0notpol}-1)}}{((R_{pe}/2) \cdot \tau)^{(q_{0pol}-1)}} \tag{4.13}$$

With this equation we are going to represent for different combinations of $R_{pe} \cdot \tau$, the value of $q_{0notpol}$ against the value of q_{0pol} that maintains the single pixel rate as we had before using the polarizers. The combinations used for the representation are the ones summarized in the table (4.9) and the results are represented in figure (4.7).

In figure (4.7) the continuous lines represent the upper and lower limit in the estimation of the new value of q_0 and are going to be considered as the error of that estimation. As an example we can see by taking a look at the plot (figure(4.7)) that if we have $q_{0notpol} = 10$ ph.e./pixel for the most optimistic case if the intensity of the LONS is reduced by half its value, we can lower the pixel threshold down to a value of $q_{0pol} = 8$ ph.e./pixel and for the less optimistic case we can go down to $q_{0pol} = 9$ ph.e./pixel.

To finish this section we are going to comment how do we simulate the LONS in the camera. We are going to assume for the LONS a Poisson distribution, therefore we are going to generate Poisson randomly distributed events in the camera. The probability that a certain pixel gives N photoelectrons according to a Poisson distribution is given by:

$$P(N) = \frac{\mu^N}{N!} \cdot e^{-\mu} \tag{4.14}$$

where μ is the mean number of photoelectrons. In our case this mean value is going to be the mean number of ph.e. per pixel and depends on the intensity of the LONS, the mirror area, integration time, quantum efficiency and angular acceptance of the pixels, according to:

$$\mu = Flux^{LONS} \cdot Mirror^{area} \cdot Q \cdot \tau \cdot str \tag{4.15}$$

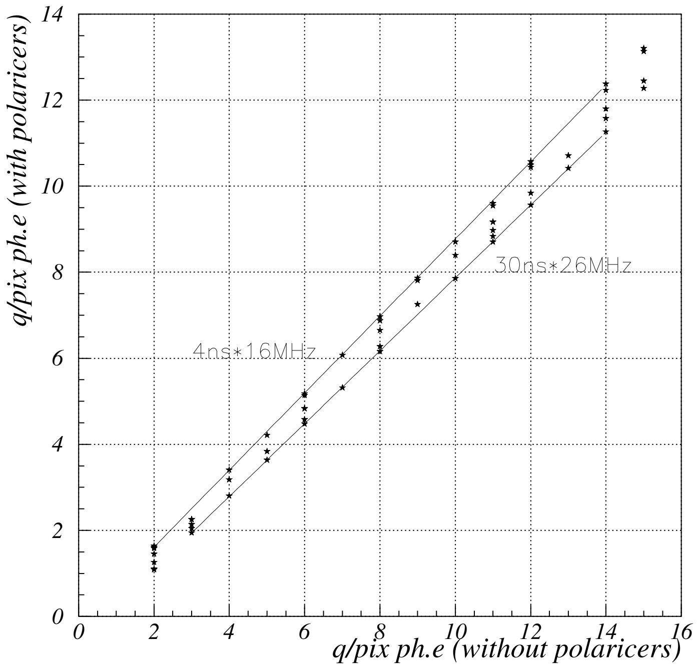

Figure 4.7: *Single pixel trigger threshold (q_0) for different combinations of $R_{pe} \cdot \tau$ are represented. In the Y-axis the value of q_0 is represented for the case of using polarizers and in the X-axis the value of q_0 is represented for the case of not using polarizers. The upper line is the upper limit given by the combination 16Hz $\cdot$ 4ns, and the lower line is for the lower limit given by the combination 26Hz $\cdot$ 30ns. Along the lines the factor $\frac{R_{pixel(notpol)}}{R_{pixel(pol)}}$ equals one.*

Where *str* are the stereo radians/pixel, Q is the quantum efficiency and τ the integration time.

With this mean value μ for the ph.e./pixel we generate the number of ph.e/pixel for each one of the 271 pixel on the camera. In order to take into account the effect of the polarizers we take each one of the ph.e. and assign each one of them a 50% probability to go through the polarizer. This 50% takes into account the unpolarized nature of the light. As an example we can take a look at figure (4.8), where a 271 pixel camera has been simulated. On the upper figure we can see the number of ph.e./pixel due only to the LONS without taking into account the effect of the polarizers, and in the lower figure we have the same camera image but taking into account the effect of the polarizers on the LONS.

In figure (4.9) we can see four different plots taken out from our simulation in order to test the LONS simulation made. In figure (4.9A) the number of photoelectrons per camera due only to the LONS is represented from a total of $\sim$ 8600 camera images. In figure (4.9B) the same value is represented but taking into account the effect of the polarizers. As expected the number of ph.e./image using polarizers is reduced by a factor 2 with respect to the *normal* situation as can be seen in figure (4.9C) where the intensity cutoff in the camera by the polarizers is represented against the core distance. The larger errors seen at close core distances is only due to the less statistics that we have near the core. We have less telescopes for close core distances than for large core distances. Last, in figure (4.9D) the number of ph.e./image against the number of ph.e./image taking into account the effect of the polarizers is represented just as a comparison between both of them

With this we finish the overview to the LONS simulation. Now we go on to the simulation of the camera images and the determination of the Hillas image parameters.

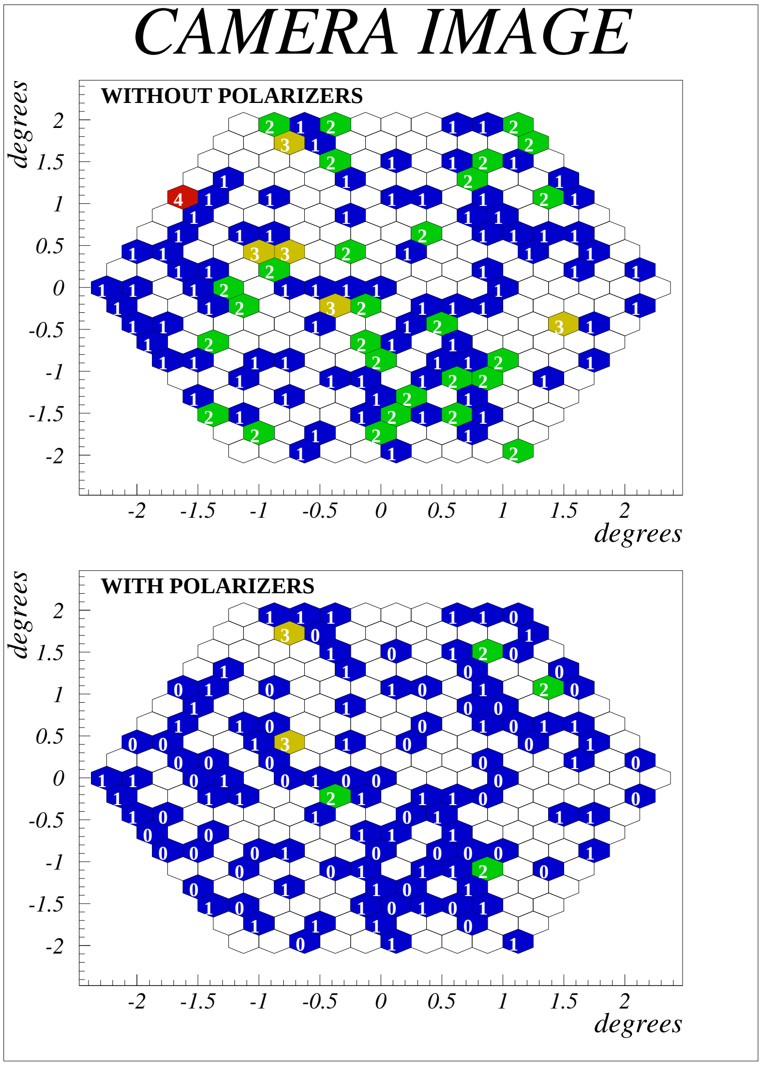

Figure 4.8: *Simulation of LONS on the camera.*

4.3.3 Image Analysis

For the analysis of the shower images we developed a second program. With this second program we intent to study mainly two things. We have talked about the expected modification that the images might suffer due to the placement of polarizers onto the camera, so we are going to study the Hillas image parameters for both situations, with and without polarizers, and see if those modifications take place. Secondly, because the intensity of the LONS is reduced by half and

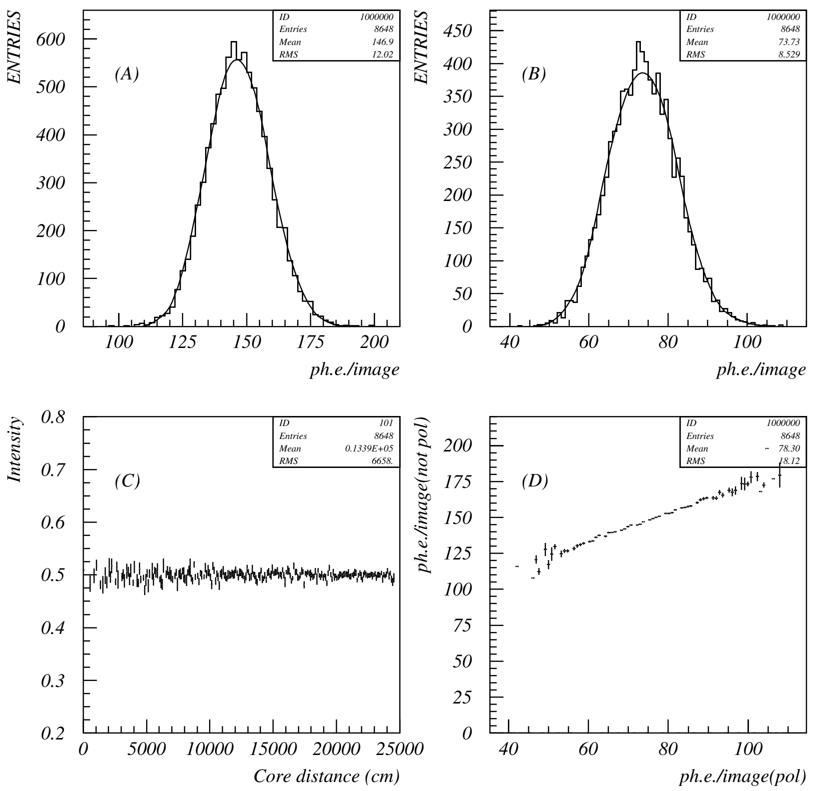

Figure 4.9: *LONS parameters.*

the LONS is the factor that limits the energy threshold of the telescope, we will study the possibility of lowering the energy threshold of the telescope by using polarizers. There are two critical factors for our study and the results obtained depend very strongly on those factors. One is the trigger condition of the telescope and the other one is the 'tail cut' applied for the image analysis. Both things are going to be explained on detail. This program also simulates the LONS according to the procedure explained in the last section. The parameters used for the simulation of the camera are summarized in tables (4.10) and (4.11).

Now we will explain the simulation of the trigger condition, image 'tail cuts' as well as the supercuts applied and procedure to obtain the effective area of the telescope.

- **Trigger condition:** As already explained a trigger condition has to be set

$Flux^{LONS}$ **(ph/$m^2 \cdot str\cdot$ s)**	τ **ns**	**str/pixel**
$1.7 \cdot 10^{12}$	25.0	1.5^{-5}

Table 4.10: LONS simulation parameters.

$Mirror^{area} m^2$	**Number of pixels**	**deg/pixel**	**Quantum eff. of the PM**
8.5	271	0.25^0	0.1

Table 4.11: Parameters of the simulated detector.

on the number of ph.e a certain combination of pixels has to have in order to trigger the telescope. In our simulation two trigger conditions have been set; one trigger condition for the situation in which polarizers are not used and the other one using polarizers. For our purpose the trigger condition we asked for is 2NN/271 $> q_0$, where q_0 is:

q_0 **(ph.e.) Without Polarizers**	q_0 **(ph.e.) With Polarizers**
10	8

Table 4.12: Trigger threshold.

The number of ph.e in 2NN/271 was chosen to be 10 if no polarization assumption is made, according to the value found in reference [19, A. Konopelko 1998]. For the situation in which polarizers are used the trigger condition was chosen according to figure(4.7). As a remainder, this value of 8 ph.e. is such that the relation $\frac{trigger \quad rate \quad without \quad polarization}{trigger \quad rate \quad with \quad polarization}$ remains constant. Another interesting fact can be pointed out from figure (3.3). From this figure we can obtain the amount of light that is going to be lost when reaching the camera, and going through the polarizers, at the hump to be around 20%. So lowering the trigger condition from 10 to 8 ph.e. should not affect the gamma trigger rate at the hump even if some light is cut off when using polarizers. It has to be mention that this is a pure coincidence, because we chose this new value of 8 ph.e. according to the accidental trigger rate and not to the gamma rate. By taking a look at the same plot we can see that around 50% of the light is going to be lost for hadron showers at all core distances, so is around the hump where we expect to gain more in what trigger refers, because the difference in intensity loses between gamma and hadron events is bigger. Related results would be presented in the next chapter.

- **Hillas image parameters:** Cherenkov images are described by parameters related to the first and second order moments of the intensity distribution in the camera. The camera pixel continuously collect the background light of a different kind. Thus the measured Cherenkov light flashes contain the background light in each camera pixel. The influence of the background light is very strong for the pixels being at the *tail* of the Cherenkov light images. Usually, noisy pixels are excluded from the analysis by requiring a certain minimum amplitude. The two-level tail-cut technique to extract the shower image from the measured intensity of the pixels was suggested in [31, M. Punch *et al* 1992]. This technique consist on the following. A first cut is applied, what is called *higher tail-cut*, in order to identify what are called *picture* pixels in which Cherenkov light from the air shower dominates above the background light. The second cut defines the so called *boundary* pixels with an amplitude above a *lower tail-cut* but less than the *higher tail-cut*. This boundary pixels are significantly influenced by the background light. By using only picture pixels and boundary pixels which neighbor at least one picture pixel, the background dominated pixels can be almost entirely excluded from the analysis, having better image quality.

  As we did for the trigger condition we defined a different set of picture and boundary tail-cut for the common situation and for the polarizers case. For the common case we again refer to reference [19, A. Konopelko 1998] and for the polarizers situation we had to define our own picture and boundary tail-cut. The values for the tail-cut are defined in table (4.13).

	Picture tail-cut	**Boundary tail-cut**
Without polarizers	6 (ph.e.)	3 (ph.e.)
With polarizers	5 (ph.e.)	3 (ph.e.)

Table 4.13: Image tail-cut.

  Two criterions were followed to adecuate the 'tail-cut' to our situaion:

  - **Length and Width images:** We generated several showers at 600 GeV with different set of 'tail-cuts' for the case of polarization keeping the 'tail-cut' for the common case. We tried the set of 'tail-cuts' summarized in table (4.14). Both, the length and width parameter, are represented in figure (4.10). From this figure we can see that the set

	Picture tail-cut	**Boundary tail-cut**
Without polarizers	6 (ph.e.)	3 (ph.e.)
With polarizers(1)	6 (ph.e.)	3 (ph.e.)
With polarizers(2)	5 (ph.e.)	3 (ph.e.)
With polarizers(3)	4 (ph.e.)	2 (ph.e.)

Table 4.14: Set of different tail-cuts applied for testing.

of 'tail-cut' that better adjust both distribution, with and without polarization, is the case of *picture* tail-cut equals 5 and *boundary* tail-cut equals 3. For example by taking a look at the parameter distributions for the case of *picture* 'tail-cut' equals 4 and *boundary* 'tail-cut' equals 2, we can see a tail in the distributions, both for length and width, that is related with the non elimination of the pixels from the tail of the image because the 'tail-cut' is not hard enough on the image.

- **Poisson distribution:** This second method used for the selection of the image 'tail-cut' consists on the following. The mean number of ph.e. generated in each pixel due to the LONS is equal to μ=0.6. With the polarizers this mean value is divided by two, being μ=0.3. If we take a look at table (4.15) we can see that the probability of having 6 ph.e. (picture 'tail-cut') with mean value 0.6 is equal to 3.88E-05. Now if we move to the mean value of 0.3 ph.e., we look for the number of ph.e. with the same probability of having 6 ph.e. for the case of mean value 0.6. This number of ph.e. corresponds approximately to 5 ph.e. The same is applied in the selection of the boundary 'tail-cut'.

This a critical point in our work because the distribution of the second moment image parameters depend crucially on the amount of background light per pixel. With this tail-cut we eliminate pixels from the camera that do not belong to the image but that have big influence when obtaining the image parameters. A slight overestimate or underestimate of the background light content dramatically change the distributions of a number of image pixels in readout, the number of pixels above the boundary and picture tail cuts, and as a consequence the distribution of the image shape parameters.

- **Supercuts:** As already explained in Chapter 2 a set of image cuts have to be applied in order to achive a good γ-hadron separation. The set of Supercuts used in our study is the following :

$$0.6(^o) < dist < 1.1(^o)$$

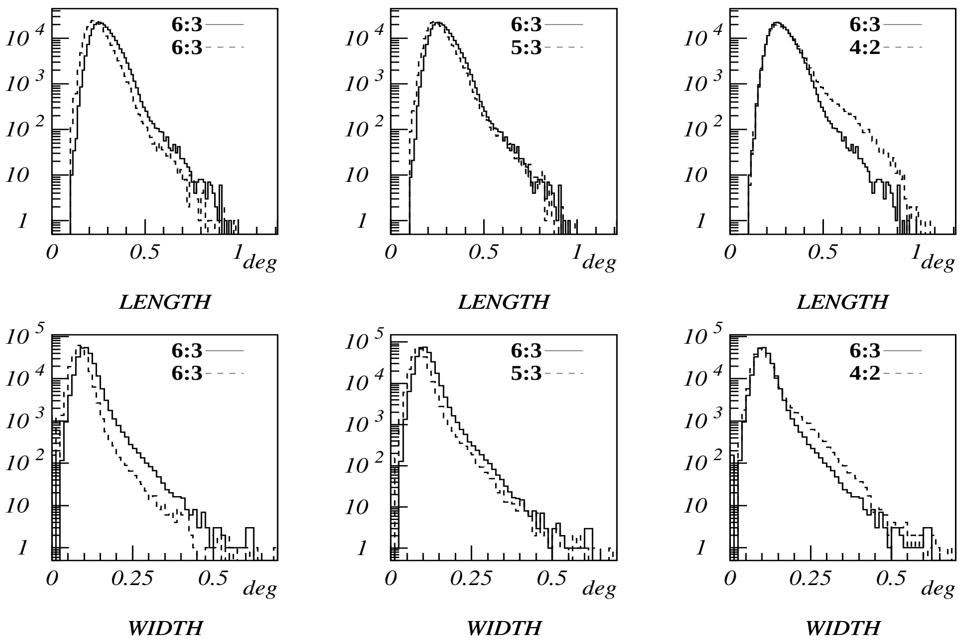

Figure 4.10: *Tail cuts. The continuous line represent the parameter distribution for the case of not using polarizers, while dashed line is for the distribution using polarizers. Three set of tailcuts are represented (6,3), (5,3) and (4,2) for comparison. The first number in brackets is the picture tail-cut and the second one the boundary tail-cut. This image parameters were obtained for* 10^5 *showers of 600 GeV where the tail-cut plays a more important role than for higher energies.*

$$0.18(^o) < length < 0.375(^o)$$
$$0.06(^o) < width < 0.2(^o)$$
$$alpha < 15.(^o)$$

These cut are chosen to be in agreement with those used by the HEGRA collaboration and no difference is made between the non polarization and polarization case. The same set of supercuts is used for both situations. Nevertheless it has to be mention that this cuts could be optimized for the polarization case in order to take full advantage of the technique. It has been mentioned that the image parameters suffer modifications due to the use of polarizers, for example length and width move towards smaller values. This displacement is different for gamma distributions and for hadron distributions, so the Supercuts can be optimized to better exploit this fact

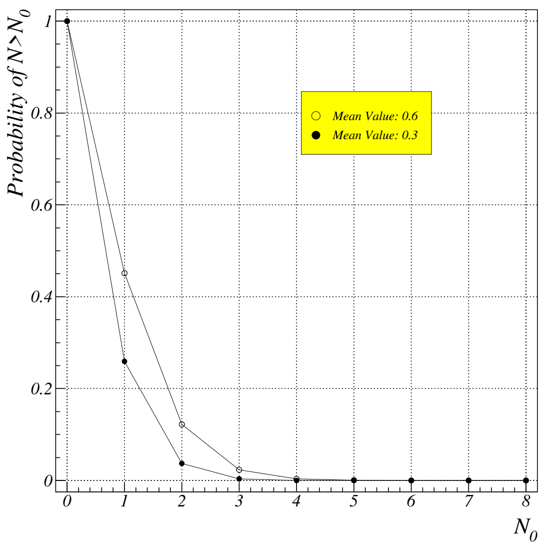

Figure 4.11: *The probability of having $N > N_0$ events according to a poisson distribution for to different mean values, μ, of the distribution.*

	μ = **0.6**	μ = **0.3**
N_0	PROB($N > N_0$)	PROB($N > N_0$)
0	1	1
1	0.4511	0.2591
2	0.1219	0.0369
3	0.0231	0.0036
4	0.0033	0.00030
5	0.0004	1.58E-05
6	3.88E-05	7.83E-07
7	3.29E-06	3.34E-08
8	2.45E-07	1.25E-09

Table 4.15: *Probability of having $N > N_0$ according to a poisson distribution for to different mean values.*

in order to achieve a better γ-hadron separation strategy. This is not going to be done in this work and will be left for further studies.

- **Energy threshold:** An advantage of the atmospheric Cherenkov technique is the big collection area they can achieve. The lowest energy shower detectable is imposed by the fluctuations of the LONS, and, as we saw, trigger conditions have to be imposed in order to suppress accidental triggers. We have a level beyond which now shower is detected. Assume we detect a shower of a given energy with impact parameter equals to zero. Next we can ask ourselves how far can the impact point be from the telescope in order to detect it. This way we can evaluate for a given energy the probability of detecting a shower at different core distances, $P_\gamma(E,r)$. For a given energy this probability depends only on the impact parameter, and gives us an idea of the dependance of the detection of gamma ray showers with the distance of the shower core from the telescope. This yields a high detection rate of the gamma ray induced air showers. The collection area for the gamma ray induced air showers is evaluated as:

$$S_\gamma(E) = 2 \cdot \pi \int_0^\infty P_\gamma(E,r) \cdot r dr \tag{4.16}$$

where $P_\gamma(E,r)$ is the trigger efficiency or probability of detecting gamma ray air showers of primary energy E at different distances.

The suppression changes for the background of hadronic induced shower. For this background events we have to consider zenith angle of incidence. This time the probability of detecting a shower depends on this angle too, $P_{cr}(E,r,\theta)$. This fact has to be taken into account and the collection area is then written as :

$$S_{cr}(E) = 4 \cdot \pi \int_0^{\pi/2} sin(\theta) \cdot d\theta \cdot \int_0^\infty P_{cr}(E,\theta) \cdot r dr \tag{4.17}$$

We can plot the collection area against the energy to obtain the following plot (figure(4.12)).

Looking at the plot we can see a different behavior for gamma and hadron events. This behavior is determined by the shape of the lateral distribution of the Cherenkov light pool at the observation level. We can find the reason in the following arguments: i) at low energies a gamma showers produced more light than a hadron induced shower of the same energy, thus the collection area is bigger for gamma events; ii) the number of ph.e. in an hadron shower is lower than in a gamma shower and the hadron shower produces a more diffuse image which turns in a poorly detection efficiency and iii) at high energies the number of ph.e. in gamma and hadron images

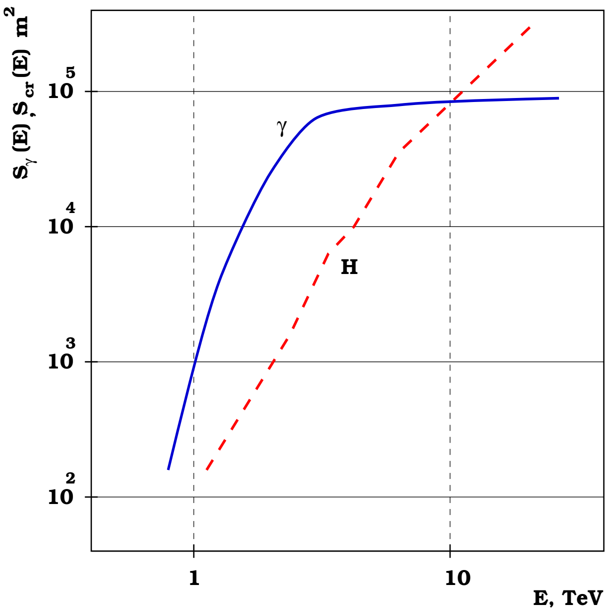

Figure 4.12: *Collection areas.*

is high enough and i) and ii) don't have to much relevance, so we can expect to have the same collection area. Instead because the field of view is limited for gamma showers , S_γ tends to a constant value and the shower image moves away out of the field of view for showers with impact parameter greater than $\sim$ 100 m. For hadronic showers the events can be detected at distances greater than 100 m.

Using the collection areas we can determine the detection rate for the gamma showers:

$$R_\gamma = \int_0^\infty S_\gamma(E) \cdot A_\gamma \cdot E^{-\alpha_\gamma} \cdot dE \qquad (4.18)$$

and for hadron events:

$$R_{cr} = \int_0^\infty S_{cr}(E) \cdot \frac{dN_{cr}}{dE} \cdot dE \qquad (4.19)$$

With this two equations and a given energy spectrum, S_γ and S_{cr}, we can evaluate the detection rate at different energies. If we make the plot detection rate against energy we can see a peak at a certain energy. This energy corresponds to the maximum detection rate and can be considered as the energy threshold of the telescope. This maximum is set at different energies for gamma and hadron events. In this definition the energy threshold depends on the intrinsic features of the γ ray source, that is mainly the energy spectrum.

In our simulation we evaluate the probability of detecting an event just by comparing the number of telescope that fulfill the trigger condition against the total number of telescopes:

$$P_{\gamma/CR}(E,r,\theta) = \frac{Number \quad of \quad triggered \quad telescopes}{Total \quad number \quad of \quad telescopes} \tag{4.20}$$

Once we have this probability we evaluate the effective area just by multiplying this factor $P_{\gamma/CR}(E,r,\theta)$ by the total area covered by the telescopes. The simulation evaluates the trigger probability up to a distance of 250m in radii. Two things are taken into account here, one the drop of the Cherenkov light pool around 150 meters and the other one the limited field of view of the detector. The field of view limits the detector in a way that light is collected only from within a small angular radius θ from the axis. From geometry, if a shower falls, say 100 m from the telescope, only the part above an altitude of $100/\sin(\theta) \sim 12$ Km, is seen. As already showed in previous chapters this is above most of the emitting region. Thus the amount of light collected falls off more rapidly with core distances. So the collection area also depends on the field of view.

Last, we have used to evaluate the differential detection rates the following differential power-law energy spectra for a Crab like γ ray source and a background spectra with the following characteristics:

γ differential spectrum: $\frac{dJ_\gamma}{dE} = A_\gamma \cdot E^{-\alpha_\gamma}$
with $\alpha_\gamma \equiv$ power law index = **2.6**
and $A_\gamma \equiv dJ_\gamma$ (>1 TeV) (flux normalization) = **2.8** $\cdot 10^{-11} s^{-1} cm^{-2} TeV^{-1}$

Cosmic ray background differential spectrum: $\frac{dJ_{CR}}{dE} = A_{CR} \cdot E^{-\alpha_{CR}}$
with $\alpha_{CR} \equiv$ power law index = **2.7**
and $A_{CR} \equiv dJ_{CR}$ (>1 TeV) (flux normalization) = **1.6** $\cdot 10^{-5} s^{-1} str^{-1} cm^{-2} TeV^{-1}$

Only background events within the angle range $0°$ and $3°$ have been generated, so to obtain the flux normalization factor we have to multiply by the correpondant factor 0.00861 str.

With this we finish the overview to the simulation procedure.

4.4 Monte Carlo Data Base

We have used CORSIKA 5.61 version from April 21, 1998 (Capdevielle et al. 1992), to simulate a handful of events to test the ideas exposed along this work. The events generated are gamma events and proton events. Night Sky Background was included in the simulation as described before.

- **Gamma events:** The gamma events library contains 100 showers at 15 different energies going from 200 GeV up to 1600 GeV. All the events have been generated at 0^o zenith angle. Each energy has been simulated separately what means that no energy spectrum has been considered. All the Cherenkov photons at ground are collected if they fall within the 250 m radii area, centered on the core.

- **Hadron events:** The hadron events generated are protons, which for the energies involved in our work represent around 50% of the cosmic ray flux. The events have been generated according to the solid angle between 0 degrees and 3 degrees zenith angle and energy between 600 GeV and 4800 GeV. A hundred showers have been generated at each energy. For the computation of hadron events it is assumed that Cherenkov photons light production by hadronic showers is three times lower than for gamma showers of the same energy, in order to have approximately the same light intensity per unit of area as for the gamma events. This is due to the fact that hadronic showers should produce less light because not all of the primary energy goes into the electromagnetic cascade, from which most of the fraction of Cherenkov light produced in an EAS comes. With the aid of the Gaisser-Hillas ([34, T. K. Gaisser and A. M. Hillas, 1977]) and Greisen ([33, K. Greisen 1956]) formula (1.18), light production by proton showers can be compared with that from gamma showers. For $1TeV < E < 10^4 TeV$ the Cherenkov light produced by a proton shower of a given energy is less than that from a gamma showers of the same energy by a factor ([35, P. Sommers and J. W. Elbert, 1987]):

$$f = 0.680 + 0.063 \cdot log_{10}(E/1000TeV) \qquad (4.21)$$

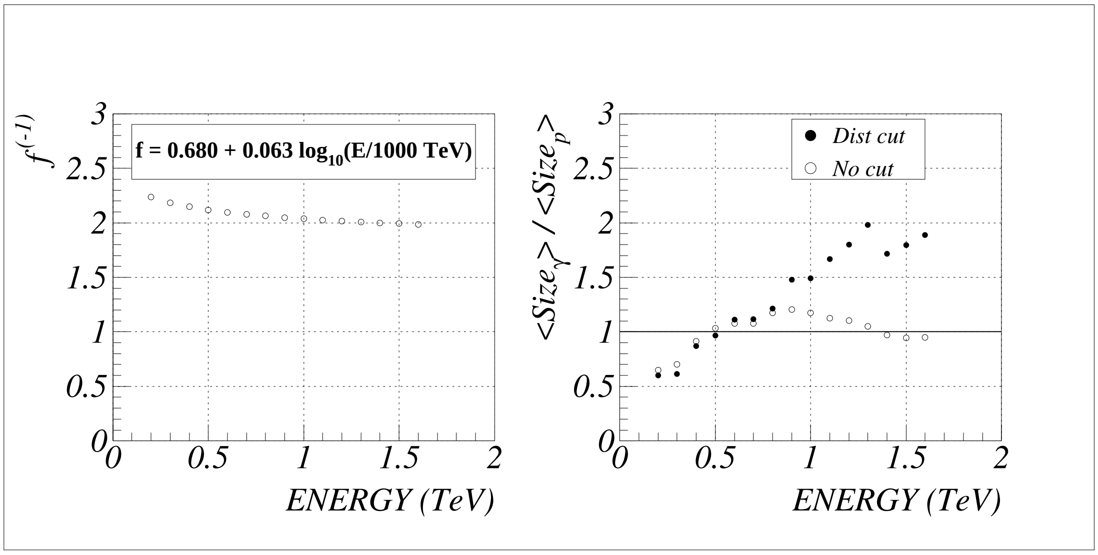

Figure 4.13: *On the left figure the factor f^{-1} is ploted for the energy range 0.2 TeV and 1.6 TeV. According to this figure in order for the light produced in gamma showers and proton showers to be comparable, the last ones have to be generated with an energy twice the energy of the gamma shower. On the right figure the rate between $size_\gamma$ and $size_p$ is represented for the events simulated in this work that has passed the telescope trigger condition, and for two cases, with no image cut applied (empty circles) and with the dist cut applied (filled circles). In this plot gamma showers and proton showers of energy three times higher are compared.*

As shown in figure Fig.(4.13) left, this factor is around two for the energy range involved ($1TeV < E < 10^4TeV$). For our simulation we can compare the mean size of gamma images on the camera with that of proton images. The comparisson is shown in figure Fig.(4.13) right. In this plot the x-axis is the energy of the gamma events. Each gamma event is compared with a proton event of an energy three times higher. The distribution should be centered around ($< size_\gamma > / < size_p >$) ~ 1 if the light generated in a gamma shower of a certain energy is comparable to that of a proton shower of an energy three times higher. We have plotted the rate between the mean size of the gamma and proton images for two cases:

$\frac{<size_\gamma>}{<size_p>}$ with no image cuts.

$\frac{<size_\gamma>}{<size_p>}$ with the *dist* cut applied.

In this plot, and for both cases, only images which have triggered the telescope are being taken into consideration, so actually this result cannot be extrapolated to light produced in the shower. This plot (figure (4.13) right) only gives a rough idea of the size of the gamma images and background images being compared for each simulated gamma energy.

To increase the sample statistics we simulate the same event in many non-overlapping telescopes covering an area of 250 meters of radius centered on the core. In this way we have a sample of the order of 10^6 gamma events, highly correlated, at each energy and a total sample of gamma events of 10^7 highly correlated. For hadron events we generated proton shower having the same sample as for gammas. Our results should be correct with respect to sampling fluctuations, but not to fluctuations of physical origin.

In the following tables the events library is summarized.

Energy (GeV)	**Zenith angle (^{o})**	**N^0 showers**
200	0	100
300	0	100
400	0	100
500	0	100
600	0	100
700	0	100
800	0	100
900	0	100
1.000	0	100
1.100	0	100
1.200	0	100
1.300	0	100
1.400	0	100
1.500	0	100
1.600	0	100
TOTAL:		1500

Table 4.16: Gamma library.

Energy (GeV)	**Zenith angle (^{o})**	N^0 **showers**
600	0-3	100
900	0-3	100
1.200	0-3	100
1.500	0-3	100
1.800	0-3	100
2.100	0-3	100
2.400	0-3	100
2.700	0-3	100
3.000	0-3	100
3.300	0-3	100
3.600	0-3	100
3.900	0-3	100
4.200	0-3	100
4.500	0-3	100
4.800	0-3	100
TOTAL:		1500

Table 4.17: Proton library.

Chapter 5

Results

In this chapter we present the results found through out our simulation. The chapter will be divided in three main sections concerning several features of the intrinsic polarization of EAS, telescope performance and finally the Hillas image parameters.

5.1 General Characteristics

Through out our study we have found several interesting features of the polarization of the Cherenkov radiation in EAS that we would like to summarize in this section. In Chapter 3 we have studied the basic physical ideas of the polarization of the Cherenkov radiation in the frame of EAS and we introduced two approximations, the ideal case and the real case. On the basis of these two approximations most of these features can be understood and explained.

Polarization distribution on ground and its dependence with the core distance and energy: In Chapter 3 we have explained how the particular distribution of the polarization vectors on ground is set over different core distances and the implications of such a distribution for our study. Now we will present the results obtained.

In a previous chapter we defined the *radial direction* as the one joining the shower core with the impact point of the photons on ground and the *transverse direction* as the one perpendicular to it (Fig.(5.1)). The angle between the polarization vector, $\vec{pol}$ and the radial direction is also defined on the figure and will be called θ_{pol}.

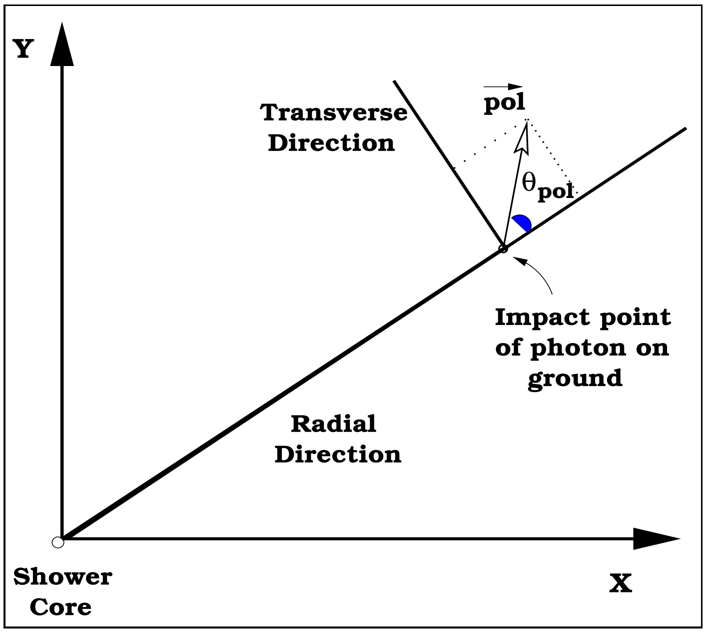

Figure 5.1: *Definition of radial and transverse direction.*

With these two directions defined we can study the distribution of the polarization vectors on ground according to their components along the radial and transverse directions and the dependence of such distributions with the core distance and primary energy and nature. First we are going to give some relations to help to understand the results that will be extracted from figures Fig.(5.4) and Fig.(5.5). We define ϵ as the rate between the transverse and radial components of the polarization vector. This rate can be expressed as a function of the polarization angle (θ_{pol}), defined in figure Fig.(5.1), as:

$$\epsilon = \frac{Transverse \quad Component}{Radial \quad Component} = \frac{< sin^2(\theta_{pol}) >_r}{< cos^2(\theta_{pol}) >_r} \tag{5.1}$$

where the mean value is taken over all the photons falling on a given differential area. The rate ϵ can be translate into relative intensity along both directions with the following relations:

Radial Intensity: $\frac{1}{1+\epsilon}$
Transverse Intensity: $\frac{\epsilon}{1+\epsilon}$

The established relations between the rate ϵ, the relative intensity along both directions and the angle θ_{pol}, are represented in Fig.(5.2). It has to be mention that this relations are true if we consider totally linear polarized light. In this case we can approximate $(< sin^2(\theta_{pol}) >_r)/(< cos^2(\theta_{pol}) >_r)$ by $< tg^2(\theta_{pol}) >_r$ and thus equalize ϵ to $< tg^2(\theta_{pol}) >_r$.

Once this relations have been introduced, we can look at figures Fig.(5.4) and Fig.(5.5) where the rate between the transverse and radial component of the polarization vector is represented as a function of the core distance, both for γ and hadron showers respectively, for three different energies.

Several implications can be pointed out from this two figures (Fig.(5.4) and Fig.(5.5)):

i) The arrangement of polarizing filters **on the camera**, described in Chapter 4, has as a direct consequence a loss of light collected on the camera. This loss depends on the nature of the primary particle initiating the shower and the impact parameter of it. In principle this intensity loss seems to make the polarizing arrangement not to be a very good option since any lost of light is critical for the IAC technique. But if we take a closer look at the problem we can see that is not as bad as it seems. First of all the loss of light in the camera is partially compensated by the reduction of the trigger threshold, at least around the hump region for gamma events. In second place, the loss of light is bigger for protons than it is for gammas. The reason is twofold: 1) Cherenkov light in proton showers

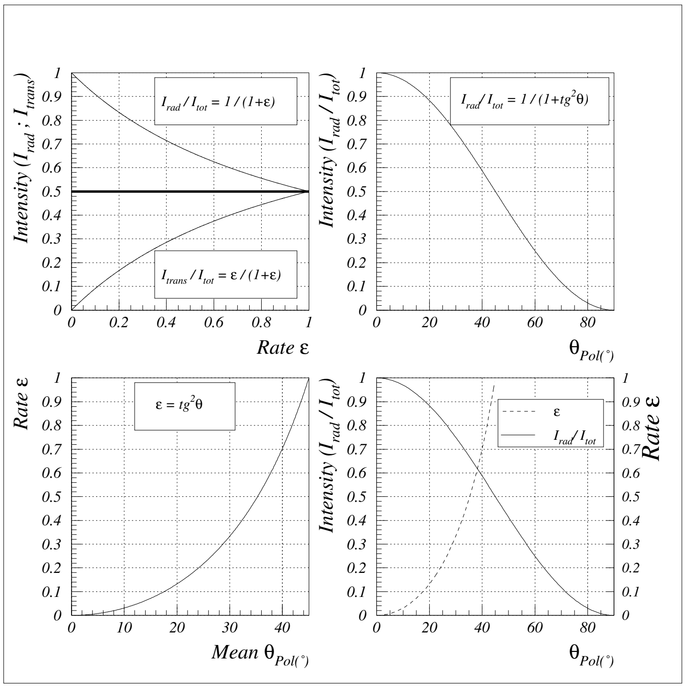

Figure 5.2: *Relations between intensity, the rate ϵ and the angle of polarization θ_{pol} for totally linear polarized light.*

is less polarized than for gammas, 2) The particular setup of polarizing filters on the camera makes the radial direction as the privilege direction, what means that only the intensity fraction along this direction goes through the polarizers placed on the camera. Ground polarization does not translate into camera polarization for proton EAS, as it does for gammas.

In Fig.(5.3) a 1 TeV gamma and two 3 TeV proton event at 0° and (0° − 3°) are represented as an example. In both figures Fig.(5.3)c the continuous line represents the ideal radial intensity as a function of the angle θ_{pol}. On dashed line the intensity obtained **on the camera** as a function of the same angle. For the gamma event both curves are approximately identical, demonstrating that the information contained in the polarization distribution on ground is translated to the camera. For the proton event at 0° zenith angle this is also approximately true, but for the proton event generated within the zenithal angle (0° − 3°) this is not true. The explanation can be found in the fact that in this last case the major axis of the elliptical images does not follow the radial direction as happens with gamma images.

Taking a look at the distribution of polarizing vectors on ground (Fig.(5.4) we could make an estimation of the fraction of light that is going to be lost in

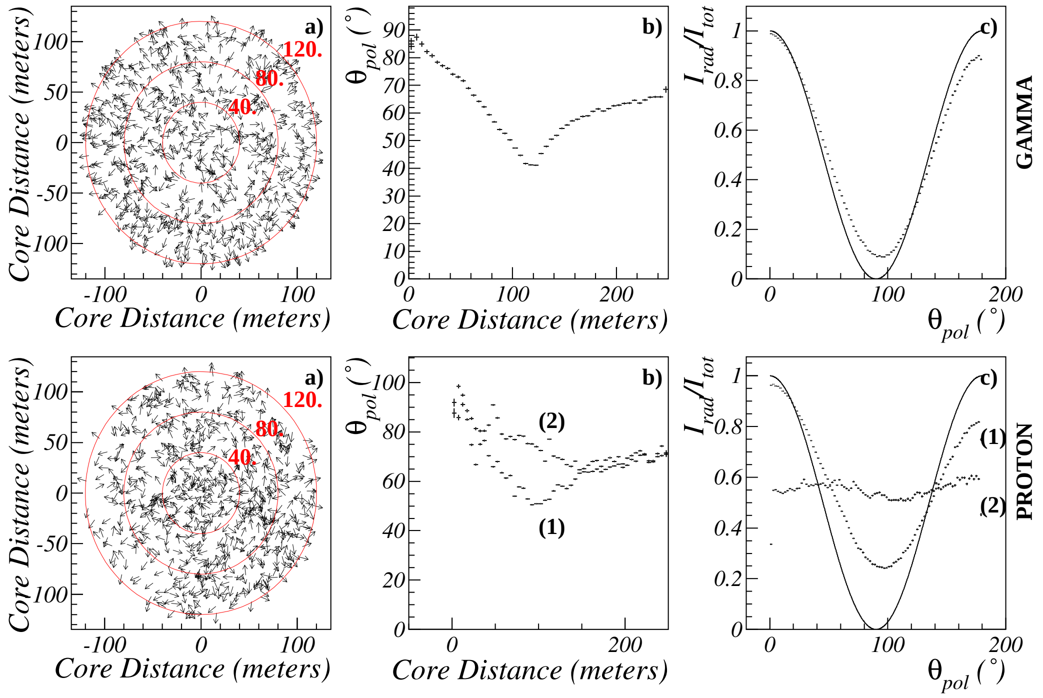

Figure 5.3: *Two examples of the polarization vector distribution on ground for a 1 TeV gamma event, top row, and in the bottom row two proton events of 3 TeV at* $0°$ *of zenith angle* **(1)**, *and* $0° - 3°$ *zenith angle* **(2)**. *In figure* **a)** *Polarization vector distribution on ground;* **b)** *Mean polarization angle over different core distances;* **c)** *Ideal radial intensity curve (continuous line) and intensity measured* **on the camera** *(dashed line) as a function of the polarization angle. The difference in figure* **c** *for protons between the event at* $0°$ *and within* $0° - 3°$ *is due to the fact that the radial direction is not aligned with the image major axis.*

the camera, transverse intensity, due to the polarizers. For gamma events this fraction ranges from 50% at close core distances to 25% around the hump. On the other hand, the *dist* parameter cut rejects images from showers whose core falls at distances greater than ~ 130 m from the hump and closer than ~ 50 m. So actually we only accept events falling within a core distance between ~ 50 m and ~ 130 m. If we take a look again at figure Fig.(5.4) and consider only events in such a range of distance the mean value of ϵ is around ~ 0.5. So the mean intensity lost in the camera by the polarizers for gamma events is around $\sim 30\%$. In figure, Fig.(5.6), the mean intensity cut off suffered by the images in the camera for different energies is represented. This plot is in complete agreement with the arguments just given, relative to the mean intensity cut off suffered by

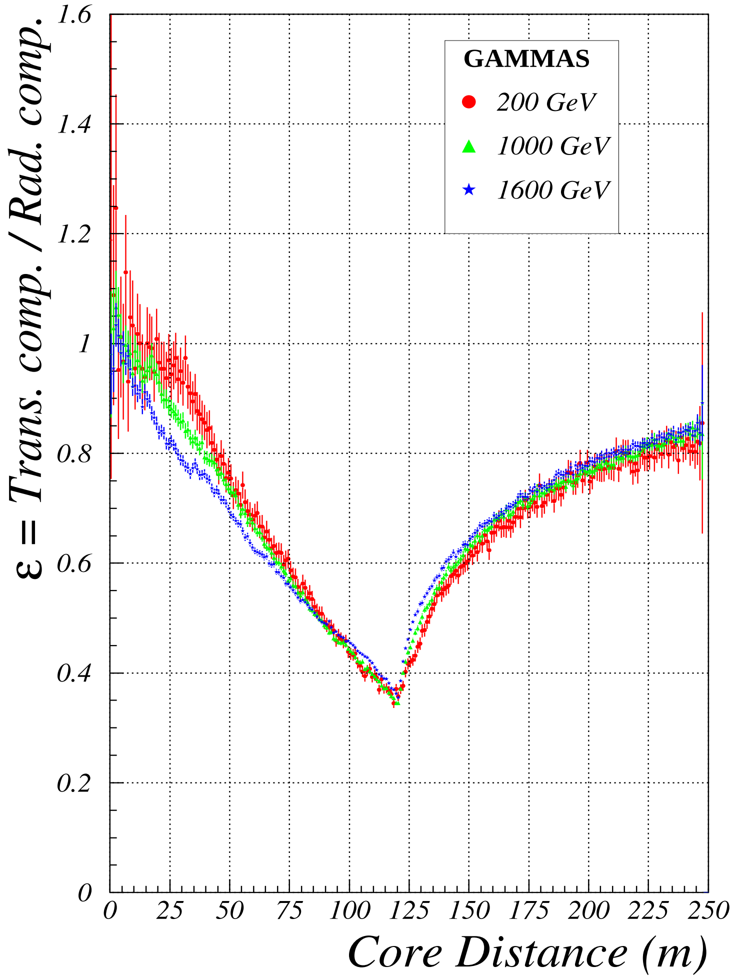

Figure 5.4: *Representation of the rate between the transverse component and radial component of the polarization vector against the core distance for three different gamma energy values. Each energy curve is a mean curve taken out of 10 gamma events generated at zero degrees of zenithal angle.*

the images extracted from figures Fig.(5.4). For background events this can not be done since information contained on ground is not translated into the camera as reflected in Fig.(5.3)c. Also in Fig.(5.7) the mean intensity cut off suffered by hadron images is represented.

ii) There is an energy dependence in the distribution of the polarization vectors on ground, although it is not very big.

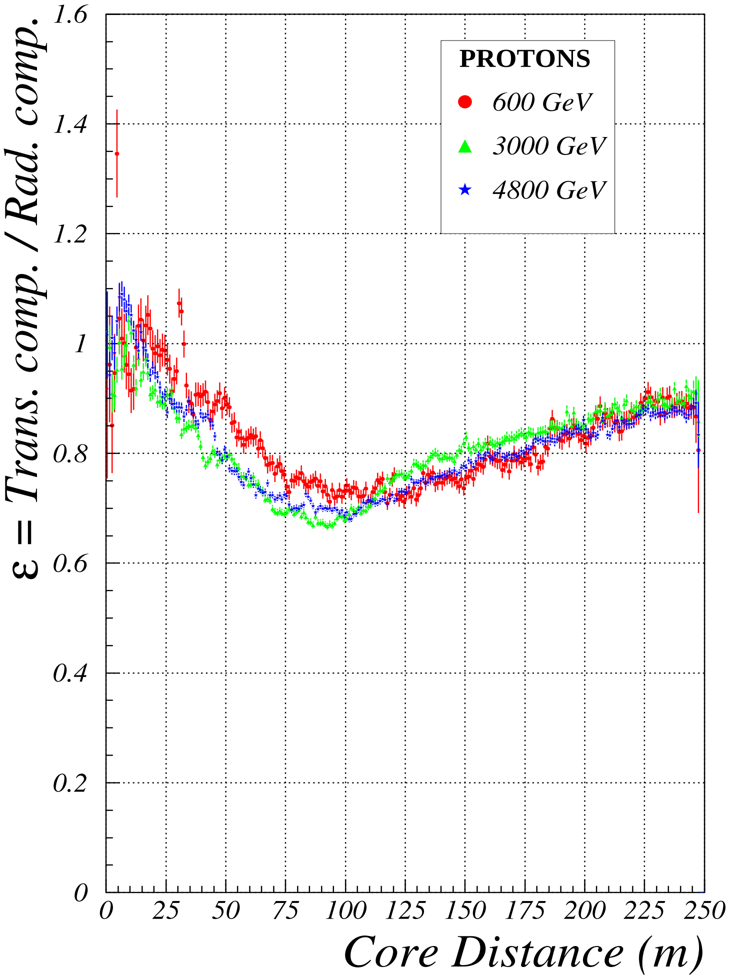

Figure 5.5: *Representation of the rate between the transverse component and radial component of the polarization vector against the core distance for three different proton energy values. Each energy curve is a mean curve taken out of 10 protons events generated within a zenithal angle between 0 and 3 degrees.*

1. **Gamma events.** The plot Fig.(5.4) shows two well defined regions with different behavior. These two regions are distances lower and higher than the hump region. At the hump the rate ϵ remains about the same for the three energies. At distances between the core and the hump, showers with higher energy tend to show a distribution on ground slightly more dominated by the radial component of the polarization vector, closer to the ideal case, higher than that of showers with lower energy. This could be

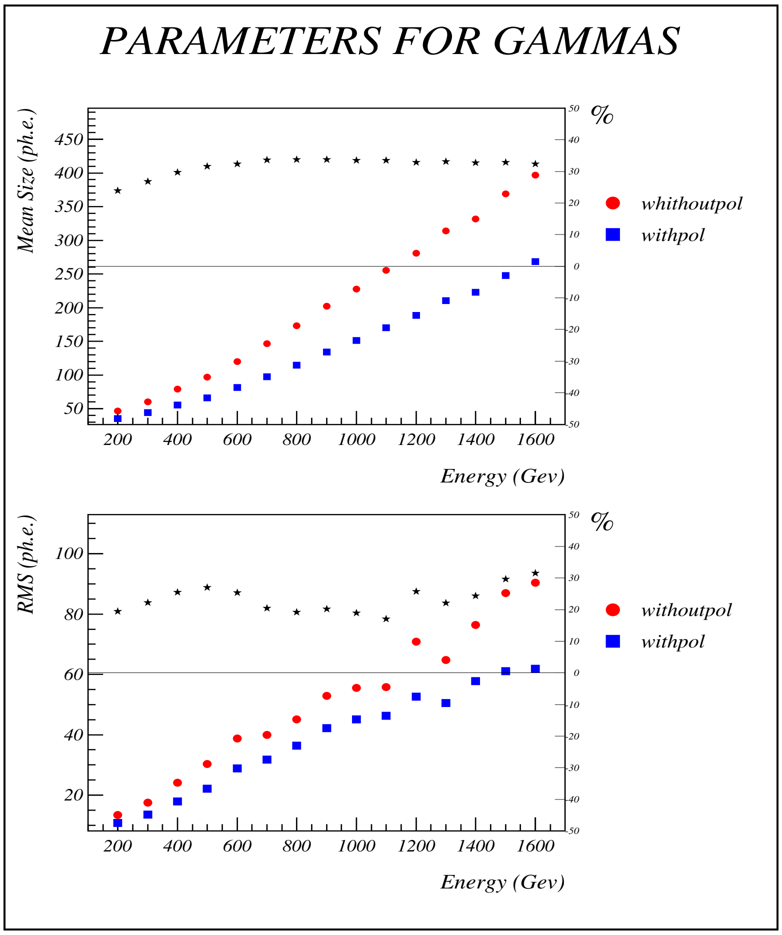

Figure 5.6: *Comparison between the mean size of gamma images with and without polarization assumption for different energies. The stars represent the difference in % between mean sizes.*

explained by the fact that shower of higher energy have their maximum at lower altitudes above ground and more penetrating power, thus particles reaching ground had suffer less from multiple scattering being closer to the ideal case. In any case at close core distances the radial direction is not so well defined and photons coming from all parts of the shower reach all close core regions. For distances greater than that of the hump the situation is the opposite. Showers of lower energy are closer to the ideal case than showers of higher energy. We could find the reason for this in the fact that showers of higher energy develop closer to the ground and thus, the Cherenkov photons reaching high core distances come from particles that had suffer more the multiple scattering effect, thus the distribution of the polarization vectors on ground is far from the total polarization assumption.

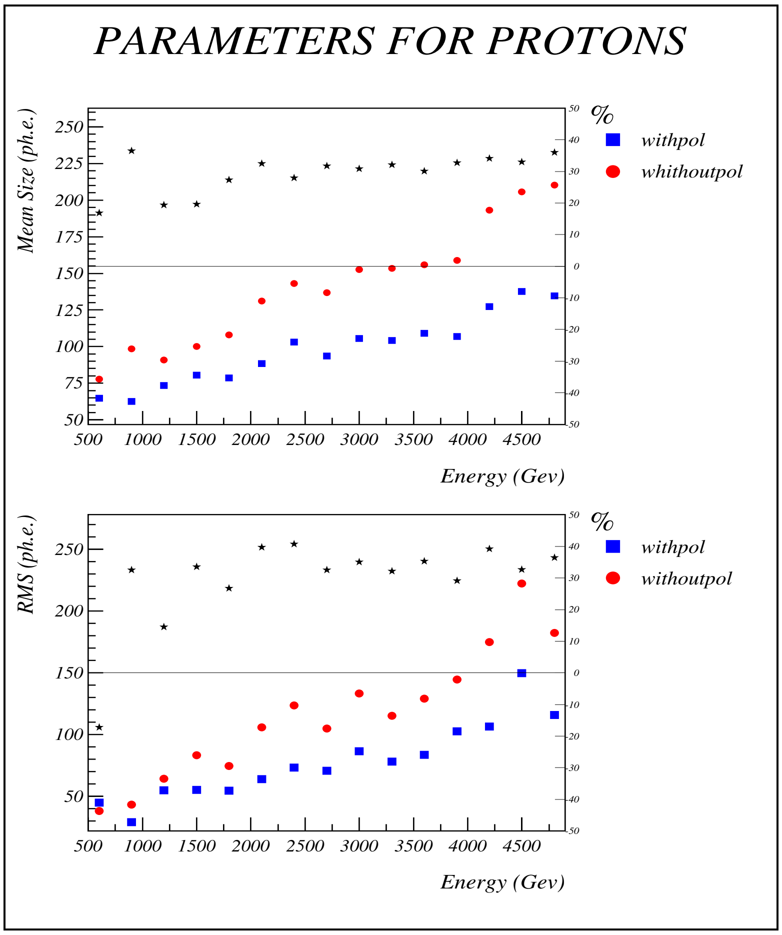

Figure 5.7: *Comparison between the mean size of proton images with and without polarization assumption for different energies. The stars represent the difference in % between mean sizes.*

2. **Proton events.** For proton events this dependence is not so well defined. Conclusions cannot be pointed out since in our simulation only background events within the zenithal angle 0(°) and 3(°) have been simulated. This effect is equivalent as limiting the field of view of the detector which has a direct impact on the shape of the lateral distribution of the showers ([11, A. M. Hillas 1991]). It is expected for this distribution to be flatter than for γ's due to the nature of hadron showers. Also in Fig.(5.5) we can see a peak at a core distance of around $\sim$ 100 meters shown at all energies.

iii) The difference between the ground distribution of the polarization vectors on ground for gamma and hadron event is due to the different nature of both gamma initiated shower and hadron initiated showers. The differences in the longitudinal development of both showers is the factor that determines the distribution of the polarization vectors on ground. Proton initiated showers are farther form the ideal case.

In the following set of plots, Fig.(5.8), Fig.(5.10) and Fig.(5.10), gamma events and hadron events are represented together for comparison. Bellow each plot the angle of polarization has been represented for four core distance intervals. We can extract from the figure that as we move towards the hump, at distances between ~ 100 and ~ 150 meters from shower core, the distribution of polarization angles gets narrower around zero degrees. It is also extracted that this effect is higher for gamma events than for hadron events.

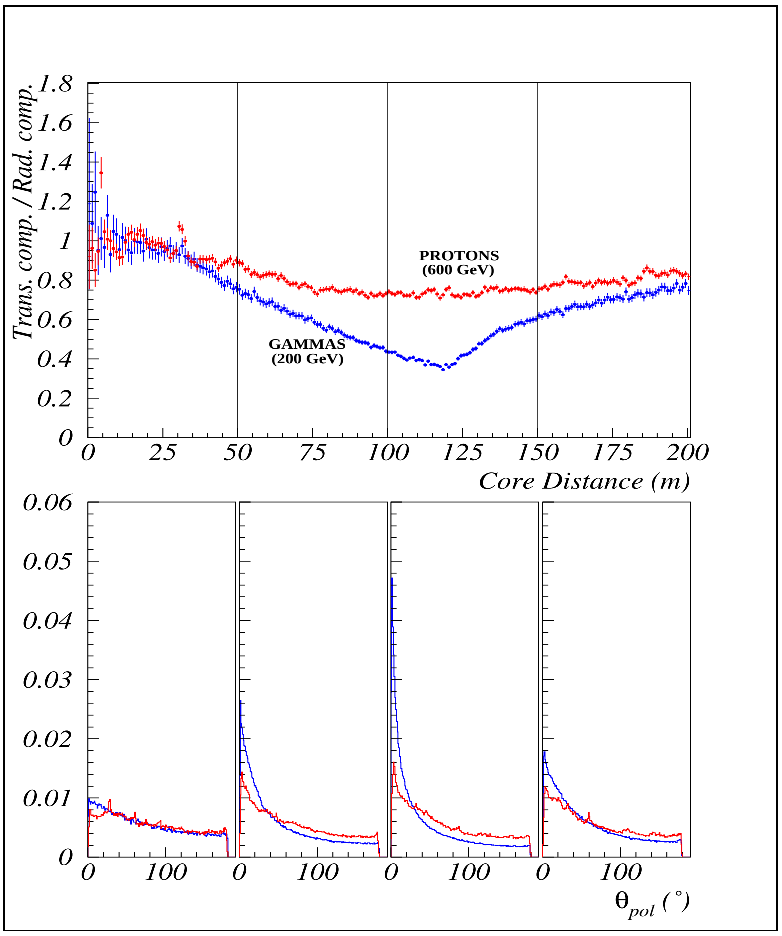

Figure 5.8: *Comparison between polarization distribution on ground for gamma and hadron events of low energy, 200 GeV and 600 GeV respectively. The angle of polarization is represented for four different core distance intervals.*

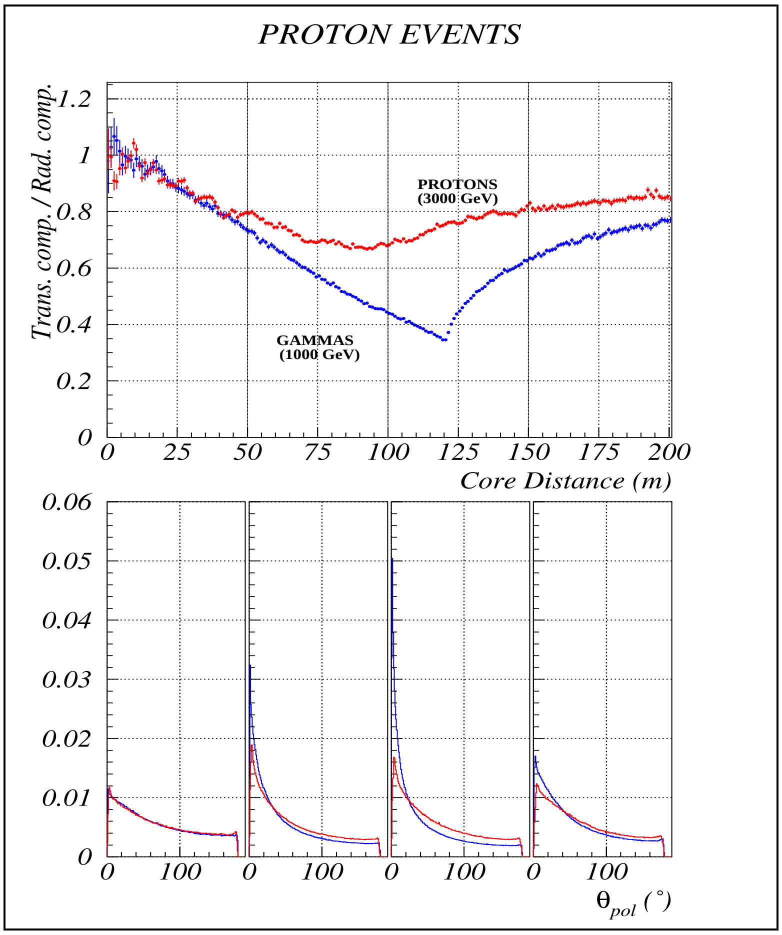

Figure 5.9: *Comparison between polarization distribution on ground for gamma and hadron events of medium energy, 1000 GeV and 3000 GeV respectively. The angle of polarization is represented for four different core distance intervals.*

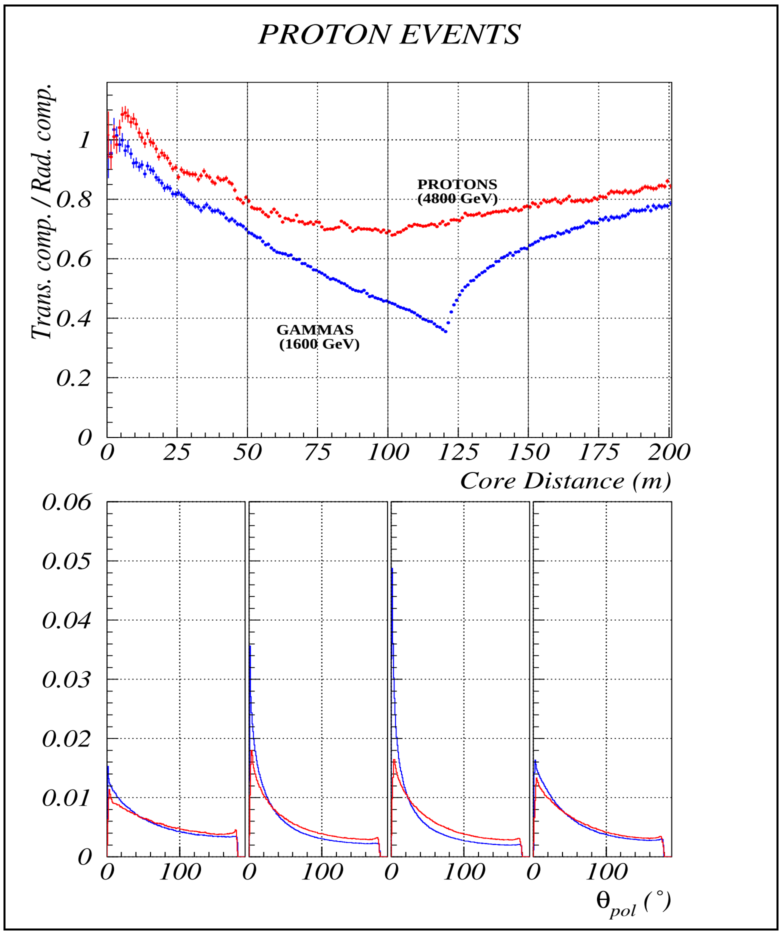

Figure 5.10: *Comparison between polarization distribution on ground for gamma and hadron events of relatively high energy, 1600 GeV and 4800 GeV respectively. The angle of polarization is represented for four different core distance intervals.*

Dependence of the intrinsic polarization of the Cherenkov radiation with height production of Cherenkov photons in the atmosphere: From figures Fig.(5.4) and Fig.(5.5) we could extract several indirect conclusions.

In previous Chapters we have explained that for gamma events, the Cherenkov radiation produced in the atmosphere that reaches the hump, comes from higher layers of the shower. An examples is given in Fig.(5.11). It is expected for the *angle of polarization* (θ_{pol}) to be closer to zero in the first steps of the shower development where the conditions are closer to the ideal case. In order to explain the dependence of the polarization distribution with height above the observation level it is necessary to study the polarization distribution in planes perpendicular to the shower axis along the longitudinal development and compare it with the ideal case. For this small study 10 gamma events of energy 1000 GeV and 10 hadron showers of energy 3000 GeV have been simulated with the first interaction point fixed at 35 Km above sea level, in order to merge together different events. In Fig.(5.12) the height of Cherenkov photon production versus θ_{pol}, is represented. The height interval has been chosen such as to represent one radiation length (37 g/cm^2) although the simulation program used, CORSIKA, does not follow the exponential atmosphere model needed to obtain the height of light production as a function of the radiation length.

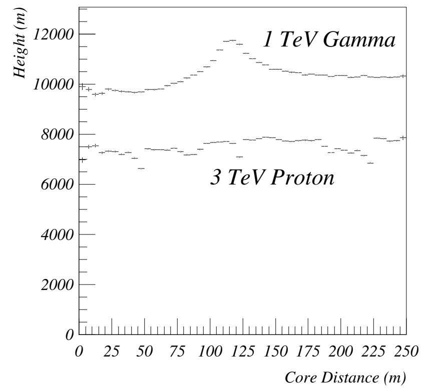

Figure 5.11: *Mean value of height of Cherenkov photon production against core distance for a gamma and hadron event.*

The behavior shown in Fig.(5.12) can be easily explained on the basis of the ideal case. First, in the early steps of the shower development the particles had suffer less from multiple scattering than particles produced in later steps of the shower development, being closer to the ideal case. Secondly, the differences between gamma and proton events can be easily explained on the basis of the differences in the transverse development along the longitudinal development, where on average particles have higher transverse momentum and the shower spreads more. In the last case particles do not keep the track of the primary particle and move away from the ideal case. The vertical bars in Fig.(5.12) represent the height interval within which the mean value of θ_{pol} has been obtained. For the horizontal bars, since the distribution of θ_{pol} (Fig.(5.13)) is asymmetric, we obtained a *left* width and a *right* width representing the interval within which 16%-50% and 50%-84% of the events are contained respectively. The right width is higher due to the existence of a tail in the θ_{pol} distribution towards high values of θ_{pol} (Fig.(5.13)).

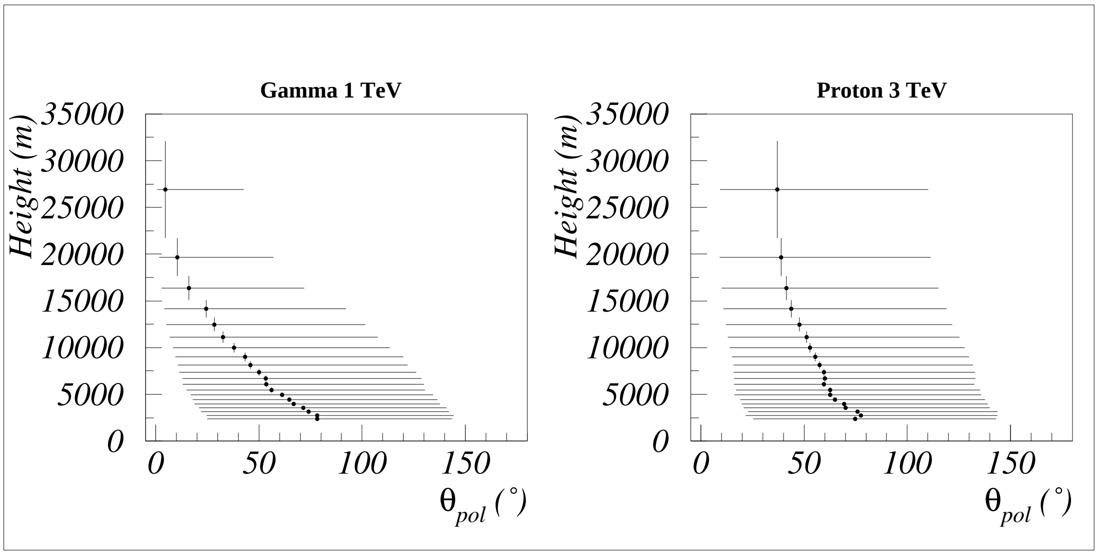

Figure 5.12: *Dependence of the polarization angle θ_{pol} with height of Cherenkov photon production both for gamma events of energy 1 TeV, left, and proton events of energy 3 TeV, right.*

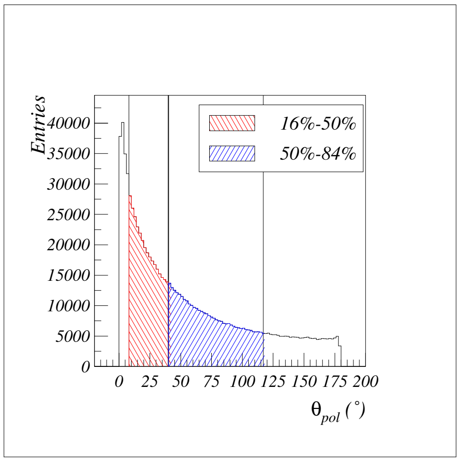

Figure 5.13: *θ_{pol} distribution including all heights, for a gamma event of 1 TeV with the first interaction point fixed at 35 km above sea level. Lines represent limits within which 16%-50% and 50%-84% of the events are contained.*

Dependence of the arrival time distribution of Cherenkov photons at ground with the polarization angle: To study the dependence of time of arrival of Cherenkov light at ground with the polarization distribution on ground, we simulated a 1 TeV gamma shower at zero degrees zenith angle and a 3 TeV proton shower at zero degrees zenith angle, both with the first interaction point fixed at 35 Km above sea level. To see the correlations between the Cherenkov photons and its time of arrival on ground, we will separate the Cherenkov photons in two groups defined by $\theta_{pol} > 32°$ and $\theta_{pol} < 32°$. The value of 32° was chosen because it is the median value of the θ_{pol} distribution for the shower, equivalent as to consider values of $abs(cos(\theta_{pol})) > 0.85$. In figure Fig.(5.14) the distribution for abs(cos(θ_{pol}) is shown for the 1 TeV gamma event.

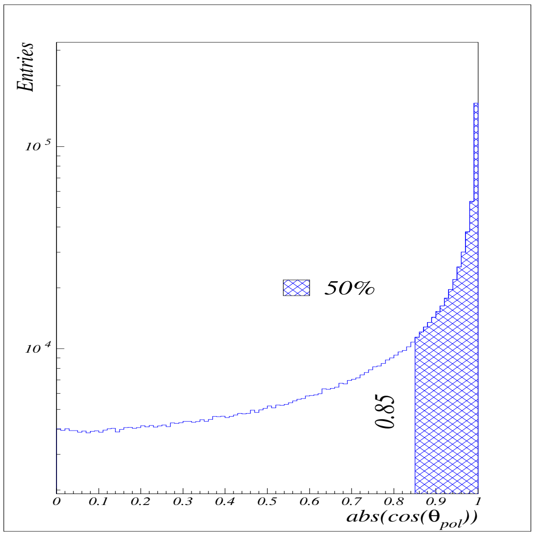

Figure 5.14: *abs(cos(θ_{pol})) distribution for the 1 TeV gamma event. A value of* $abs(cos(\theta_{pol})) > 0.85$ *is equivalent as to have angles* $\theta_{pol} < 32(°)$.

Once we have the polarizers approximation defined, we plotted mean arrival time versus the core distance for events with abs(cos(θ_{pol})) > 0.85, considered for the polarizers approximation, and compare it with the same distribution for all the events. To obtain the mean arrival time at a given core distance, we take the median of the time distribution at that distance. We also obtain the rms of the time distribution, taken such as to contain the 34% of the events between the 50% and the 84% of the total events. This way we identify the rms of the time distribution with the decay time of the Cherenkov pulse. This fall time seems to be more sensitive to the primary species ([36, V. R. Chitnis and P. N. Bhat 1999]). As an example in figure Fig.(5.15) several time distributions are plotted for three different core distance intervals for a 1 TeV gamma event and a 3 TeV proton event, both at 0° with the first interaction point fixed at 35 Km above sea level.

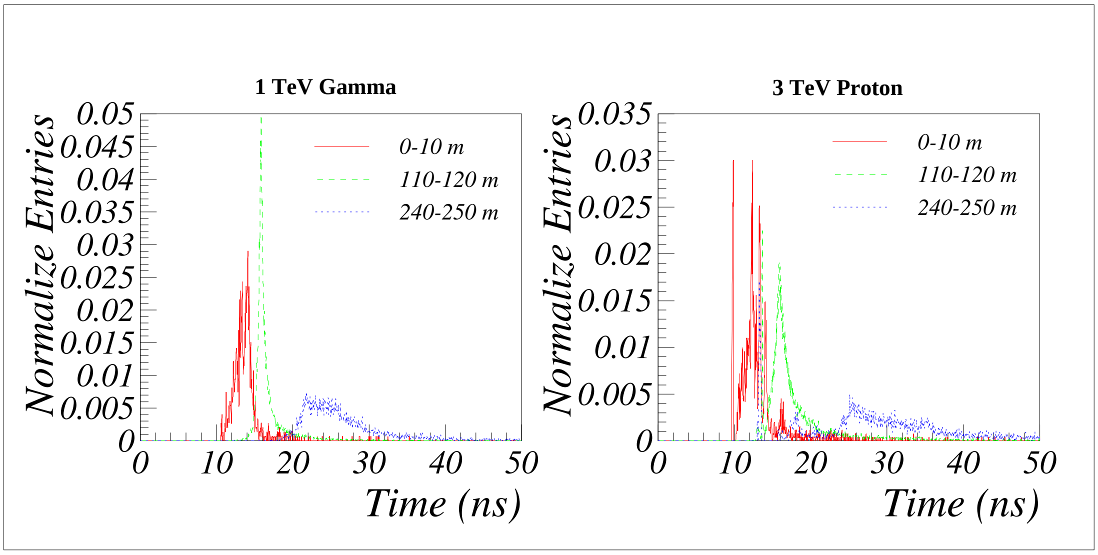

Figure 5.15: *Time profiles for the not polarization case at three different core distances for a 1 Tev gamma event and for a 3 TeV proton event both at 0° zenith angle with the first interaction point fixed at 35 Km above sea level.*

The final results of the mean arrival time and rms versus core distance are collected in figures Fig.(5.16) for the gamma event and Fig.(5.17) for the proton event. Three types of curves are represented in the plots, the circles stand for the not polarization assumption, the squares stand for the polarization assumption and stars represent the difference in % between *with* and *without* polarization (related to the not polarization case).

From plots Fig.(5.16) and Fig.(5.17) we extract the following conclusions:

1) The value of the mean arrival time of the Cherenkov light front at different core distances does not depend on the polarization distribution on ground. The difference in both distributions, with and without the polarizers approximation, is negligible on the basis of Fig.(5.16) and Fig.(5.17). The above stated applies for the gamma event and for the proton event.

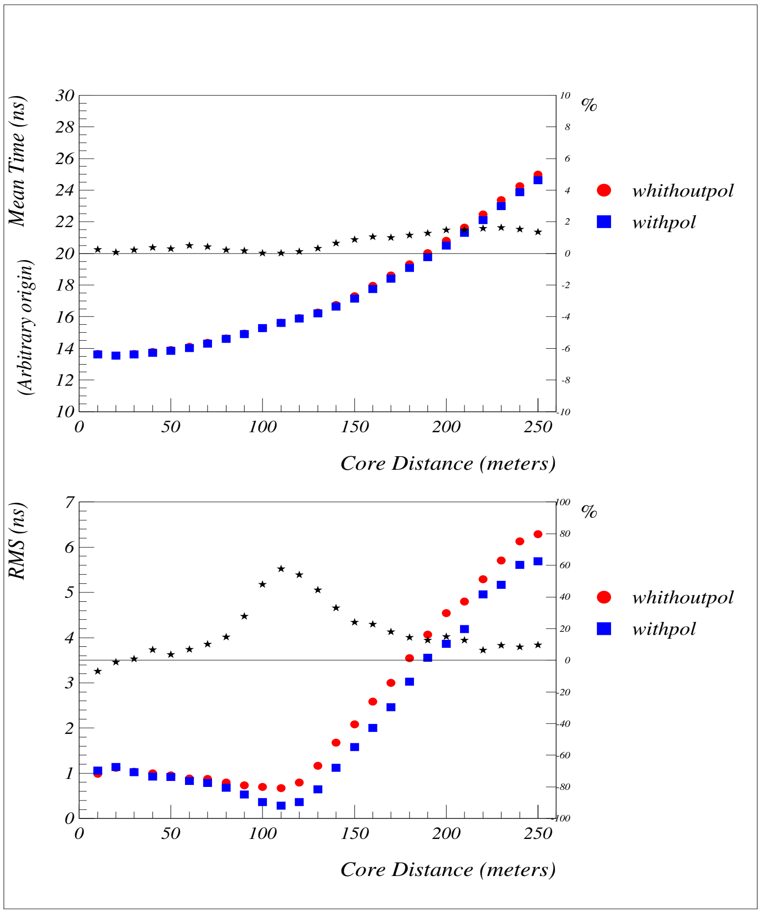

Figure 5.16: *Mean arrival time at different core distances for a 1 TeV gamma event at zero degrees zenith angle with the first interaction point fixed at 35 Km above sea level. On the top plot the arrival mean time at different core distances is represented. The origin of the y-axis is arbitrary. On the bottom plot the rms of the time distribution at different core distances is represented.*

2) The width of the Cherenkov light pulse, especially the value of the fall time, depends on the polarization distribution on ground and hence depends on the core distance. The Cherenkov light pulse becomes narrower in the polarizers approximation. This state is valid both for gamma and hadron events. For gammas, the effect becomes more prominent as we move away from the core until it reaches a maximum around the hump region. Hence, the arrangement of polarizing filters on the camera will reduce the pulse width, by reducing the tail of the pulse, what might allow lower ADC gates. For the proton event this reduction is also shown although it is not so prominent as it is for the gamma event.

It is not the aim of this work to discuss the modifications of the Cherenkov light pulses with the arrangement of polarizing filters on the camera, proposed in this work, and would be left for further studies.

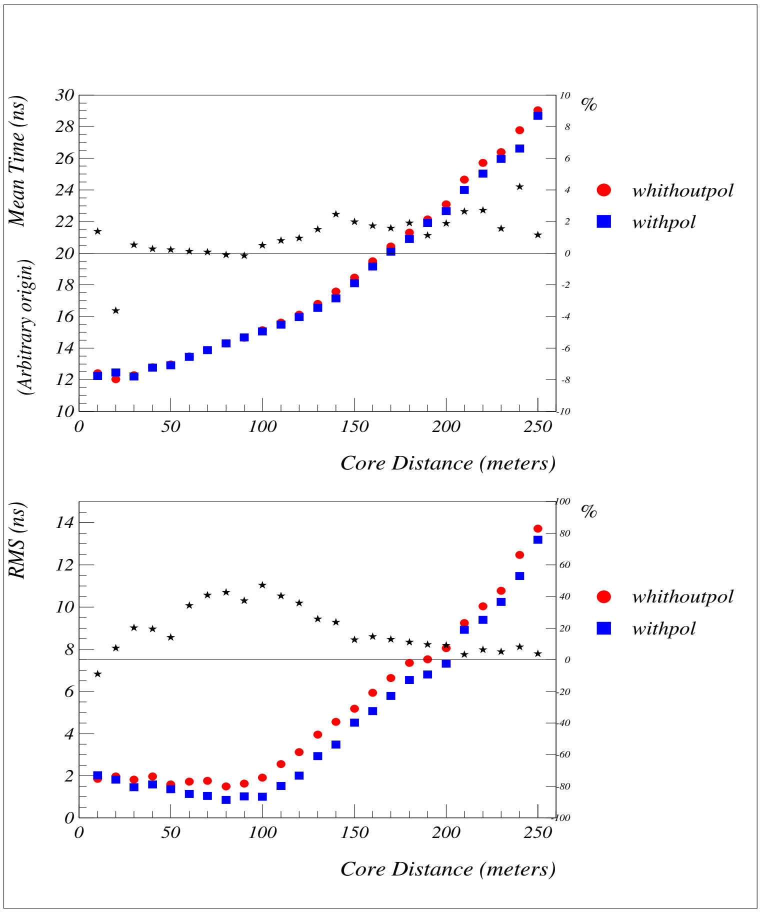

Figure 5.17: *Mean arrival time at different core distances for a 3 TeV proton event at zero degrees zenith angle with the first interaction point fixed at 35 Km above sea level. On the top plot the arrival mean time at different core distances is represented. The origin of the y-axis is arbitrary. On the bottom plot the rms of the time distribution at different core distances is represented.*

5.2 Energy Threshold

There are two parameters with great relevance for determining the statistics of the detected showers and hence the performance of the telescope, effective area and energy threshold. These two parameters depend on several factors such as the mirror collection area, photon to photo-electron conversion factor and trigger condition imposed by the pixel trigger threshold q_0.

Both parameters, effective area and energy threshold, are obtained for gamma and hadron events in this work, in order to make a comparison between the common situation and the polarizers assumption. The obtainance of the effective area and energy threshold of the telescope in the first case allows us to test the performance of the telescope simulated and the second one to see the effect of the polarizers on such performance in order to compare it with the common case. For this purpose, first the probability curves P(E,r), obtained with the method explained in chapter 4, are generated using the showers simulated at each energy (tables (4.16) and (4.17)). We can see this curves both for γ and proton events in figures Fig.(5.18) and Fig.(5.20) respectively. Also in figures Fig.(5.19) and Fig.(5.21) the probability detection curves are represented for comparison for different primary energies and with and without polarization assumption, both for gammas and proton events respectively.

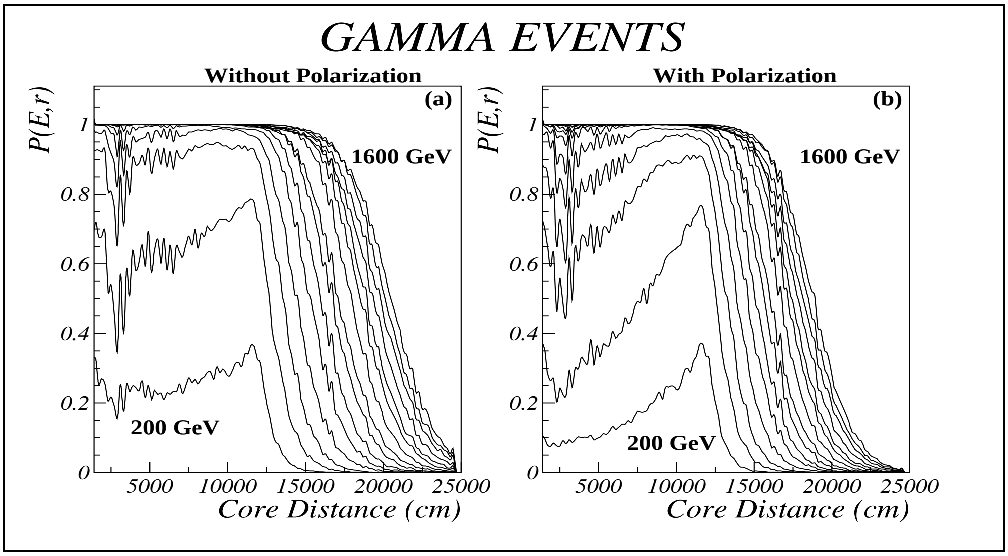

Figure 5.18: *Trigger probability as a function of the energy and core distance. In plot* **(a)** *the probability curves for the not polarization case is represented, while in plot* **(b)** *we have the probability curves for the polarization case. The energy ranges from 200 GeV up to 1600 GeV.*

With the aid of these figures we extract the following conclusions:

i) Gamma events: The probability curves, in general, give an idea of the response of the telescope to the arrival of the Cherenkov light coming from an EAS, as a function of the primary energy of the particle initiating the shower and the impact parameter of the shower. One fact that should be keep on mind in order to understand these plots is the following. The pool of Cherenkov light falling on ground may be considered as composed of three parts ([11, A. M. Hillas 1990]), mainly: 1) A ring of light peaking typically near $\sim$ 120 m from the shower axis where intensity fluctuations from shower to shower are low. In a low energy gamma ray this is the dominant pattern of light falling on ground. 2) If the tail of the shower penetrates close to the observer, its radiation has not spread an contributes with a peak near the shower axis. This time intensity fluctuations are very high from shower to shower. 3) Light from muons. In Fig.(5.18)**a** the probability curves for the common case are represented. The probability curves reflect the lateral distribution of the showers. At low energies the peak near the shower axis is shown as well as the ring of light around $\sim$ 120 m from the shower axis.

Two facts contribute to the differences found between the probability curves obtained for *with* and *without* the polarizers assumption, between plots Fig.(5.18)**a** and Fig.(5.18)**b**. The comparison between both is shown in Fig.(5.19).

- **The shower energy**. The amount of Cherenkov light produced in an EAS grows with the energy of the primary particle initiating the shower. At low energies we have less Cherenkov light than at high energies and the effect of the polarizers plays a more important role. At energies higher than $\sim$ 1 TeV the behavior of the probability curves is the same at distances lower than that of the hump and shows a small difference at energies higher than that of the hump.

- **The core distance**. The effect is more prominent at low energies where the amount of light collected is critical. At low energies the probability of detecting a shower at close core distances is reduced by around 50% when using polarizers. Fluctuations from shower to shower at close core distances are high and at close core distances the radial direction is not so well defined. Around the hump, where we are close to the ideal case and fluctuations from shower to shower are lower, the probability of detecting a shower it is not affected by the use of polarizers on the camera.

All the modifications of the probability curves have a direct effect in the collection areas where the difference between *with* and *without* polarizers can be quantify. In figure Fig.(5.22) the collection areas achieved by the simulated telescope in this work are shown, and will be commented later.

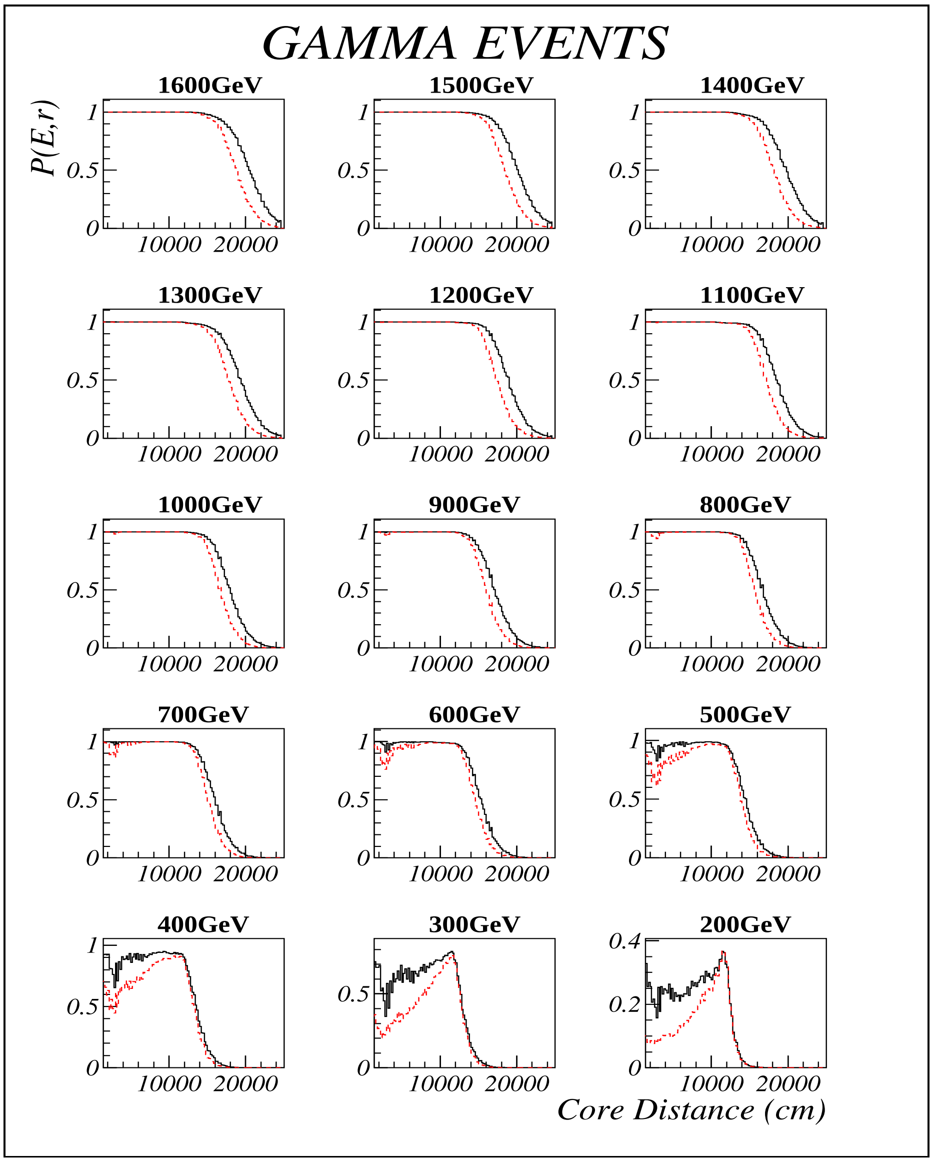

Figure 5.19: *Trigger probability curves for gamma events as a function of the core distance for different energies. In red dashed line the polarization case is represented while the not polarization case is represented in continuous black line.*

ii) Proton events: The probability curves for protons are different than for gamma events (Fig.(5.20)**a** and Fig.(5.20)**b**). The differences arises mainly at close core distances. In general proton showers of a given energy penetrate more in the atmosphere than their gamma counterparts being the reason for the existence of the bulk of light near core distances event at low energies. We can also find several differences in the probability curves between *with* and *without* polarizers. Although the differences exit, the dependence with the energy is not so well defined than it is for gamma events, and the differences between both cases is about the same at all energies. The dependence with the core distance is also small and the difference it is about the same at all core distance. This reflects the *unpolarized* nature of the light from proton showers and it is in agreement with plot Fig.(5.5).

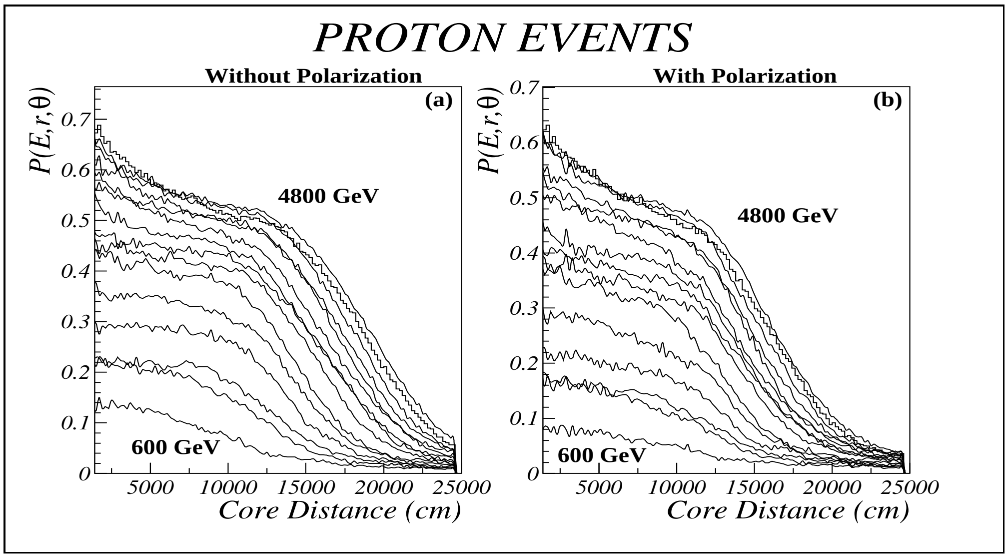

Figure 5.20: *Trigger probability as a function of the energy and core distance. In plot* (**a**) *the probability curves for the not polarization case is represented, while in plot* (**b**) *we have the probability curves for the polarization case. The energy ranges from 600 GeV up to 4800 GeV.*

Because only 100 proton showers were generated at each energy, fluctuations in the trigger probability derived from shower physical origin at low energies, are bigger than at higher energies due to the bigger fluctuations from shower to shower at low energies. The reduction of the trigger probability is reflected in the effective area that would be explained later on.

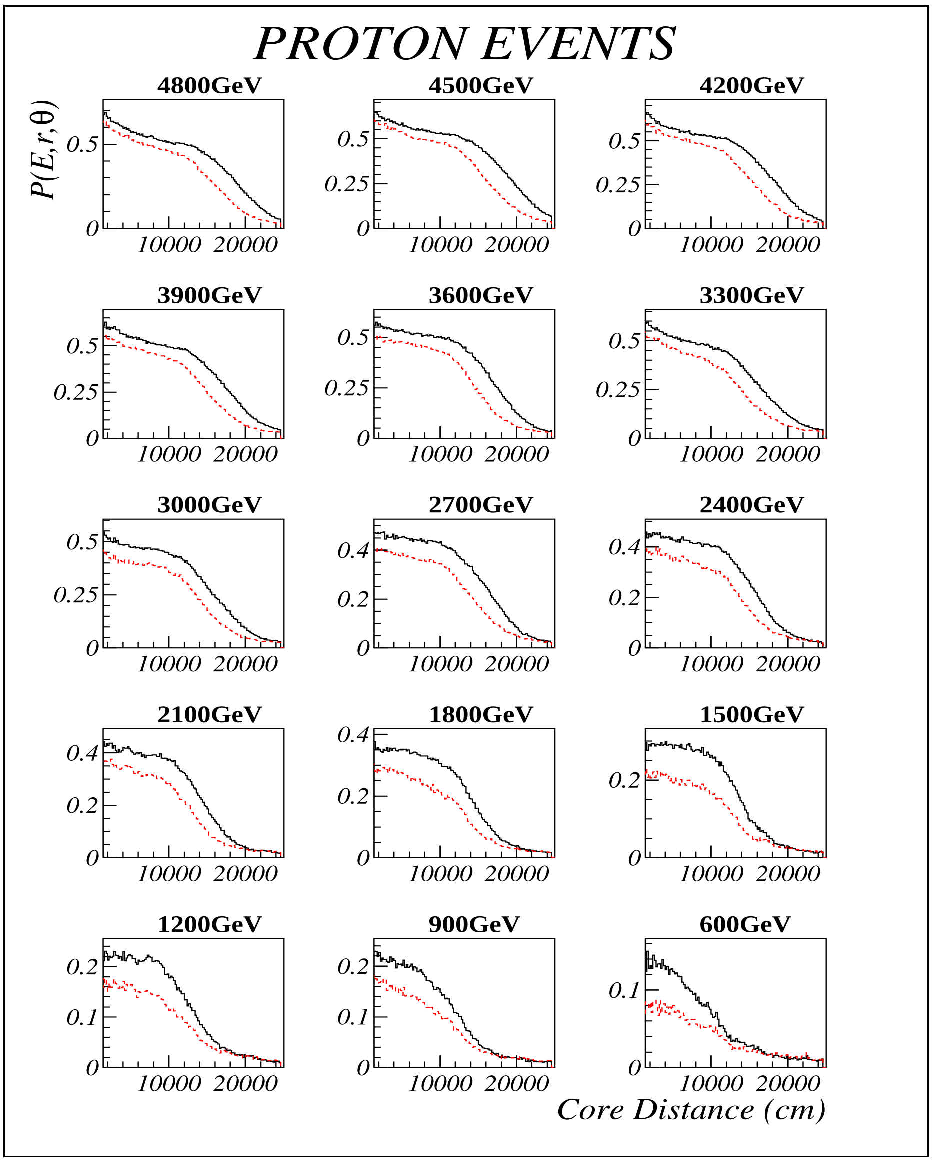

Figure 5.21: *Trigger probability curves for proton events as a function of the core distance for different energies. In red dashed line the polarization case is represented while the not polarization case is represented in continuous black line.*

In figure Fig.(5.22) the **effective areas** are plotted for gamma and hadron events. Together with the value of the effective area are plotted the errors obtained. The gray shadowed region represents the error limits for the not polarization case and the error bars are for the polarization case. To obtain the errors we consider a distribution of N_{tot} telescopes and two probability states, triggered or not triggered. We associate this to a binomial distribution of N_{tot} events with p=$\frac{N_{triggered}}{N_{tot}}$ to evaluate the error in the effective area as:

$$\Delta N_{triggered} = (Area_{total}/\sqrt{N_{tot}}) \cdot \sqrt{p \cdot (1-p)} \tag{5.2}$$

where $Area_{total} = 250^2 \cdot \pi\ m^2$, and N_{tot} is the number of telescopes simulated (100 showers $\times$ 8719 telescopes). The different images of a shower in different telescopes are correlated, meaning that the statistic of independent events is smaller than N_{tot}. It is difficult to estimate the effect of this correlation. Being conservative we will consider the images totally correlated and replace N_{tot} with 100, so the final expression will be:

$$\Delta N_{triggered} = (Area_{total}/\sqrt{100}) \cdot \sqrt{p \cdot (1-p)} \tag{5.3}$$

Once we have introduced the way the effective area is evaluated and by looking at Fig.(5.22), we can conclude that:

1) The effective area is always smaller when using polarizers. Just by looking at Fig.(5.22) we can see that at all energies, and both for gammas and protons, the effective area is always smaller. In Fig.(5.22) the two bottom plots represent the mentioned difference in percentage showing the loss in effective area. Even with the reduction of the trigger condition from 2NN/271 > 10 ph.e. to 2NN/271 > 8 ph.e. no gain is achieve by the use of polarizing filters on the camera of an IACT. For gammas, from figure Fig.(5.19), we can see that the main loss in effective area comes from the reduction of the trigger probability at close core distances. The cut imposed in the *dist* parameter in the image analysis only accepts showers whose core falls within a core distance between $\sim$ 50 m and $\sim$ 130 m, hence any lost in collection area in any distance range out of this one, does not have to much relevance.

2) The loss in effective area is bigger **for protons** than for gammas. This is true at all energies. If we take a look at the bottom plots of Fig.(5.22), where the difference in percentage is plotted, we can see that for gamma events the difference tends to a constant value for energies above 1400 GeV. For protons the fluctuations are bigger although it seems that the loss of effective area tends to be smaller as we move up towards higher energies. The values of the effective area are summarized in tables (5.1) and (5.2) for a better comparison, both for gammas and protons respectively. The difference in percentage, related to the not polarization case, between the effective areas obtained *with* and *without* polarization is also shown.

ENERGY (GeV)	Without Pol. (m^2)	With Pol. (m^2)	Diff. (%)
200	15397.00	12004.85	**22.03**
300	40493.95	32162.76	**20.57**
400	58182.57	50197.95	**13.72**
500	68833.98	61061.95	**11.29**
600	78401.50	69964.24	**10.76**
700	85822.90	76265.05	**11.13**
800	93487.05	82223.11	**12.04**
900	98301.78	85997.20	**12.51**
1000	107808.1	93193.85	**13.55**
1100	114731.1	98437.35	**14.20**
1200	119217.9	101907.2	**14.52**
1300	124136.3	105800.6	**14.77**
1400	129589.0	109941.1	**15.16**
1500	134434.5	114038.6	**15.17**
1600	136845.3	116084.8	**15.17**

Table 5.1: Effective areas for gammas.

ENERGY (GeV)	Without Pol. (m^2)	With Pol. (m^2)	Diff. (%)
600	4235.07	3082.28	**27.22**
900	8993.73	6718.33	**25.29**
1200	11878.5	8481.4	**28.59**
1500	17056.3	11420.5	**33.04**
1800	21644.4	15108.1	**30.19**
2100	25912.6	18733.1	**27.70**
2400	31782.4	23156.2	**27.14**
2700	35100.7	25408.4	**27.61**
3000	37320.9	27394.9	**26.59**
3300	42541.7	31327.9	**26.35**
3600	48652.4	35904.6	**26.20**
3900	52795.4	39364.8	**25.43**
4200	52881.9	39547.4	**25.21**
4500	57172.6	42818.9	**25.10**
4800	54675.3	40708.8	**25.54**

Table 5.2: Effective areas for protons.

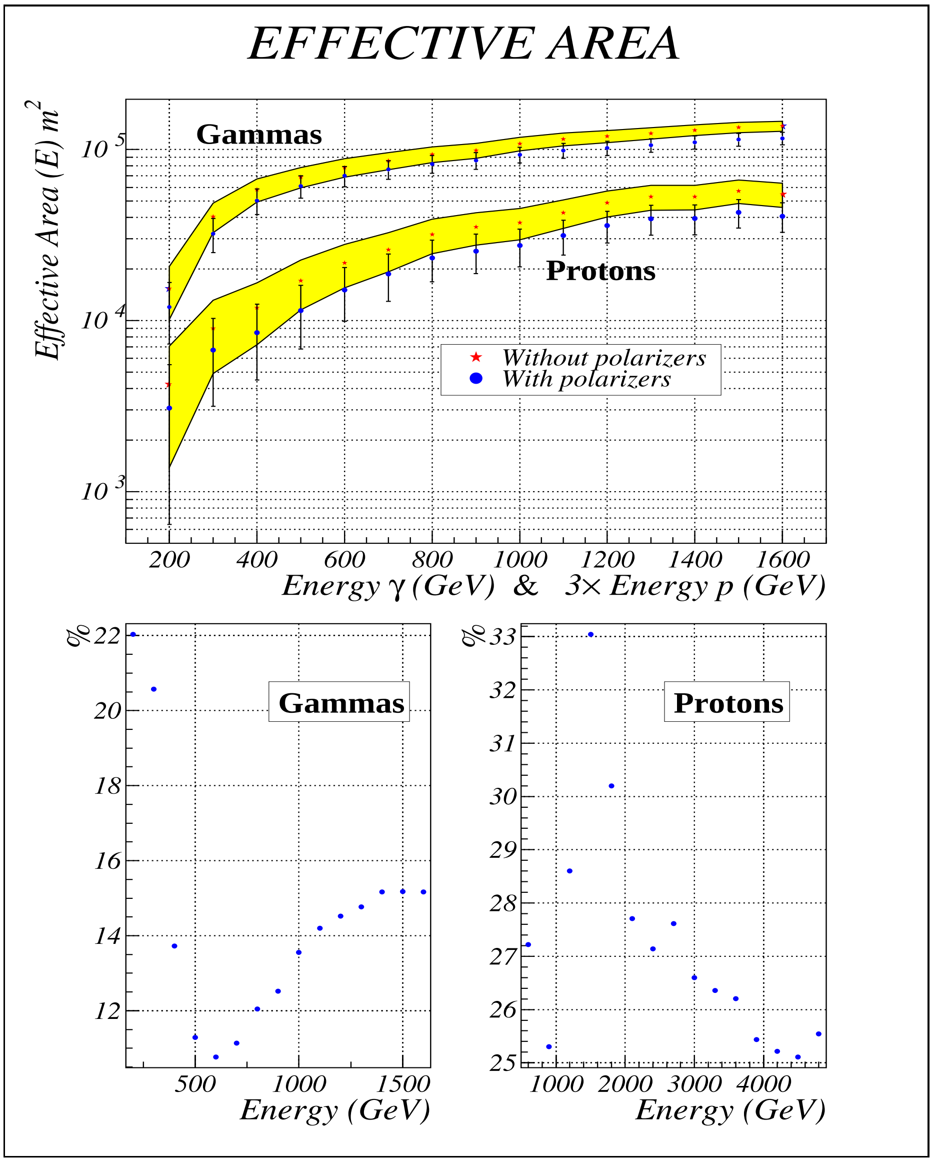

Figure 5.22: *Effective Areas.*

With the effective areas and a given differential power law spectra (page 103) we can obtain the differential rates achieved by the simulated telescope for gammas and hadron events. In Fig.(5.23) the differential rates are plotted for the common situation and the polarizers approximation. Two things can be pointed out form this figure:

1) The rates with polarizers are reduced both for gamma and proton events. This result was already derived from the effective area results. The rate for

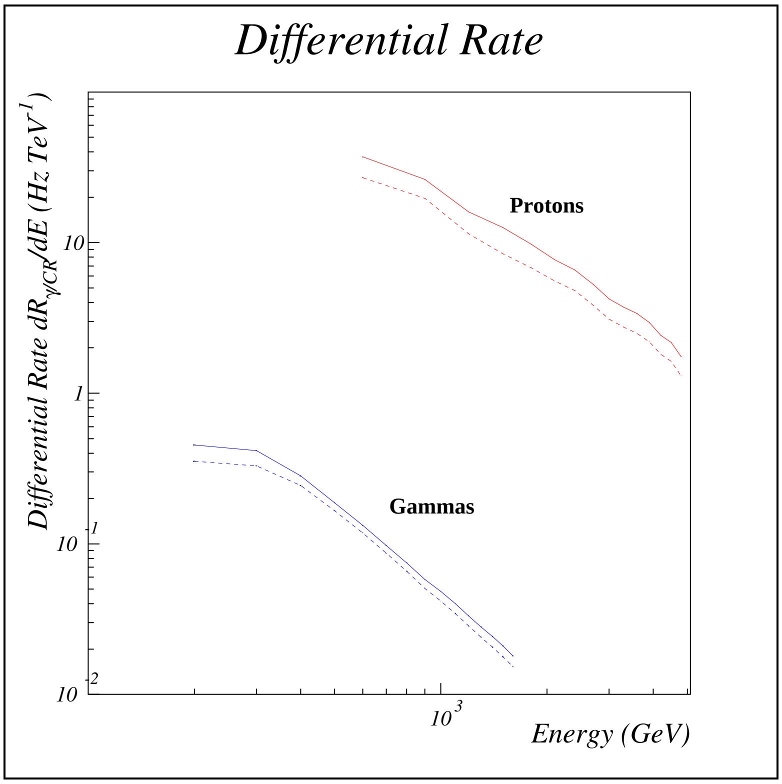

Figure 5.23: *Differential rate for gammas and hadron events both with and without polarization assumption.*

protons is reduced more than for gamma events.

2) The energy threshold of a telescope is determined by the energy at which the detection rate for gammas has a maximum. In our plots the maximum detection rates are not reach either for gammas nor for protons. This indicates that the energy threshold of the telescope simulated is somewhere bellow 200 GeV. In determining the energy threshold two facts come into play, the telescope features and the primary energy gamma spectra. The threshold depends weekly on the power law index ([19, A. Konopelko 1998]) so the reason for such a low threshold has to be looked in the features of the telescope simulated.

5.3 Image Parameters

The last point of our work covers the study of the Hillas image parameters. In Chapter 3 we explained our expectations of how these parameters should be modified on the basis of three regions defined over the image (page(54)). Now we will present the results concerning the modifications found in the Hillas image parameters centering the study on the shape parameters **length** and **width** and on the orientation parameter *alpha*. In the previous point we have seen that a direct effect of the polarizers is the intensity cut off suffered by the images, so we will present the modifications of the **size** parameter in order to quantify that loss. Finally, the quality factor Q is obtained in order to see the effectiveness of our experimental setup.

Length and Width parameters. Several conclusions can be extracted from figures Fig.(5.24), Fig.(5.25), Fig.(5.26) and Fig.(5.27) where the mean length and width of images is represented for gammas and protons, for different energies, together with the rms of the distributions.

- Images become narrower and more compact. For gammas the reduction found for the **length** parameter is a little bit less than 10% and remains constant at all energies, while for protons the reduction found is between 10% and 20% reaching the $\sim$ 35% at the lowest energies generated. The fluctuations are bigger from energy to energy. For the **width** parameter this reduction is less than 20% for gammas and constant with energy except at low energy values where the reduction is lower. For protons the reduction is between 15% and 25% with bigger fluctuations from energy to energy (plots of the Mean value).

- The distributions of the **length** and **width** parameter at each energy for gammas become narrower, being the values of the length and width parameter better distributed around the mean value. For protons both, length and width distributions, are flattened (plots of the RMS value).

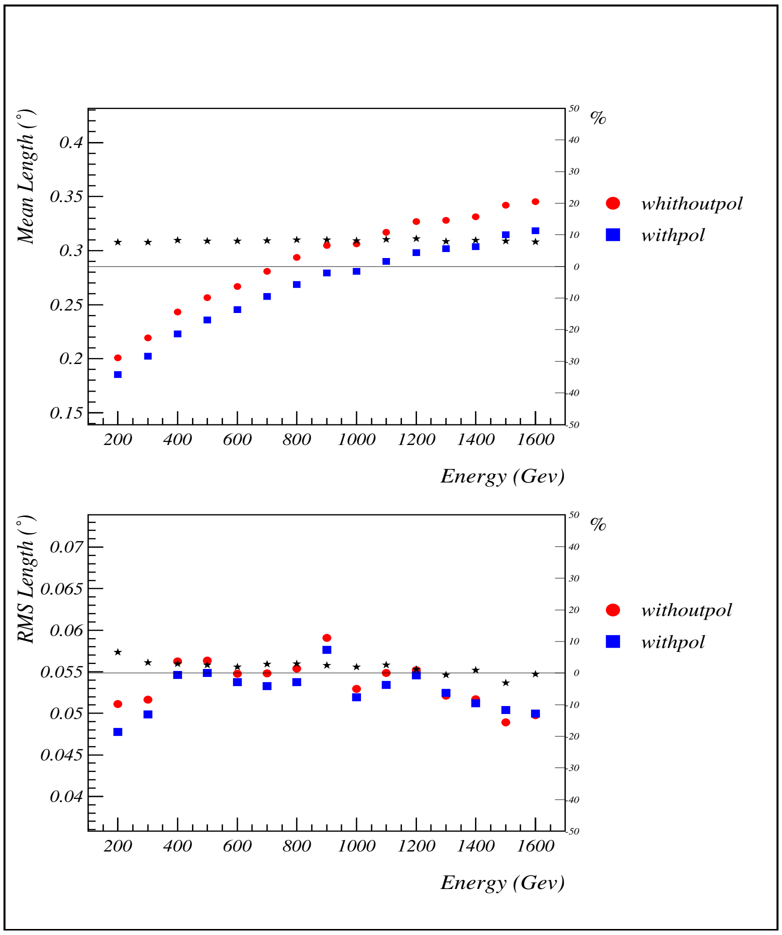

Figure 5.24: *Comparison between the mean length of gamma images with and without polarization assumption for different energies. The stars represent the difference in % between mean sizes.*

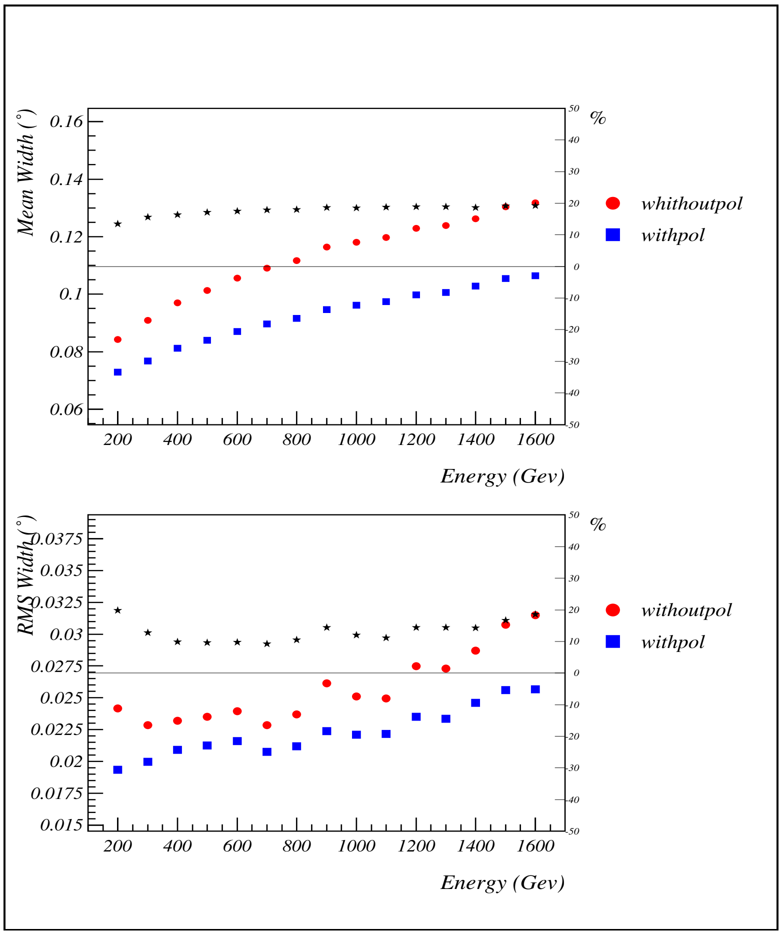

Figure 5.25: *Comparison between the mean width of gamma images with and without polarization assumption for different energies. The stars represent the difference in % between mean sizes.*

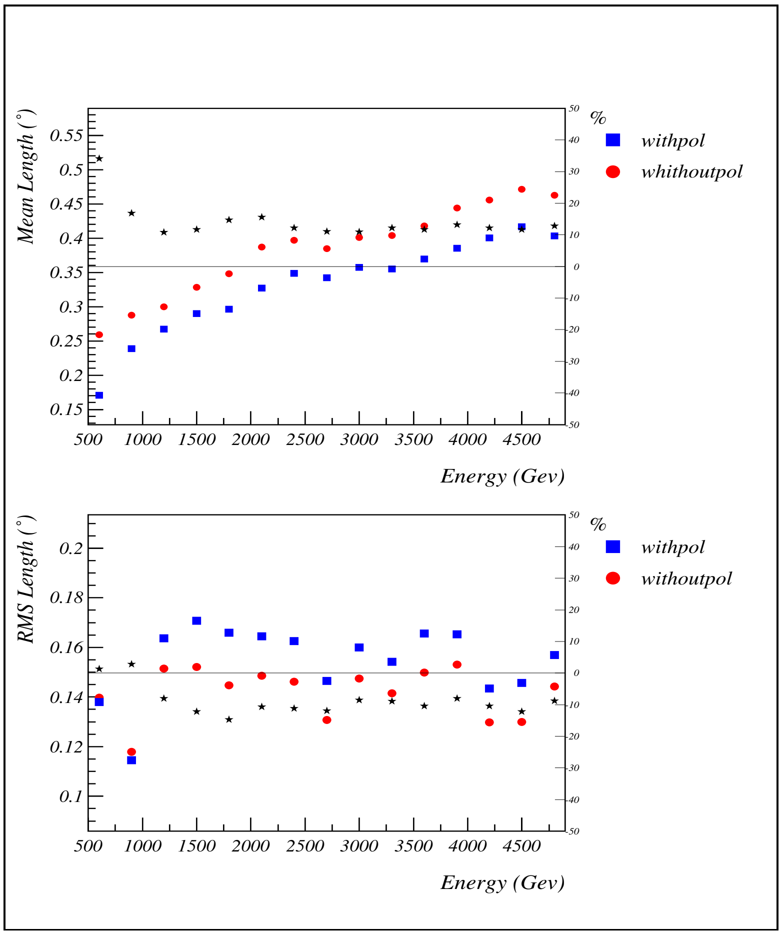

Figure 5.26: *Comparison between the mean length of proton images with and without polarization assumption for different energies. The stars represent the difference in % between mean sizes.*

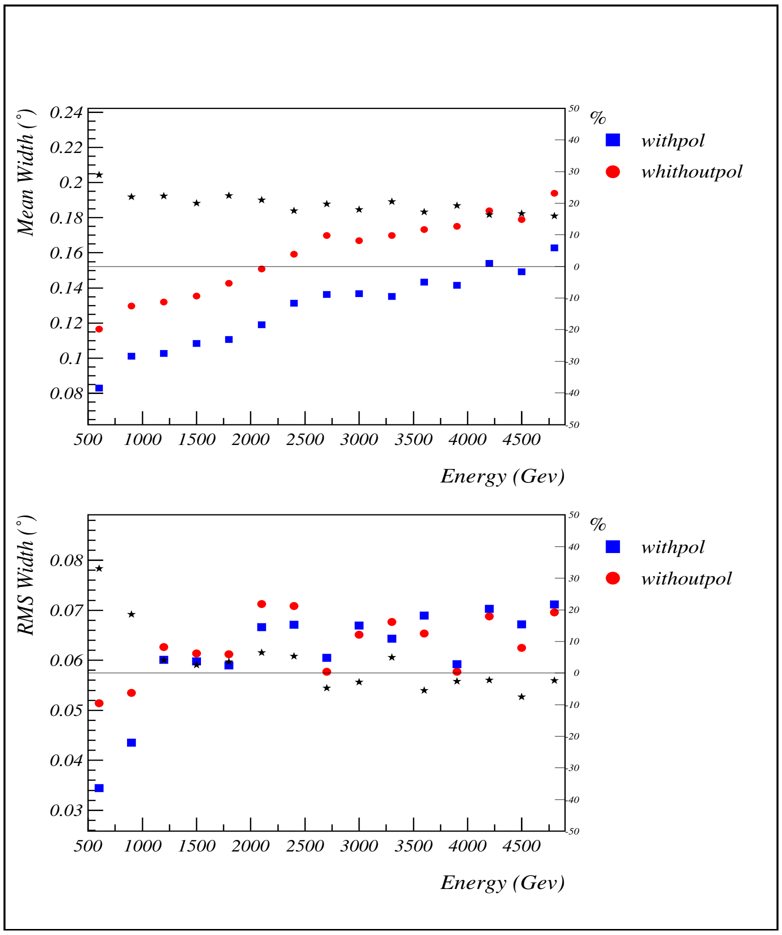

Figure 5.27: *Comparison between the mean width of proton images with and without polarization assumption for different energies. The stars represent the difference in % between mean sizes.*

Alpha. In figures Fig.(5.28) and Fig.(5.29) the mean alpha parameter is represented for gammas and protons respectively.

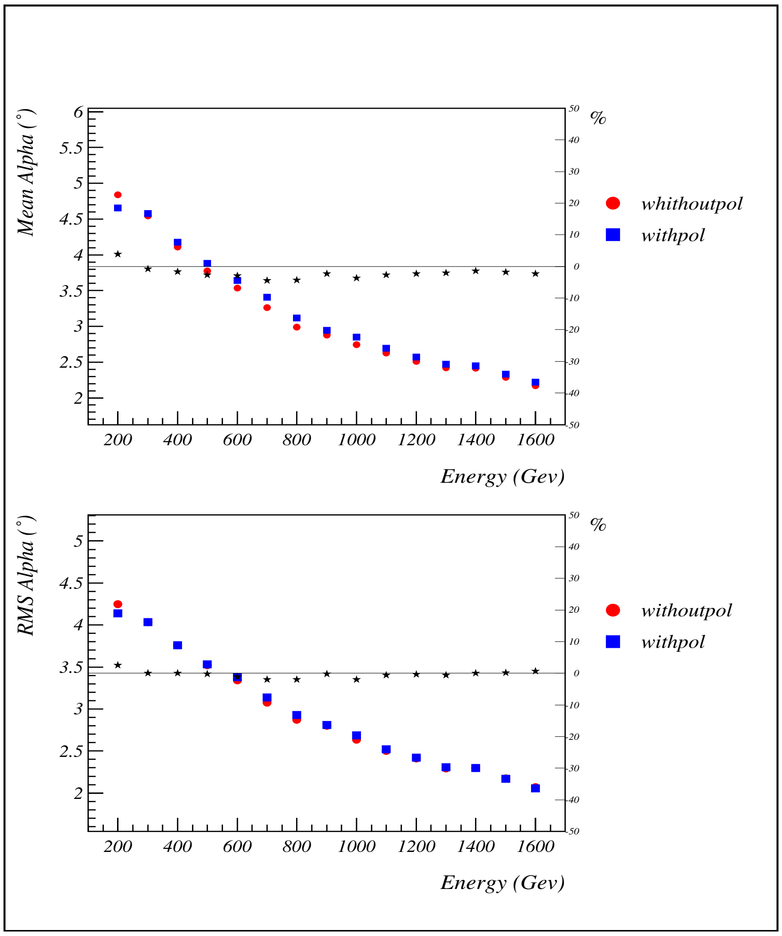

Figure 5.28: *Comparison between the mean alpha of gamma images with and without polarization assumption for different energies. The stars represent the difference in % between mean sizes.*

The conclusion extracted relative to the alpha parameter, is the following:

- The alpha parameter does not suffer any relevant modification with the polarization assumption. This states for gammas and for proton images. The reduction is between 0-5 %. The rms of the alpha distributions are not modified either. The value of alpha for gammas is not better determined around the value of zero degrees.

Size. In figures Fig.(5.6) and Fig.(5.7) the mean size of gamma and proton images is represented.

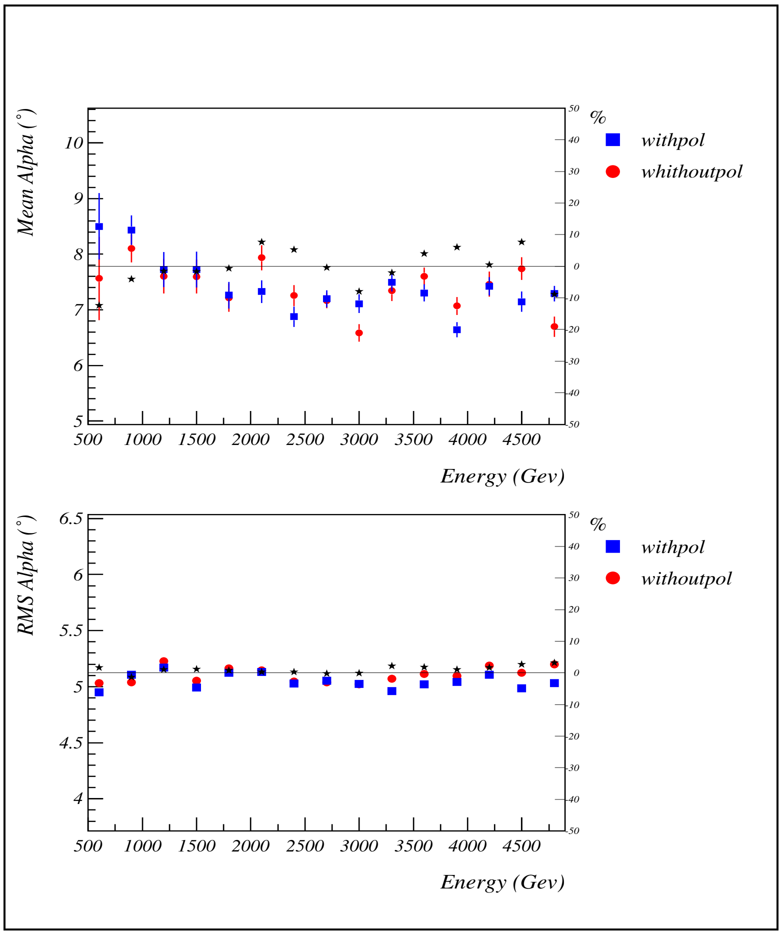

Figure 5.29: *Comparison between the mean alpha of proton images with and without polarization assumption for different energies. The stars represent the difference in % between mean sizes.*

The conclusion extracted from this figures is the following:

- For gammas around 30% of the light is loss at all energies except at the lowest energies where the loss ranges the 20% - 30% of the total image light. For protons this loss ranges between 20% at the lowest energies and 40% at the highest. Bigger fluctuations exist from energy to energy for proton events. The cut off suffered by the gamma and proton images is as expected from what we have seen in point **5.1** of the General Characteristics.

The final conclusion extracted from the analysis of the Hillas image parameters is that even with the more compact images the alpha parameter is not better determined as expected.

Quality factor. Last, the quality factor is obtained. In figure Fig.(5.30) the quality factor is plotted for the polarizers assumption and the common situation. The stars on the plot have to be looked in the right axis. They represent the difference in percentage between both cases. If the stars are above 0% means that our method achieves better results than the common case. The shadowed region is the error region for the common case while bars are the errors for the polarizers case.

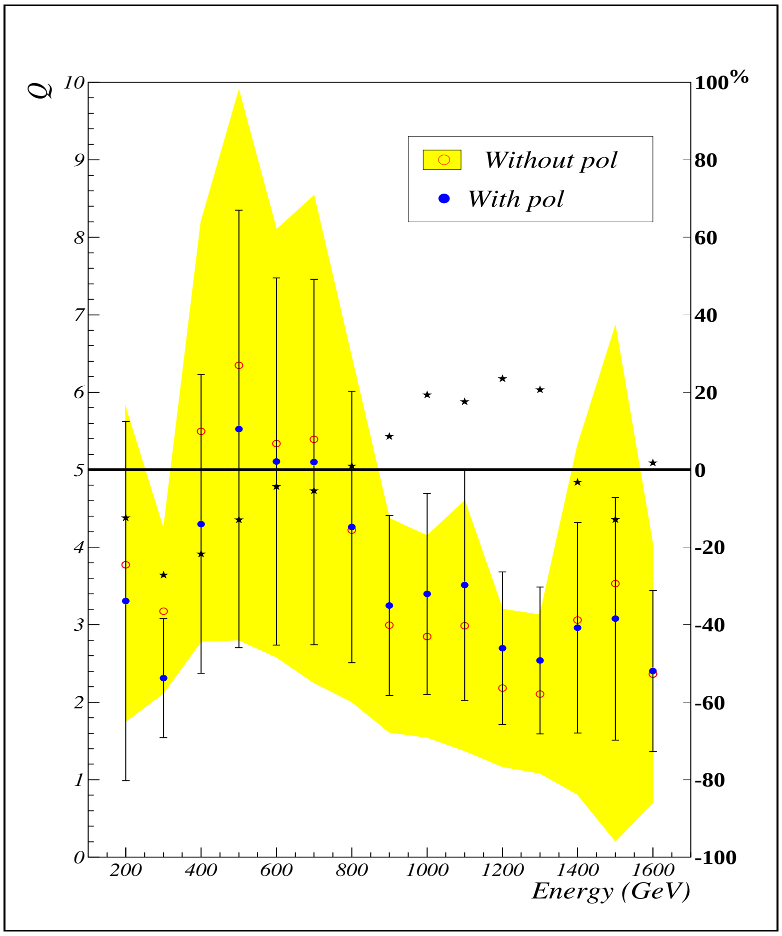

Figure 5.30: *Quality factor.*

The procedure followed to obtain the quality factor is the following:

$$Q = \frac{\epsilon_\gamma / \epsilon_{\gamma trig}}{\sqrt{\epsilon_p / \epsilon_{ptrig}}} = \frac{\Gamma_\gamma}{\sqrt{\Gamma_p}} \tag{5.4}$$

where:

$\epsilon_\gamma \equiv$ gamma events accepted after cuts.
$\epsilon_{\gamma trig} \equiv$ gamma events in trigger.
$\epsilon_p \equiv$ proton events accepted after cuts.
$\epsilon_{ptrig} \equiv$ proton events in trigger.

This way we obtain a quality factor as a function of the energy for the polarizers assumption and for the common case, just by taking into account the different value of the ϵ parameters for each case.

To obtain the errors we consider a distribution of N_{trig} events and two probability states, event taken after cuts or not taken after cuts. The cuts used are the ones from page(98). We associate this to a binomial distribution of N_{trig} events with p=$\frac{N_{aftercut}}{N_{trig}}$ to evaluate the error of Q as:

$$(\Delta Q)^2 = (\frac{1}{\sqrt{\Gamma_p}})^2 \cdot (\Delta\Gamma_\gamma)^2 + (\frac{1}{2} \cdot \frac{1}{(\Gamma_p)^{3/2}})^2 (\Delta\Gamma_p)^2 \tag{5.5}$$

where:

$\Gamma_\gamma = \epsilon_\gamma / \epsilon_{\gamma trig}$; $\quad \Delta\Gamma_\gamma = \sqrt{\frac{p_\gamma \cdot (1-p_\gamma)}{100.}}$
$\Gamma_p = \epsilon_p / \epsilon_{ptrig}$; $\quad \Delta\Gamma_p = \sqrt{\frac{p_p \cdot (1-p_p)}{100.}}$

and:

$p_\gamma = \frac{N_{aftercut\gamma}}{N_{trig\gamma}}$
$p_p = \frac{N_{aftercut\mathrm{p}}}{N_{trig\mathrm{p}}}$

Again, it is difficult to estimate the effect of the correlation between different telescopes. Being conservative we will consider the images totally correlated and replace N_{trig} with 100 (number of showers) to estimate $\Delta\Gamma_\gamma$ and $\Delta\Gamma_p$.

The conclusion concerning this point is:

- Between 800 GeV and 1300 GeV our method achieves better results, being the γ acceptance higher. For energies lower than 800 GeV and higher than 1300 GeV the Q factor is smaller for the polarization case than it is for the common case.

Camera Images. Before finishing this results chapter we would like to show some camera images as obtained with the simulation program developed for this work.

- **Figure Fig.(5.31):** *Upper left*, a 200 GeV gamma image in which the telescope is not triggered in the common case and triggered in the polarization assumption. *Upper right*, a 200 GeV gamma image in which the telescope is triggered in both cases and the length and width parameter is reduced with polarization. *Lower left*, a 1000 GeV gamma image in which both length and width are reduced. *Lower right*, a 1000 GeV gamma image with the impact point at a distance typical of the hump, in which both length and width are also reduced.

- **Figure Fig.(5.32):** *Upper left*, a 1200 GeV proton image in which the image parameters, length and width, are reduced. More than 50% of the light is cutted off by the polarizers. *Upper right*, a 1800 GeV proton image where no significant cut off in intensity is achieved. *Lower left*, a 3000 GeV proton image. Again around 50% of the light is cutted off. *Lower right*, a 4800 GeV proton image not triggered with polarization and triggered in the common case.

- **Figure Fig.(5.33):** The four images are muon rings and arcs obtained in proton showers of different primary energy.

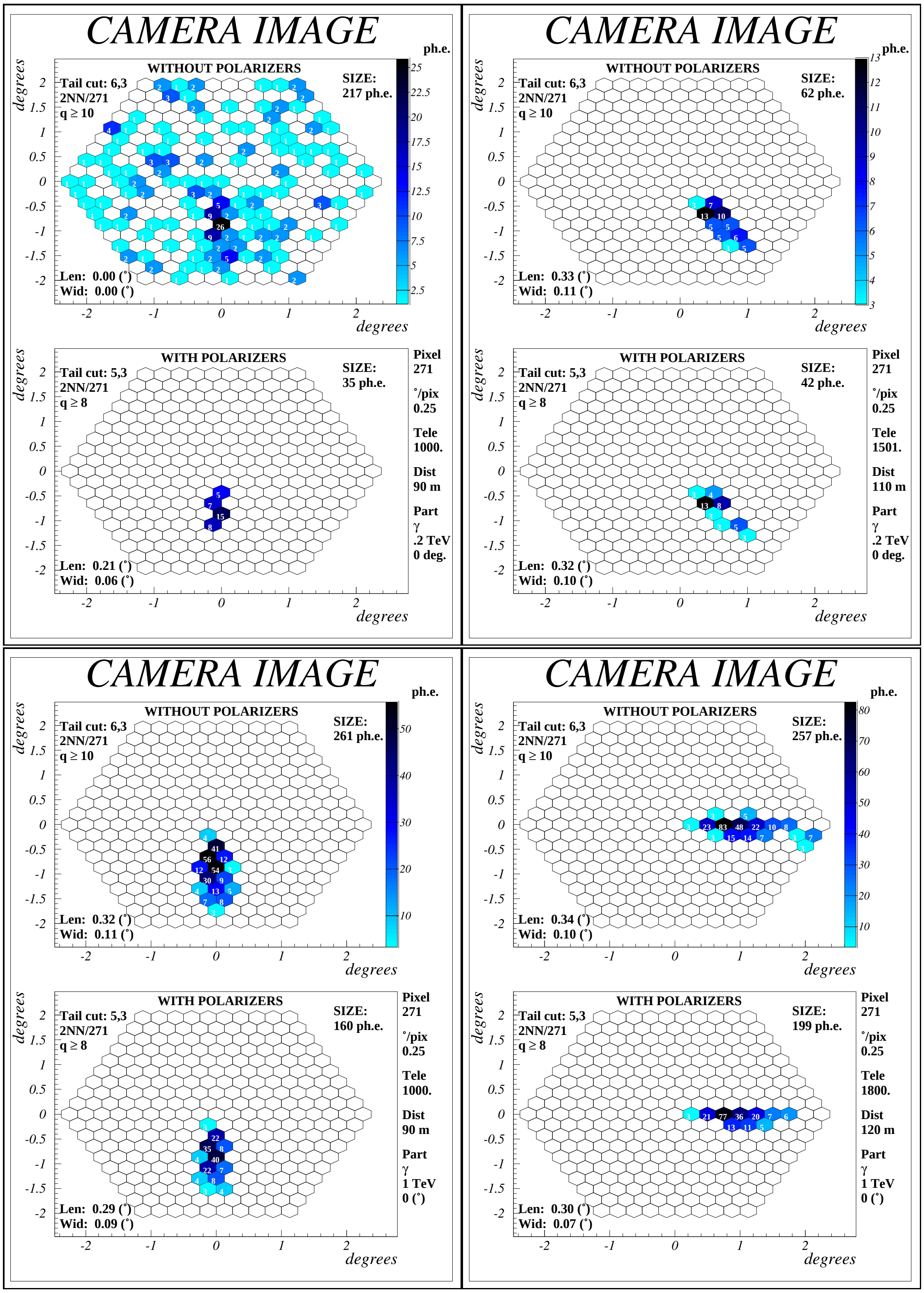

Figure 5.31: *Gamma images on the camera. In the upper row two 200 GeV gamma shower image. Lower row two 1 TeV gamma shower image.*

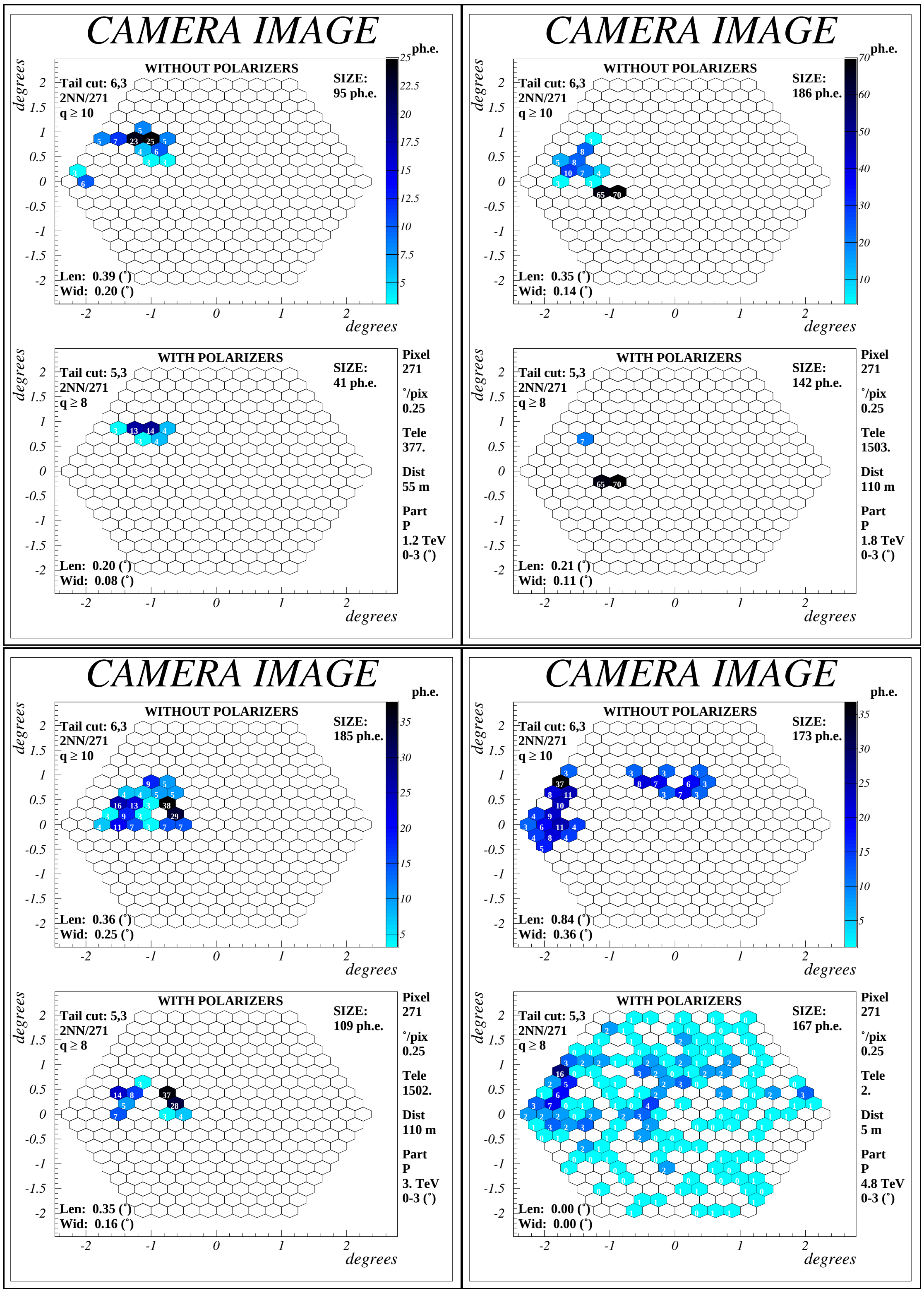

Figure 5.32: *Proton images of different energies, on the camera.*

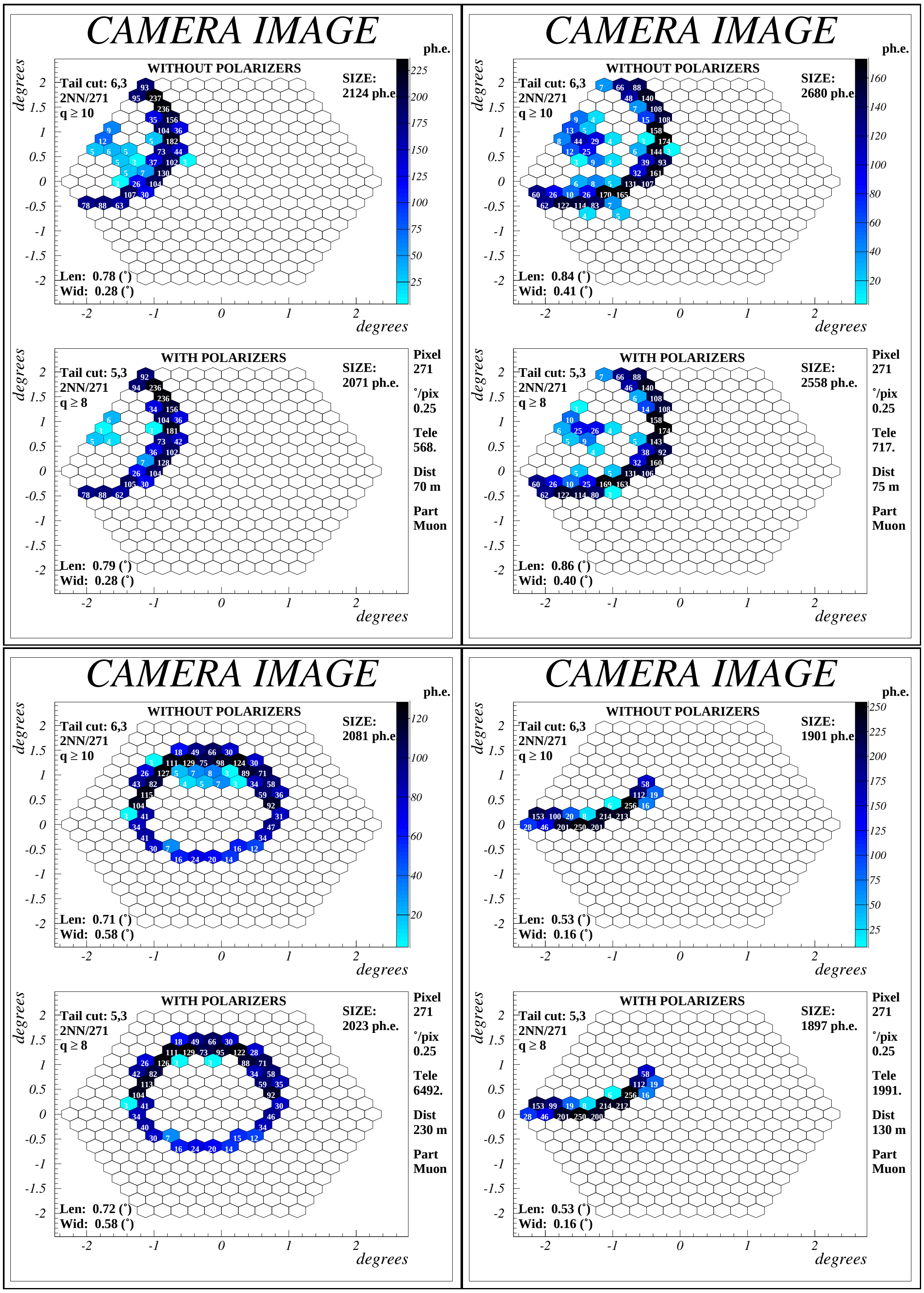

Figure 5.33: *Muon rings and arc.*

Chapter 6

Conclusions

The main task of this work is the study of the intrinsic polarization of the Cherenkov radiation produced in Extensive Air showers. The particular features of the polarization of Cherenkov radiation makes it an interest source of information, not exploited nowadays, that could have benefits for the Imaging Atmospheric Cherenkov technique.

Little information exists in the literature about the polarization of Cherenkov radiation in the frame of EAS. Hence the first task of this work includes the study of several intrinsic features of the polarization of the Cherenkov radiation in the frame of EAS. This first study covers the distribution of the polarization vectors along the longitudinal development of the shower, that is, the dependence of such a distribution with height of Cherenkov photon production; secondly we study the dependence of the lateral distribution of the shower with the polarization vectors distribution on ground, and look for an energy and primary particle dependence of such a distribution. Finally we carried out the study of the dependence of this polarization distribution on ground with the time of arrival of the Cherenkov photons at the observation level. The conclusions of this first study are that there is dependence of the polarization distribution with height of Cherenkov photon production; there is a dependence of the polarization distribution on ground with the core distance and a small dependence with the energy of the primary particle, and finally there is dependence of the polarization distribution with time of arrival of Cherenkov photons at ground. In the three cases the dependence is different depending on the nature of the primary particle initiating the shower.

In order to take advantage of the intrinsic polarization of the Cherenkov radiation in EAS, an experimental setup has been proposed in this work. This setup consists on the arrangement of linear polarizing filters on the camera of an IAC telescope. With this particular setup we can take advantage of the particular distribution of polarization vectors on ground and find whether reliable results can be achieved with this new method. *A priori* conclusion that we can extract from the arrangement of linear polarizing filters on the camera is the suppression of 50% of the light of the LONS being a simple effect of natural light going through a linear polarizer.

With this experimental setup the performance of the telescope is tested and compared with the common well established technique existing at the moment, without polarizing filters placed on the camera. To test the performance of the telescope the effective areas are obtained for both situations and both for gamma and proton initiated showers, with the final aim of studying the differential rates and hence the energy threshold of the telescope. From the conclusion extracted in the first point related to the dependence of the distribution of polarization vector on ground with the nature of the primary particle, we expected to increase the energy threshold for proton events and reduce the energy threshold for gamma events. After the study, our conclusions are that the effective areas are reduced for gammas and proton events but with a bigger reduction in the last ones. The differential rates are hence affected by this reduction in effective area and again the differential rate for protons is reduced more than for gamma events. Related to the trigger threshold of the telescope no conclusion is achieved because this energy falls bellow the energies of the events generated.

The last study carried out in this work is related with the modification of Hillas image parameters due to the placement of polarizing filters on the camera of an IAC telescope. On the basis of the ideas exposed in chapter three we expected to have narrower and more compact images with the use of polarizing filters allowing us to better determine the alpha parameter. After our study, the conclusion is that with the polarizing filters, images are actually shrank in length and width with greater shift in width making images narrower and more compact as expected. There is little dependence in the modification of these parameters with the energy and some small differences exist when taking into account the nature of the primary particle. Nevertheless the alpha parameter does not suffer relevant modifications as expected either for gammas nor for protons, and even at some energies is slightly worst determined with the use of polarizing filters. The alpha parameter plays an important role in the γ-hadron separation technique. We expected to have better determined the alpha parameter for gamma events than for proton events making the γ-hadron separation more efficient with the use of polarizing filters. This is reflected in the quality factor, Q, that is determined in this work for both cases, with and without the polarizers assumption. The conclusion, in what quality factor refers, is that even not having the alpha parameter better determined, our method achieves better results at energies between $\sim$ 700 GeV and sim 1400 GeV. Another parameter with big relevance is the size parameter. This parameter give us an idea of the mean amount of light lost in the camera by the placement of polarizers at different primary energies. We expected to loss around 30% for gamma events on the basis of Fig.(5.4) and around 40% for proton events on the basis of Fig.(5.5). Our conclusion is that for gamma events the intensity loss is $\sim$ 30%, as expected, at all energies except at the lowest energies generated where the loss is a little bit lower. The loss of light for proton events is a little bit higher than $\sim$ 30% at all energies except for the lowest energies, but anyway not reaching the 40% expected.

Bibliography

[1] T. C. Weeks 1985, *The Gamma-Ray Universe*; *Infinite Vistas* Cornell and Carr Editors.

[2] J. V. Jelley and T. C. Weeks 1995, *Ground-Based Gamma-Ray Astronomy*; Sky and Telescope, pag. 20, Sep. 1995.

[3] D. J. Fegan 1997, *γ-hadron separation at TeV energies*; J. Phys. G: Nuclear Part. Phys. **23**: 1013-1060.

[4] J. V. Jelley 1958, *Cherenkov Radiation and its Applications*; Ed. Pergamon Press.

[5] J. M. Cabrera 1993, *Optica Electromagnética*; Ed. Addison-Wesley Iberoamericana.

[6] A. M. Hillas 1996, *Differences Between Gamma-Ray and Hadronic Showers*; Space Sciense Reviews **75**: 17-30.

[7] W. R. Leo 1987, *Techniques for Nuclear and Particle Physics Experiments*; Ed. Springer-Verlag.

[8] P. Sokolsky 1988, *Introduction to Ultra High Energy Cosmic Ray Physics*; Ed. Addison-Wesley.

[9] R. Mirzoyan 1997, *Constrains in Reducing the Threshold of Imaging Cherenkov Telescopes*; Towards a Major Atmospheric Cherenkov Detector V, Proc. Kruger National Park ed O.C. de Jager p298.

[10] D. Petry 1997, *Development of Dynamical Supercuts for the HEGRA 5 m^2 Cherenkov Telescope*; Towards a Major Atmospheric Cherenkov Detector V, Proc. Kruger National Park ed. O.C. de Jager p368.

[11] A. M. Hillas 1990, *Characteristics and Brightness of Cerenkov Shower Images for Gamma-Ray Astronomy near 1 TeV*; J. Phys. G: Nucl. Part. Phys. **16**: 1271-1281.

[12] J. Knapp 1997, *High Energy Interactions and Extensive Air Showers*; 25^{th} International Cosmic Ray Conference, Durban, South Africa.

[13] J. Knapp and D. Heck, *Extensive Air Shower Simulation with CORSIKA*; User's Guide, version 5.61 April 1998.

[14] D. Heck, J. Knapp, J. N. Capdeville, G. Schatz and T.Thouw 1998, *CORSIKA: A Monte Carlo Code to Simulate Extensive Air Showers.*

[15] R. Mirzoyan and E. Lorentz, *Measurement of the Night Sky Light Background at La Palma*; Internal report of the HEGRA collaboration.

[16] R.Mirzoyan, E. Lorenz, D. Petry, C. Prosch 1997, *On the influence of afterpulsing in PMTs on the trigger threshold of multichannel light detectors in self trigger mode*; Nuclear Instruments and methods in Physics Research A 387, 74-78

[17] G.Hermann, C. Kohler, T. Kutter and W. Hofmann 1995, *Triggering of Imaging Air Cherenkov Telescopes: PMT trigger rates due to night-sky photons*; Astro-ph **v2** Aug 1995.

[18] *The MAGIC Telescope for Gamma-Ray Astrophysics above 10-30 GeV*; Letter of Intent, June 1998.

[19] A. Konopelko 1998, *The Monte Carlo Characteristics of the HEGRA system of Imaging Air Cherenkov Telescopes. Elsevier preprint*, May 1998.

[20] M. Ulrich, A. Daum, G. Hermann and W. Hofmann 1997, *An Improve Technique for the Determination of Shower Geometry from Single and Stereo IACT Images*; J. Phys. G: Nucl. Part. Phys. **24**: 883-897.

[21] J. Sanchez Almeida and V. Martinez Pillet 1992, *Instrumental Polarization in the focal plane of telescopes*; Astron. Astrophys. 260, 543-555.

[22] J.L. Contrera, I. de la Calle and J. Cortina 1998, *A Study of the Polarization of the Cherenkov Radiation in Extensive Air Showers of Energy Around 1 TeV*, Proc. 16^{th} European Cosmic Ray Simposium, ed. J. Medina. p. 467.

[23] A. M. Hillas 1985, *Cherenkov Images of EAS Produced by Primary Gamma-Rays and by Nuclei*; Proc. 19^{th} ICRC (La Jolla) **3** 445.

[24] F.A. Aharonian, W. Hofmann, A. K. Konopelko and H.J. Volk 1997, *The potential of Ground Based Arrays of Imaging Atmospheric Cherenkov Telescopes. I. Determination of Shower Parameters*; Astroparticle Physics **6**: 343-368.

[25] Rao and Sinha 1988; J. Phys. G: Nucl. Part. Phys. **14**: 811.

[26] P. T. Reynolds *et al* 1993; The Astrophysical Journal, **404**: 206-218, 1993 February 10.

[27] D. A. Lewis *et al* 1993; Proc. *23rd* ICRC (Calgary) **1** 279

[28] G. Mohanty *et al* 1997; Astroparticle Physics.

[29] S. Le Bohec and B. Degrange 1995. Towards a major atmospheric Cherenkov detector IV Proc. Padova Workshop, ed. M. Cresti, p378.

[30] A. M. Hillas and M. West 1991; Proc. *22nd* ICRC (Dublin) **1** 472.

[31] M. Punch *et al* 1992; Nature, Vol 358, 477.

[32] M. S. Longair 1992; *High Energy Astrophysics*, Ed. Cambridge Universiy Press.

[33] K. Greisen 1956; Prog. Cosmic Ray Phys. 3.

[34] T. K. Gaisser and A. M. Hillas 1977; Proc. *15th* ICRC, Plovdiv **8** 353.

[35] P. Sommers and J. W. Elbert 1987; *Ultra-High gamma-ray Astronomy Using Atmospheric Cherenkov Detectors at Large Zenith Angles*; J. Phys. G:Nucl. Phys. **13** 553-566.

[36] V. R. Chitnis and P. N. Bhat 1999; *Simulations on Arrival Time Distributions of Cherenkov Photons in Extensive Air Showers.*; astr-ph/9902253 18 Feb 1999.

List of Figures

List of Tables